Polyglycerol-based Biointerface Materials for Cellular Studies

Inaugural-Dissertation
to obtain the academic degree
Doctor rerum naturalium (Dr. rer. nat.)

Peng Tang

Department of Chemistry, Biology, Pharmacy
Institute of Chemistry and Biochemistry
Freie Universität Berlin

2024

The research projects in this dissertation were carried out within the research group of Prof. Dr. Rainer Haag from August 2020 until January 2024 at the Institute of Chemistry and Biochemistry of the Freie Universität Berlin.

1. Reviewer: Prof. Dr. Rainer Haag, Freie Universität Berlin

2. Reviewer: Prof. Dr. Marie Weinhart, Freie Universität Berlin

Date of defense: 2024.06.06

Acknowledgements

This work would not have been possible without the support and contributions of a few people and I would like to express my sincere gratitude to them. First of all, I want to thank Prof. Dr. Rainer Haag for being my supervisor and continuously supporting me in every possible way during my Dr. rer. nat. career. He offers me useful and sufficient scientific advices and right amount of freedom in my research projects. His kindness and understanding has always been helpful and invaluable.

I would also like to thank Prof. Dr. Marie Weinhart for being my second supervisor in this thesis.

In addition, I want to thank Prof. Dr. Leixiao Yu's support from the very beginning of my Dr. rer. nat. He guided me in practical polymer synthesis and offered me great help in my first project.

I would like to thank Dr. Smriti Arora, Dr. Boonya Thongrom for the help in the later projects we worked on. We worked as an efficient team with interesting idea bursts and fruitful outcomes. They also helped with the proofreading of this dissertation. They are wonderful colleagues and friends, with whom I really enjoyed working with.

I want to express my gratitude to all former and present AG Haag group members. With everyone's contributions we have a lovely and nice work environment. Especially, I would like to thank Dr. Wiebke Fisher, Eike Ziegler and Anja Stöshel for being so kind and professional in coordinating all the big and minor things within the group. I would like to thank Katharina Achazi, Stefanie Wedepohl, Elisa Quaas for being of great help in the biolab. Besides, I would like to thanks Cathleen Hudziak, Katharina Goltsche, Marleen Selent, Daniel Kutifa for their help with synthesis, GPC measurement and chemistry lab management.

I would like to acknowledge the SupraFAB building and Core Facility BioSupraMol for providing useful facilities such as NMR, SEM and AFM. Especially I want to thank Andrea Schulz and Anke Schindler for their help with SEM.

I would like to thank Dahlem Research School for providing me scholarship for the first three years to support my living in Germany.

I am grateful to my colleagues and peers, Chuanxiong, Fan, Rui, Jun, Raju, Shaohui and Philip, for their collaborative spirit and valuable discussions. Especially I want to thank Guoxin for being my best friend at/out of work, I couldn't achieve this far without her

company and help. My deepest gratitude also goes to all the other kind members of AG Haag for their heartwarming support. I truly feel lucky to work with them.

I also want to thank all my friends for their emotional support, understanding and encouragement. They are my family in Berlin, people that I can always count on in all my ups and downs.

In the end, I can never thank enough my parents for their sacrifices and unconditional love through all these years. It is their tremendous cares and supports that made my doctoral education possible.

Declaration of Authorship

I hereby declare that I alone am responsible for the content of my doctoral dissertation and that I have only used the sources or references cited in the dissertation. Intellectual property of other authors has been marked accordingly. I also declare that I have not applied for an examination procedure at any other institution and that I have not submitted the dissertation in this or any other form to any other faculty as a dissertation.

Peng Tang

Berlin, March 2024

Contents

1. Introduction

A biointerface is defined as the interface or region between biological systems and synthetic materials. It involves the relations and interactions of biological entities, such as biomolecules, cells or tissues, in response to non-biological environment, e.g. metals, ceramics or polymers.[1,2] In this sense, biointerfaces are of considerate interest in numerous research fields including biomedicine, biotechnology and biochemistry. The study and manipulation of biointerfaces offers vital cues for the development of biomedical devices, biocompatible materials and biosensing technologies. Taking insights from the molecular and cellular interactions between biointerfaces, better designs of cellular substrate, drug delivery systems, medical implants and biosensors can be achieved, aiming at optimizing the biocompatibility, minimizing immunogenic responses and guiding cells' fate.[3]

One typical example of biointerfaces is the play around cells and their substrate. Given that most cells are traditionally cultured in special flasks and well plates, by modifying the surfaces of the substrates, the interaction and adhesion behavior can be controlled.[4] Depending on the applications, enhanced adhesion promotes the cell capture, growth and culture. On the other hand, modified substrates can also regulate the adhesion of unwanted biomolecules and cells thus achieve bio-antifouling.[2,5]

With the increasing demand for a better and more sophisticated model for biointerface studies, three-dimensional (3D) matrices emerged as a new platform owing to the better mimicry of *in-vivo* biological environments.[6] A 3D model that closely imitate extracellular matrix (ECM) can not only offer physical and structural support, deliver vital biomolecules but also trigger certain biological processes.[7] Many kinds of 3D scaffolds were developed to fit the purposes, among them, hydrogels, crosslinked networks with high water content, appear to be perfect candidates as 3D biointerface materials.[8]

In this work, cellular studies were carried out among different biointerfaces. Different polymeric systems were designed to fabricate scaffolds ranging from polymer coated substrates and 3D synthetic polymer hydrogels. The objective is to discover enhanced cell-substrate interactions, ensuring the targeted capture of specific cells in biosensing applications, while creating a versatile platform for the culture of multicellular spheroids in a three-dimensional environment.

2. Theoretical Background

2.1 Functional Surface Coatings

2.1.1 Surface Modification of Polymers

The functions of materials are not only determined by their bulk properties but also by their surface features. However, most of the conventional materials fail to meet the increasing demand of modern applications. A practical approach to alter or improve the performance of materials is to modify the surface characteristics when they already possess excellent bulk properties.[9] Surface modification simply refers to the act of modifying the properties, characteristics or functionality of a material's surface area by means of physical or chemical methods. This technique is able to enhance a material's durability and compatibility with other materials, bringing desired physical, chemical or biological properties.[10,11] Therefore, it is widely implemented in various fields including material science, engineering, chemistry and biotechnology.

Polymer has emerged as one of the most commonly applied materials in our daily lives, industry and science. With their outstanding versatility, durability, biocompatibility, recyclability and adaptability, polymers can fit into every aspect of fundamental material world.[12,13] The evolution of polymers has endowed them stable and robust bulk properties such as thermal resistance[14], optical[15] and electrical[16] characteristics. However, a wide range of applications are limited by the surface properties of polymers, modifications thereby are necessary in polymer design and engineering.

Surface modification, on the one hand, involves the physical change of the surface morphology, such as the roughness, thickness and topography.[17] These can be done through polishing[18], mechanical or chemical abrasion[19], chemical etching[20], corona/plasma treatment[21] or laser induced patterning[22]. Through which, the modified surfaces can be endowed accordingly with higher/lower surface area, fouling/antifouling properties, change of friction and tailored microstructures. On the other hand, chemical surface modification normally focuses on altering the chemical composition of the surface, tuning the hydrophilicity, surface charge, surface energy, reactivity, and biocompatibility. Methods such as chemical vapor deposition[23], grafting to/from chemistry[24] and so on, can be employed. Nonetheless, the physical and chemical approaches are not independent, based on the bulk materials and their intrinsic properties, various techniques can be used to fit the specific application synergistically.

Polymers have been proven to be promising materials for a multitude of biomedical applications for their outstanding bioinert properties. With proper modifications, polymers with suitable surface functionalization and modification are able to conquer the limitations in their pristine form, interact properly with different biomolecules in wider range of applications.[12,25,26] In the process of cell adhesion to a substrate, cell firstly adheres to a surface via non-covalent bonding, e.g. hydrogen bond, van der Waals, electrostatic ion and polar interactions, followed by the adhesion of extracellular matrix molecules, such as fibronectin, vitronectin, laminin and collagen, to cell transmembrane receptor proteins called integrins.[27,28] Notably, one of the most common peptide motif that contributes to cell adhesion to extracellular matrix is arginylglycylaspartic acid (RGD).[29] Hence, the complicated cell adhesion and proliferation mechanisms challenge the biopolymer materials for more advanced surface properties. Various surface modification techniques are implemented to satisfy the need for better biomedical use.

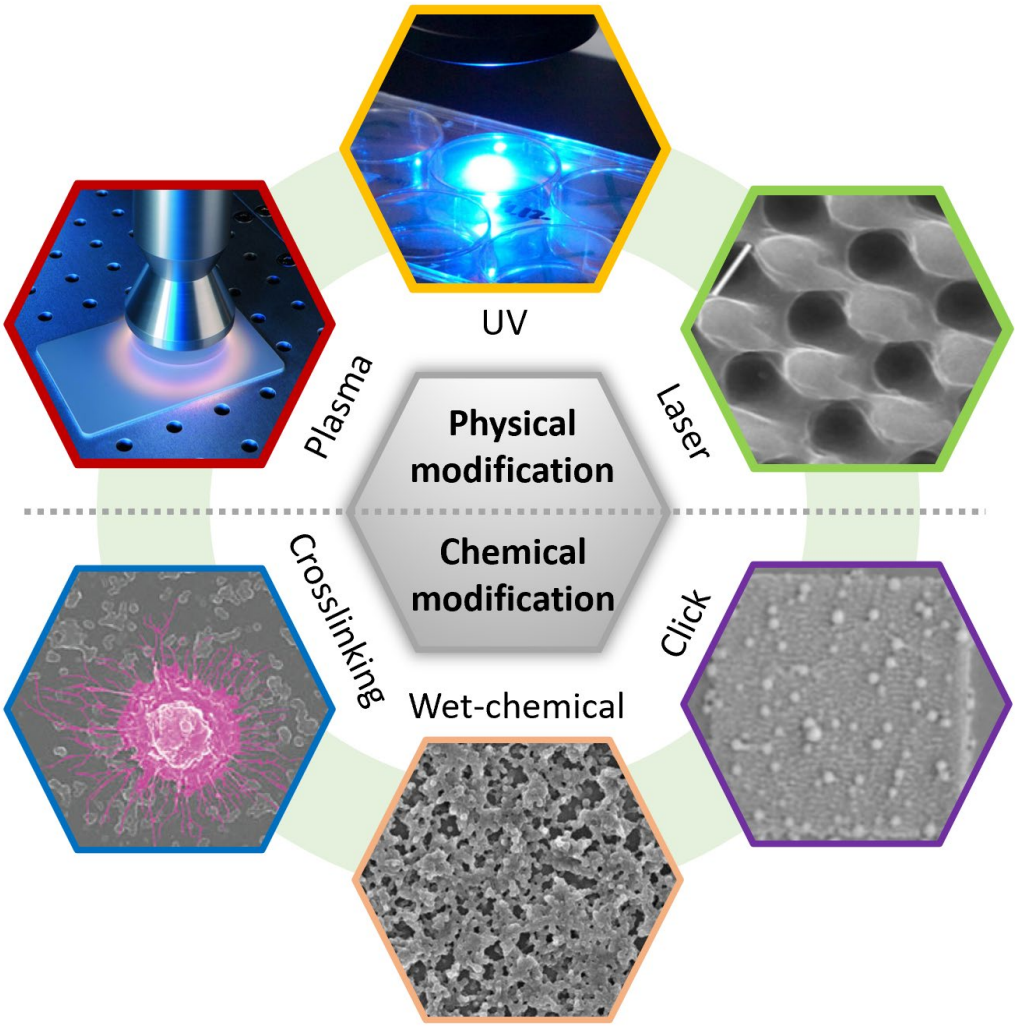

Figure 1: Overview of different methods for surface modification.

As depicted in Figure 1, in physical surface modification, one common method is plasma-induced treatment. The electrons and ions with high energy generated through the plasma ionization process interact with the polymer surface, causing various changes such as oxidation, functionalization, polymerization and so on, yielding the physical or chemical modifications on the treated surface area.[24] For instance, Barbarash et al. found that the cellular viability and adhesion were enhanced on plasma-treated poly-ε-caprolactone (PCL) substrates due to the increasing hydrophilicity.[30] Das's research also showed high cell viability with argon/oxygen plasma treated polyvinyl alcohol/chitosan nanofibers.[31] Apart from plasma, UV (ultra violet) light is often used in polymer surface modification. Energetic UV light is able to trigger photophysical/photochemical processes and initiate chemical crosslinking with photo initiators, thus altering the surface chemistry, polarity, charge on the surface.[32] Even after 10 min of UV radiation on polyamide nanofibers, the surface of which can be activated and the cell behaviors can be enhanced.[33] Satish et al. crosslinked laminin peptides with polyvinyl cinnamate (PVCi) nanofibers with photo initiator under UV radiation. Cell adhesion rate and differentiation were positively improved with the modified nanofibers.[34] With even higher energy source such as laser, the surface topographical structures can be modified by laser beams. The femtosecond laser can be applied for lithographical patterning with high precision, fabricating various surface structures.[35] Jun et al. designed microscale grooves with femtosecond laser on the surface of poly (L-lactic acid) (PLLA), which could guide the cell for self-organization and orientation for a better ingrowth of myoblasts.[36]

Proteins, polysaccharides and functional groups can be incorporated onto polymer surface via different chemical reactions to improve the performance in many biomedical applications.[25] These biomolecules can be immobilized using crosslinking chemistry. N-hydroxysuccinimide (NHS),[37] 1-ethyl-3-(3-dimethylaminopropyl) carbodiimide (EDC),[38] ethylene glycol diglycidyl ether (EGDE)[39] and glutaraldehyde[40], are most frequently used crosslinkers. For example, EDC and NHS have been applied in fields like peptide chemistry for amide coupling. Similar to this strategy, click chemistry is also often used to introduce functional groups to the polymer surface to facilitate the bio-compatibility or bio-functionality. Awada et al. utilized thiol-ene chemistry to conjugate iron nanoparticles with polylactide nanofibers surface. A monolayer of iron nanoparticles were immobilized on PLA, resulting in increased biocompatibility.[41] In Nada's research, the click reaction between azide and alkyne was employed to functionalize cellulose-based scaffolds.[42] In wet chemical reaction, methods like chemical etching or polymer grafting are applied to not only modify

the surface with desired functional groups but also to change the surface topography and surface energy. For instance, chemicals like toluene and ethanol mixture were used to pretreat the surface of PLA fibers to generate swollen surface layer. This layer can absorb gelatin solution to achieve better cell adhesion.[43]

For both physical and chemical modifications, the surface of a bulk material is directly altered. Sometimes, the scaffold is inert and not subjected to easy modification, thereby introducing a surface coating aids broadening the possibilities for further functionalization. The process of a surface coating can be direct and simple, without any destruction to the coated materials. However, the stability and linkage between coating and substrate always remain problematic. Nevertheless, coating is still widely used for its great potential in surface modification.[44] Bio-based coating such as ECM or peptide sequences can be coated to desired substrate via specific linkage to encourage cell adhesion, proliferation and differentiation.[45] According to the applications, coating can also be applied to prevent the adhesion of the cells for bio-antifouling. In our previous research, it is found that hydrophilic coating such as polyglycerol-based coating material has outstanding bio-antifouling properties to prevent undesired adhesion on substrates.[46]

2.1.2 Mussel-inspired Coatings

In recent decades, polymer coatings have gained increasing voice in surface modification due to their versatility and flexibility. Substantial efforts have been dedicated to enhancing coating performance and broadening their applications.[44] Among countless types of coating strategies, mussel-inspired chemistry stands out for its outstanding universality in wet adhesion.[47] Mussels are known to attach themselves firmly to diverse surfaces in wet and dynamic surroundings through their byssal threads. This remarkable ability of mussels attributes to the proteins found in their byssus mucus, noted as mussel-foot proteins (mfps).[48] After intensive researches on these mfps, Lee et al. discovered that almost all of these proteins comprise the post-translationally modified amino acid 3,4-dihydroxyphenyl-L-alanine (Dopa).[49] Further studies revealed that the catechol group in Dopa plays the main role, while other conditions such as pH, amines and metal ions provide strong adhesion.[50,51] Catecholamines, such as dopamine, as derivatives that possess similar molecular structures to Dopa, are the most common analogues.[52] The first generation of synthetic mussel-inspired coatings are the self-polymerized dopamine, noted as polydopamine (PDA), reported by Lee and Messersmith et al.[53] PDA was proven to be able to adhere to all kinds of organic and

inorganic materials robustly. This remarkable discovery inspired many researchers to design and develop new analogues of coatings on the basis of mussel-inspired chemistry (Figure 2).

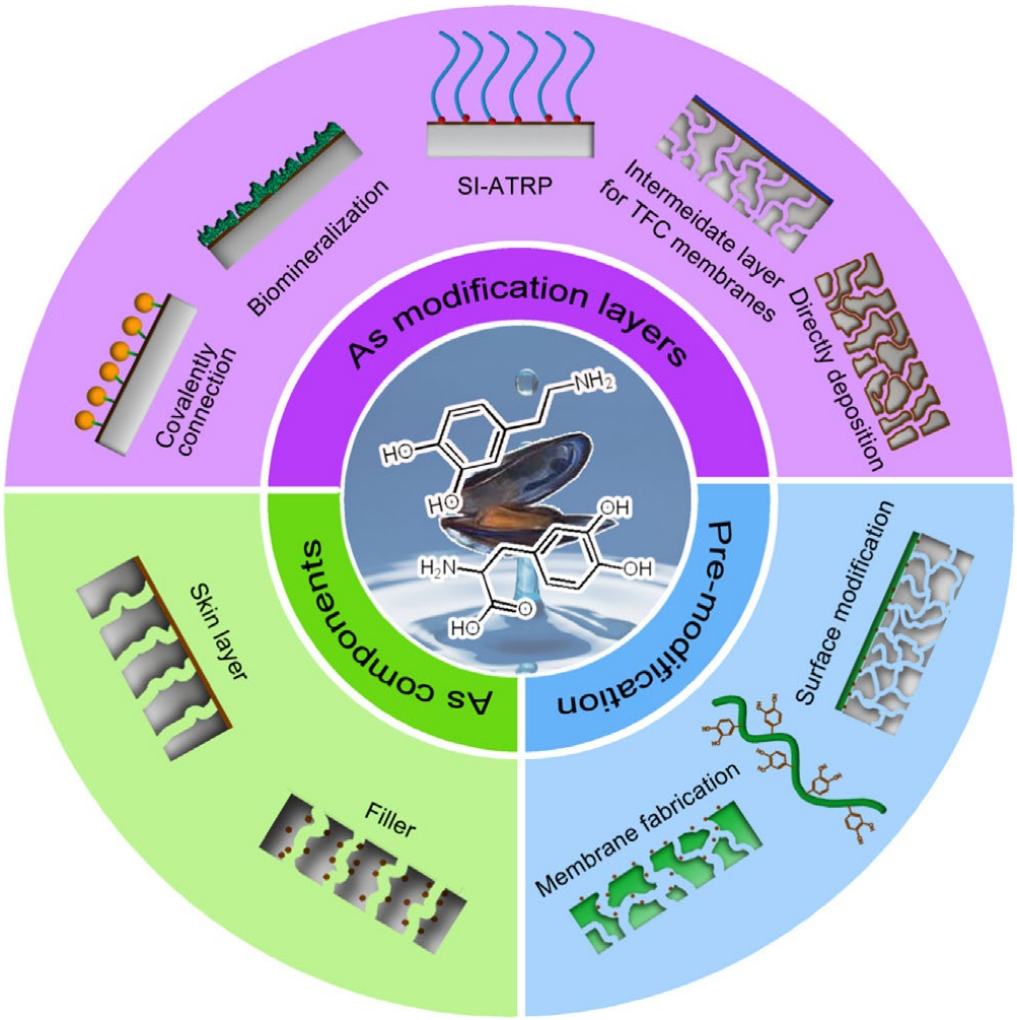

Figure 2: Illustration of mussel-inspired materials and their applications based on Dopa oxidation. Reprinted with permission from ref. [54] Copyright 2015 Elsevier.

With the development of techniques like surface force apparatus (SFA) and atomic force microscope (AFM), advances were made on revealing the essentials of mussel adhesion. The interactions between Dopa and the substrates were identified as bidentate hydrogen bond,[55] metal-ion coordination bond[56,57], π-π/π-cation interactions[58,59], redox reactions[60,61], autooxidation[62], Michael-addition[63] and electrostatic interaction[50] (Figure 3). The diverse chemical interactions via catechol chemistry offer an universal platform to improve the wet adhesion properties on various natural and synthetic materials.[64] Bidentate hydrogen bonds are in charge of the adhesion on hydrophilic substrates like mica or glass.[55] According to Bell theory and proved by SFA, bidentate hydrogen bonds have 10^6 higher bond lifetime comparing to monodentate hydrogen bonds, which greatly enhance the adhesion via

catechol molecules.[65] Dopa-metal coordination bonds are responsible for the strong adhesion on metal oxide surfaces such as TiO_2 surface.[66] Furthermore, abovementioned π-π/π-cation interactions play a critical role in adhesion on surface that are abundant in aromatic components like PS substrate.[67]

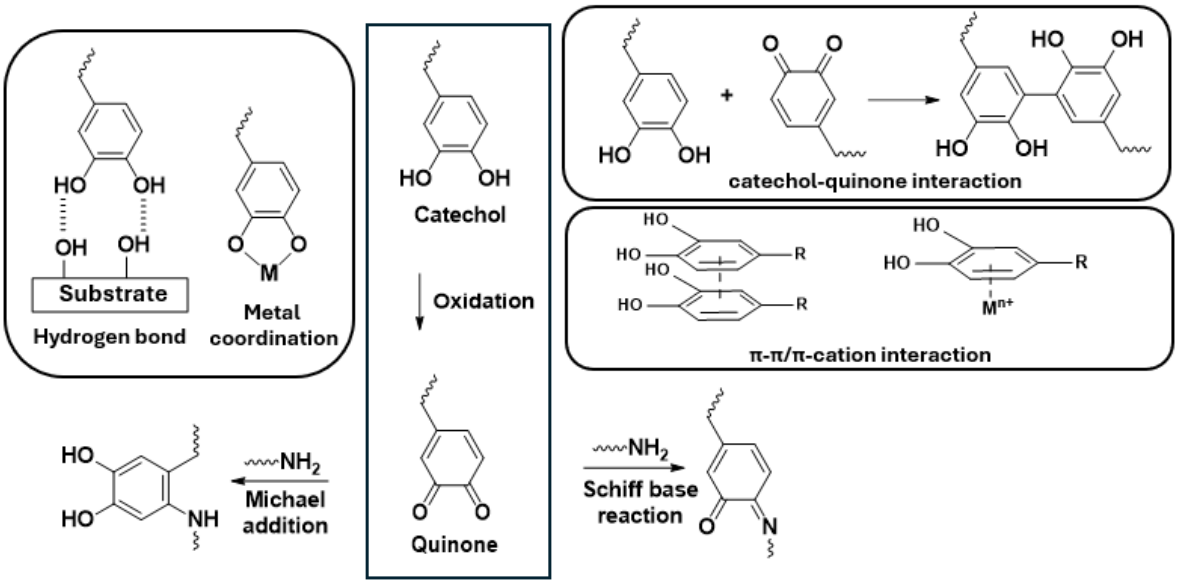

Figure 3: The mechanisms of catechol adhesion from mussel-inspired molecules.

The outstanding adhesion properties and enormous potential for post-modification have gained mussel-inspired materials substantial attention in a wide range of biomedical applications such as antimicrobial activity,[64] tissue regeneration[69] and wound healing.[70] Acting as versatile coating material, Dopa-containing polymers are capable of functionalizing various materials, including cellulose and polypeptides. Islam et al. firstly coated cellulose with Dopa, then conjugated with Ag nanoparticles via coordinative bonding. Exceptionally strong adhesion was achieved by Dopa layer to secure AgNPs on cellulose substrate. The obtained DOPA-AgNPs-modified paper showed superior antimicrobial properties against many antibiotic-resistant pathogenic bacteria.[71] Apart from coating on cellulose, Wang et al. covalently modified strontium-doped calcium polyphosphate (SCPP) with Dopa to immobilize silk fibroin (SF), which greatly enhanced the bioactivity and reduced fragility of the scaffold.[72] As another example, poly-L-lactide (PLLA) fibers were modified with PDA. Homogeneously coated PDA-PLLA demonstrated improved cell adhesion, cell spreading, alkaline phosphatase activity and osteogenic differentiation comparing to non-modified PLLA fibers.[73]

2.2 Hydrogels

2.2.1 Hydrogels and crosslinking networks

A hydrogel is a three-dimensional (3D) network of hydrophilic polymer chains that are capable of absorbing and retaining a significant amount of water within their crosslinked structure, resulting in a gel-like consistency (Figure 4).[74] The insoluble crosslinked network made of hydrophilic polymeric chains allow the hydrogel to swell in the aqueous media while maintaining its structural integrity. Hydrogels exhibit properties such as biocompatibility, high water content, and the ability to mimic certain aspects of natural tissues such as extracellular matrix (ECM), making them valuable in various biomedical, pharmaceutical, and environmental applications, including drug delivery, tissue engineering, and wound healing.

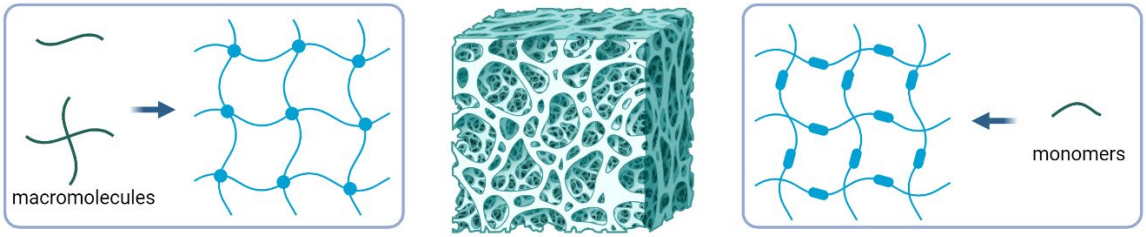

Figure 4: Schematic illustration of hydrogel network structures. Hydrogels can be formed either by crosslinking macromolecules (left) or forming network from multi-functional monomers (right). Created with BioRender.com

Natural hydrogels are normally derived from biological sources such as proteins, polysaccharides, and other biopolymers, including chitosan, alginate, dextran and hyaluronic acid. Therefore, they are inherently biocompatible and have been widely used over the past decades. The first synthetic hydrogel was made by Wichterle and Lim in 1960, hydroxyethyl methacrylate (HEMA) was crosslinked with the aim of forming a “plastic” that can contact with human tissue permanently.[75] Followed up by intensive researches, synthetic hydrogels have gained immense progress across a wide spectrum of applications. Notably, Lim and Sun successfully encapsulated cells in calcium alginate microcapsules in 1980s,[76] This inspired plenty of related work and made hydrogels attractive candidates for cellular studies and tissue engineering.

Various strategies can be implemented to form a crosslinked structure of hydrogel (Figure 5). Typically, physical crosslinking yields reversible hydrogel network, as the

involved physical interactions are normally reversible.[77] Such physical crosslinking including chain entanglement,[78,79] electrostatic interaction,[80] hydrogen bonding[81,82] and hydrophobic interaction[83,84] are non-covalent and homogeneous, thus the physical hydrogels are usually inhomogeneous, relatively weak and subject to dissociation under conditions.[85] Hence, the physical hydrogels are able to respond to certain stimuli e.g. pH, temperature, presence of ions or ligands with different affinity. In all cases, physical properties of the hydrogels can be tuned accordingly based on the crosslinking interactions. Utilizing this reversibility, fascinating applications were made possible, such as self-healing hydrogel and stimuli-responsive hydrogels.[86–88] In biomedical cases, physical gels can be fabricated through certain biospecific recognitions. For instance, Nakamae et al. formed gel complex with concanavalin A and polymeric sugar;[89] Morris et al. used avidin and polymeric biotin for physical gel crosslinking.[90]

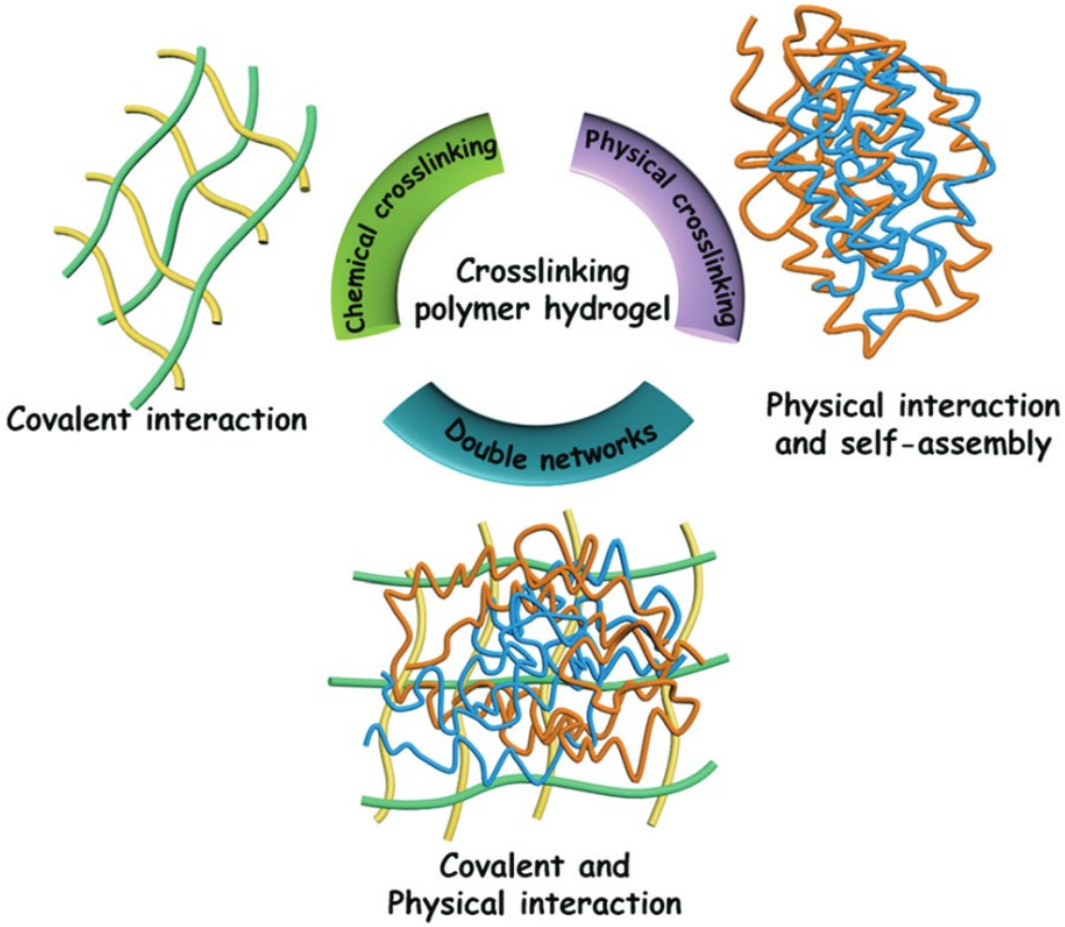

Figure 5: Hydrogels can be crosslinked physically, chemically, and dually. Reprinted with permission from ref. [91] Copyright 2019 Royal Society of Chemistry.

Chemical crosslinking forms covalent bonding between two complementary functional groups, creating 'permanent' or 'chemical' gel.[74] Chemically crosslinked network can be either made by the conjugation among two or more macromolecules or crosslinking during the polymerization process starting from monomers (Figure 4, 5).[92] Similar to physical gels, the homogeneity can also hardly be achieved with chemical crosslinking. The crosslinking region can be swollen with aqueous medium and reach an equilibrium, with higher crosslinking density, and expected lower water content. The crosslinking density is influenced not only by the reactants and the polymerization rate, but also by the types and conditions of the crosslinking reactions.[85,93] Based on the reaction mechanisms, the chemical crosslinking can be categorized as addition, condensation, and nucleophilic substitution.

The addition crosslinking involves the addition reaction of two bi- or multi-functional entities, yielding an adduct without any byproducts, forming covalently bonded three-dimensional network. Notably, due to the exceptional properties of click chemistry, such as fast reaction rate, high specificity and efficiency with mild reaction conditions, click chemistry is the most widely used in addition reaction in hydrogel formation.[94,95] Given that the mechanical properties and swelling behaviors of hydrogels are heavily dependent on the crosslinking density, click chemistry allows well-controlled and precise crosslinking of a hydrogel network. As an example, strain-promoted alkyne-azide cycloaddition (SPAAC) was employed to form hydrogels under room temperature without any catalyst, where dendritic polyglycerol (dPG) was functionalized with azide groups, then crosslinking was performed by PEG with cyclooctyne chain end.[96] Besides, thiol-ene reaction is also intensively used in hydrogel crosslinking. With the help of photo initiator and corresponding UV/vis light, a thiol-functionalized molecules can undergo fast and precise click reaction with a reactant that contains electron-rich double bonds.[97,98]

In contrast to the addition reaction, where no byproduct is generated, condensation reactions are always accompanied by release of small molecules such as water or carbon dioxide. Typical condensation reactions that are implemented in hydrogel formation are Schiff-base reaction and inverse electron-demand Diels-Adler reaction (IEDDA). These reactions are sometimes reversible, resulting in reversible hydrogels that are degradable or self-healing. Furthermore, in nucleophilic substitution, a nucleophile like thiol would substitute selectively the electrophiles, thus forming new bonds.[99] For instance, thiol-functionalized polymers can react with halogenic-functionalized polymers,[100] or disulfide containing polymers[101].

The crosslinking strategies of hydrogels are not limited to single type of reactions or interactions as mentioned above. In many cases nowadays, dual crosslinked networks which combine the physical and chemical crosslinking were designed to enhance the properties of hydrogels. Physical crosslinks provide responsiveness and adaptability, while chemical crosslinks contribute robustness and long-term stability. This dual approach allows for the fine-tuning of mechanical properties and responsiveness, which synergistically benefits the hydrogels, making them well suited for various applications. Fajardo et al. chemically functionalized chitosan and chondroitin sulfate with glycidyl methacrylate, they were chemically crosslinked with the help of a thermal initiator $K_2S_2O_8$ through free radical reaction. Later, physical crosslinked networks were achieved by immersion in stock solutions, where electrostatic interactions were established. This hydrogel exhibited different liquid uptake capacities in response to the change in the pH while maintaining strong crosslinking integrity. It showed great potential in pH-sensitive biomedical applications (Figure 6).[102]

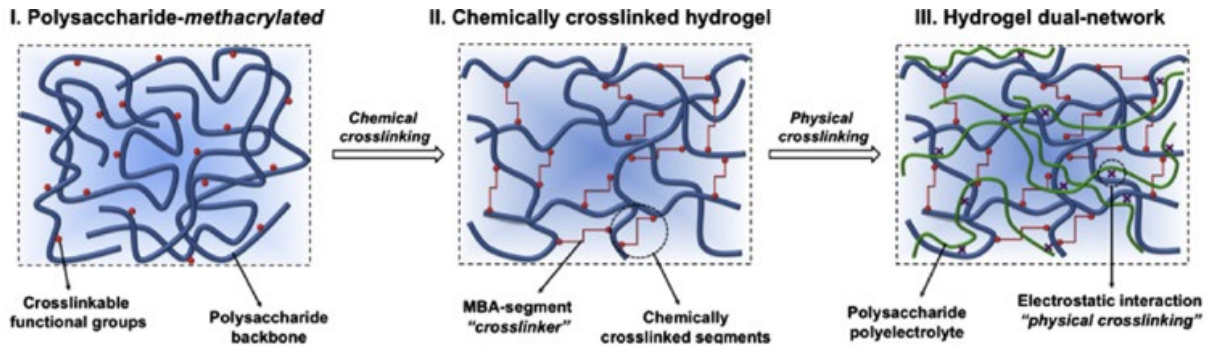

Figure 6: Example of dual-network hydrogels based on chemical and physical crosslinking. Reprinted with permission from ref. [102] 2013 Elsevier.

2.2.2 Polyglycerol hydrogels and crosslinkers

Polyethylene glycol (PEG) is one of the most intensively used synthetic polymers in pharmaceuticals, cosmetics, food, and various biomedical industrial applications. Owing to its simple chemical molecular structure with ethylene oxide repeating unit, PEG is renowned for the water-solubility, biocompatibility and low toxicity.[103,104] Notably, PEG is a FDA approved polymer that has been heavily applied in many everyday products. However, after repeated exposure to PEG, anti-PEG antibodies have been found in some individuals, which can recognize and bind to PEG molecules, potentially triggering immune responses. This phenomenon has gained attention in recent years and has implications for the safety and efficacy of PEG-containing products.[105] Even though PEG-based hydrogels are

biocompatible and suitable for numerous applications, it is yet necessary to find an alternative for the next generation of formulations. As an analogue to PEG, which is normally polymerized from monomer ethylene oxide, polyglycerol possesses the same polymeric backbone with extra hydroxyl group on each repeating unit. Polyglycerol is typically formed by ring opening polymerization of monomer glycidol. Due to the proton transfer during the polymerization process, an uncontrolled reaction would yield randomly hyperbranched molecular structure. With careful tuning of the process, linear, hyperbranched or dendritic molecular structures can be obtained.[106] Polyglycerol offers similar advantages in terms of hydrophilicity, biocompatibility and non-toxicity, while also providing more potentials for post-functionalization and structural diversity.[107]

The structure of polymer matrix plays an essential role in its chemical and physical properties. In comparison to the straightforward linear arrangement of repeating units in linear polymers, dendritic polymers have a highly branched tree-like molecular structure.[108] The symmetric branches validate multiple functional sites at each branch point, a defined size with large surface area, mono-dispersity, low viscosity and good solubility make dendritic polymer especially intriguing for various applications. However, the making of this perfect structure requires harsh synthesis process, where a well-controlled step-wise growth of the polymeric structure is needed. In that sense, degree of branching (D.B. %) was established to study branch-on-branch structures in polymer science. It is determined by the fraction of dendritic, terminal and linear units within the polymer matrix.[109] A higher degree of branching indicates a more highly branched polymer structure, e.g. linear polymer is with 0 % of degree of branching, a perfectly branched polymer is with 100 % of the value. As a compromise to the difficulties in dendritic synthesis, polymers are mostly synthesized in a less controlled, easier manner, depending on the mechanism and production, 15 – 90 % of branching can be reached and they're noted as hyperbranched polymers.[110] For instance, hyperbranched polyglycerol can be produced with high degree of branching and low polydispersity (< 1.5), which exhibits exceptional properties via ring-opening multi-branching polymerization.[111,112]

The multi-functional sites on the branched structures in hyperbranched polymer promote the formation of a crosslinked network. Thus, hyperbranched polymers are excellent candidates for hydrogel formation. Wang et al. used RAFT (reversible addition fragmentation chain transfer) polymerization technique to prepare highly branched PEG-based polymer from monomers PEGDA (polyethylene glycol diacrylate) and PEGMEMA (polyethylene glycol methyl ether methacrylate), then crosslinked by thiol-functionalized hyaluronic acid.

The obtained hydrogel was employed to encapsulate antimicrobial agent, which demonstrated great efficacy against different bacteria and enhanced cell proliferation property. The hyperbranched structure greatly facilitated the formation of a suitable hydrogel for providing a wound regeneration environment.[113]

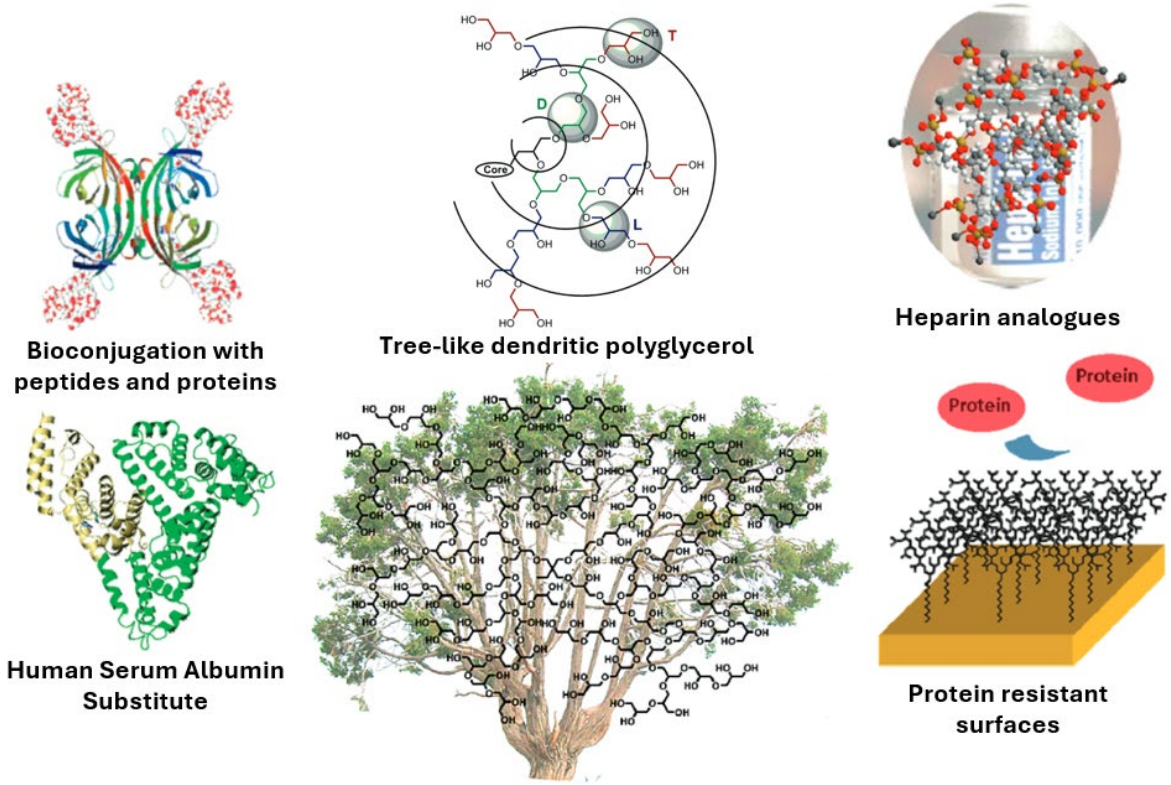

Figure 7: Dendritic polyglycerol and their potential applications. Adapted with permission form ref. [111] Copyright 2010 American Chemical Society.

Hennink et al. reported the first hyperbranched polyglycerol hydrogel in 2006.[114] Polymer was modified then crosslinked chemically via acrylate-based chemistry with the help of photopolymerization. The quick gelation and good mechanical properties were achieved, suggesting promising applications in biomedical fields. Ever since, hyperbranched or dendritic polyglycerol based hydrogels were intensively investigated by varying the chemistry and different bonding mechanisms with the purpose of fitting in various specific applications (Figure 7). The abundant hydroxyl groups on hPG/dPG (hyperbranched/dendritic polyglycerol) can be converted to various functional groups such as amines, allyls, sulfates and catechols with tailored ratio. These functional groups allow hPG to be crosslinked under proper conditions. Thongrom et al. formed hydrogels with maleimide-modified dPG and

maleimide-modified dPGS (dendritic polyglycerol sulfates) via thiol-maleimide click reaction with PEG-dithiol crosslinker. The sulfated hydrogel showed strong HSV (herpes simplex virus) binding due to the charge effect. By tuning the hydrogel properties, the antiviral function of mucus was aimed to be mimicked.[115] Variants like azide-functionalized dPG was crosslinked with cyclooctyne-functionalized PEG via SPAAC reaction, benefiting from the fast and precise reaction, a biosensing matrix with simultaneous biomolecules encapsulation can be achieved *in situ* as hydrogel. This platform offers simple and stable alternative for sensitive biosensors.[116]

2.2.3 Hydrogels as extracellular matrix(ECM)-mimicking substrates

The extracellular matrix (ECM) is a complex, dynamic network of cellular environment that exists outside of cells in multicellular organisms, which consists of proteins, glycosaminoglycans (GAGs), and other soluble molecules. Fibrous proteins such as collagen and elastin are major constituents of ECM, they provide structural support with strength and elasticity. Other glycoproteins with carbohydrate chains attached like laminin and fibronectin, regulating growth and cell-cell communication. GAGs, such as hyaluronic acid and chondroitin sulfate, contribute to the gel-like consistency of the matrix and help retain water, providing resistance to compression.[117–120] ECM is thereby not only a scaffold for cells, offering them structural integrity, elasticity, stiffness, and resilience but also crucial for tissue development, maintenance, and function. Therefore, replicating the ECM complex *in vitro* that mimics the intricate native bio-environment is the key to the successful cell culture model.[121]

Hydrogels, natural and synthetic ones are found with great potential to mimic native ECM owing to their physical, chemical, and biological properties (Figure 8). Collagen, as abovementioned, is the most abundant structural protein in the extracellular matrix in various tissues, it is thereby the most widely studied natural polymer that is applied as such tissue mimics, such as skin, blood vessel, heart valve, liver and bladder.[121] Other natural polymers that are derived from ECM or other tissues, including hyaluronic acid, chondroitin sulfate, fibrin, fibronectin, alginate, agarose and chitosan, are also used in tissue engineering and biomedical applications. Fukuda et al. successfully fabricated a co-culture system composed of hyaluronic acid, fibronectin and collagen, using layer-by-layer deposition technique. All three components were derived from native ECM and rearranged in the desire of creating a model that allows adhesion of different cell lines, making it feasible to investigate cell

behavior such as cell-cell/cell-matrix interactions.[123] In another study, chitosan was crosslinked by glutaraldehyde to form degradable hydrogels to serve as implants for brachy therapy. The degradability and release kinetics of the hydrogel were investigated both *in vitro* and *in vivo*, resulting in negligible tissue response in comparison to surgical sutures.[124]

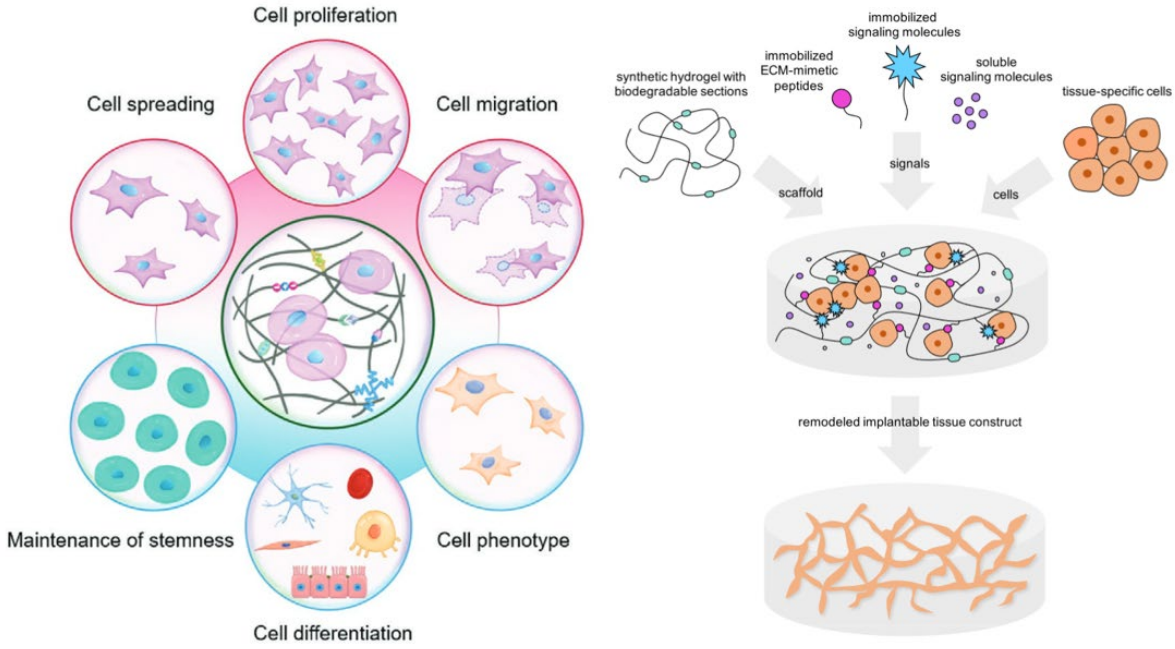

Figure 8: ECM-mimicking hydrogels can regulate various cellular behaviors (left); an example of fabrication of ECM-mimicking hydrogel (right). Reprinted with permission from ref. [27,122] Copyright 2021 Wiley-VCH, 2020 American Chemical Society.

In synthetic hydrogels, the ease of tuning their properties making them ideal tools for studying the effect of each bioactive parameters (e.g. stiffness and adhesiveness) on cells both individually and in combination.[125] For example, for bioregenerative devices in tissue engineering, they are required to be degradable and adhesive for cells. Synthetic hydrogels can be designed to be degradable passively or under actions; various bioactive peptides and proteins can be immobilized in the hydrogel chemically or physically to mimic the endogenous ECM, which consists of binding sites for cells and growth factors etc. for cell regulation.[126] Most synthetic hydrogels are intrinsically bioinert, in order to provide cells with a more hospitable environment, hydrogels can be functionalized with cell-adhesive peptides derived from ECM. Among these peptides, the most commonly used one is RGD (containing arginine, glycine, aspartic acid), which is derived from fibronectin. RGD is known to bind to integrins on most types of cells, mediating the cell attachment, facilitating

cell adhesion, migration and communication with the surrounding environment. Researches showed that varying the concentration of immobilized RGD peptide from 0.001 to 1 mM altered cell morphology, motility and polarization.[127] Standard peptide conjugation with synthetic hydrogels can be applied to RGD moieties, including click-chemistry, enzymatic ligation and peptide chemistry (Figure 8). As an example, Moon et al. employed NHS-ester chemistry to conjugate RGD with acrylate-PEG as hydrogel hub, then crosslinked together with PEGDA to form a hydrogel. Thus, RGD is grafted into the hydrogel backbone to interact with cells. There, angiogenic responses of endothelial cells were induced and regulated via micropatterning, which implied the control over cell behavior can be achieved easily by such synthetic hydrogels.[128] Besides the effective enhancement of RGD peptide on cell adhesion when applying to synthetic hydrogels, other bioactive molecules such as growth factors can also regulate many vital cellular actions such as proliferation, migration and differentiation. Soluble molecules can be freely added along with the culture medium and be dynamically encapsulated by the hydrogel. However, their efficacy is heavily dependent on the duration, concentration and spatiotemporal presentation.[129] Therefore, growth factors can also be immobilized on hydrogels to attain regulated local concentration and a sustained response. Evidence showed that increased bioactivity in EGF (epidermal growth factor)-functionalized PEG hydrogel in comparison to saturated free soluble EGF in media.[130]

2.3 Cellular Biointerfaces

2.3.1 Circulating tumor cells (CTCs)

Metastasis is the most lethal cause for cancer patients, and yet it is a complex biological process which involves the spread of tumor through the circulating system in the human body.[131] Shedding from primary tumor, mutated cells can go through epithelia-to-mesenchymal transition (EMT) then intravasate into blood (Figure 9). These tumor cells or cell clusters, denoting as circulating tumor cells (CTCs), travel in the circulating system and would potentially establish a secondary tumor in distant organ, resulting metastases. The whole process contains many complicated events including cell migration, local invasion, intravasation into blood, dissemination, landing on secondary site, extravasation at site, colonization, engraftment and eventually development of a detectable metastasis.[132] The possible timing of CTC emergence has already been proved to be early in the cancer progress, however, this is dependent on the types of cancer. Nevertheless, CTCs should be detectable weeks before the metastatic development and the count can be directly associated

with overall survival in patients with certain cancer types, including breast, prostate, lung and colorectal cancer.[133] Despite that most CTCs perish eventually in the circulation, few of them are believed to be able to initiate metastases.[134–136] More biology of CTCs and the process that it involves in are yet to be unveiled. There is a necessity to develop efficient methods or markers for CTC isolation and analysis. The challenges lie in the rarity of CTCs with 1 – 10 cells among billions of circulating blood cells and their heterogeneity on size, surface markers and other characteristics.[137,138] In recent decades, the techniques are focused on the enhancement of sensitivity, specificity and efficiency of CTC capture, which facilitates the clinical applications of CTCs in cancer screening, prognosis evaluation and treatment response monitoring.

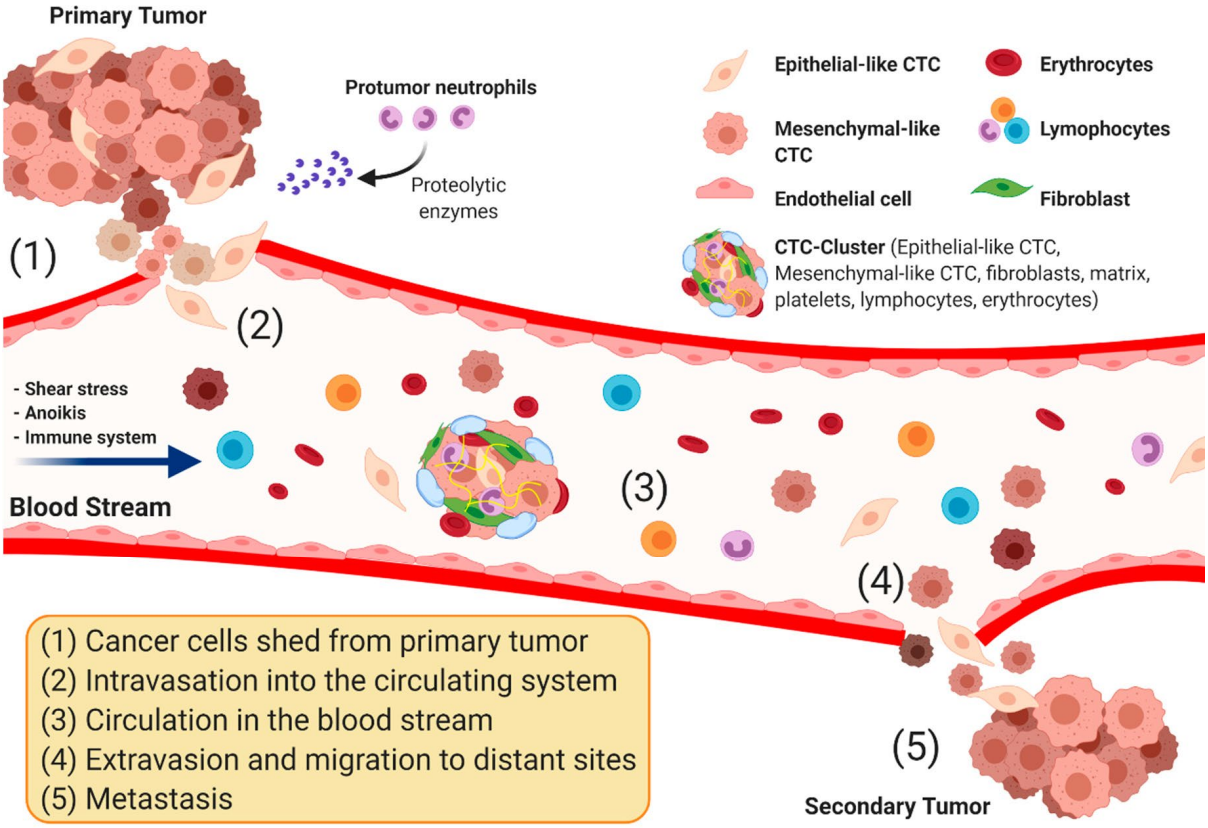

Figure 9: The process of metastasis, including the circulating tumor cells cycle. Reprinted with permission from ref. [139] Copyright 2020 MDPI.

The study of CTCs mainly consists of three core aspects: including the isolation and enrichment; identification and characterization; release and downstream analysis. The capture and enrichment are achieved through specific physical or antibody-antigen interactions between CTCs and tools. Captured CTCs are usually counted and characterized by various

devices such as fluorescence microscopy, flow cytometry etc. Once CTCs are harvested and released from the material, relevant analysis needs to be done, including further culture, genomics, transcriptomics, and proteomics.[137]

Based on the different physical properties of CTCs against normal blood cells in size, density, deformability or electrical properties, CTCs can be distinguished (Figure 10). Used polycarbonate membrane with a diameter of 8 μm to filter out epithelial tumor cells from the blood samples. Although the method was straightforward and cheap, the efficiency was low.[140] A density-based technique, Oncoquick, filters away white and red blood cells, leaving CTCs sorted in the system;[141] Apostream, employs microfluidic system in combination of dielectric electrophoresis techniques to isolate CTCs.[142] These system offer a low-cost, high-vitality solution to traditional CTCs sorting. However, the marker-independent methods normally have low efficiency, poor purity and specificity.

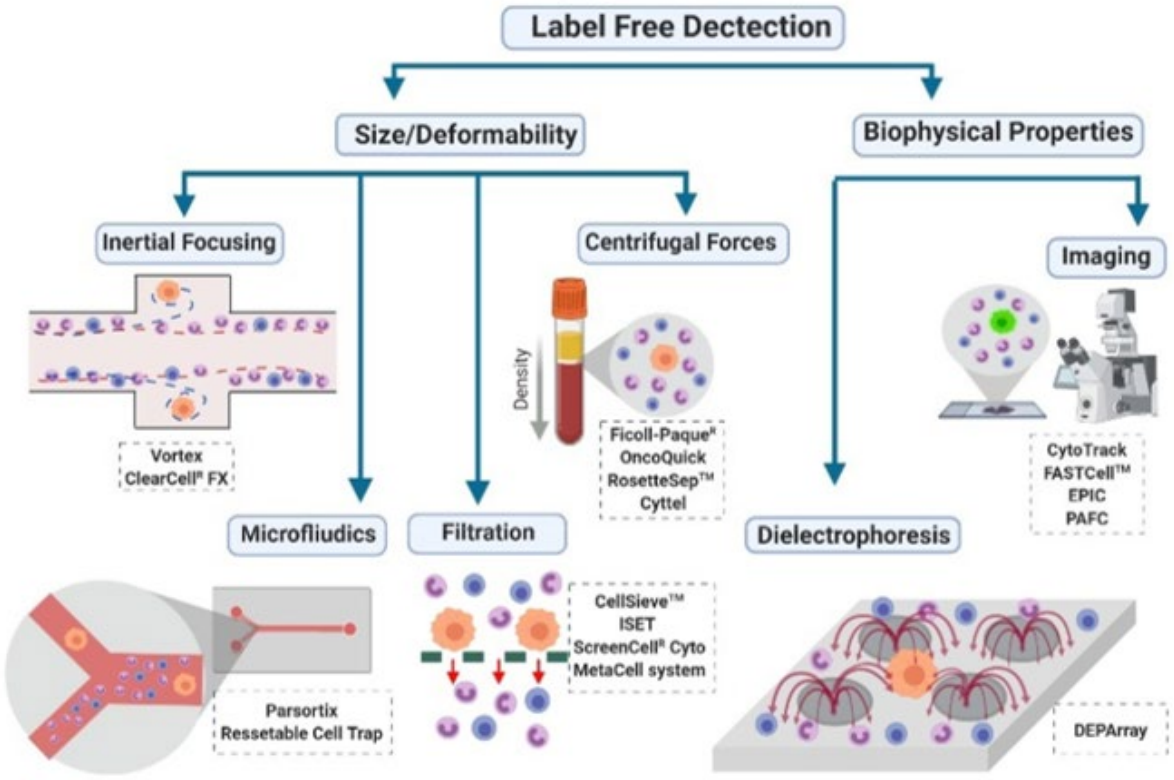

Figure 10: Summary of different label-free techniques for CTC isolation and enumeration. Reprinted with permission from ref. [139] Copyright 2020 MDPI.

Taken cues from the biological differences between cancer cells and others circulating in blood stream, specific biomarkers are used to distinguish CTCs (Figure 11). These

molecular markers vary from the cancer type, among them, EpCAM (epithelial cell adhesion molecule) is by far the most common one, as the majority of cancers originate from epithelial tissues, However, the expression of EpCAM for each cancer type is different. For cancer types like breast and prostate cancer, the strong expression of EpCAM facilitates EpCAM-based antibody-antigen conjugation, thus it is ideal for specific capture of CTCs. This applies to other EpCAM-positive cells, including cells from pancreatic, colorectal and hepatocellular cancers, but not to EpCAM-negative cells such as neurogenic cancer cells.[135] Owing to the specificity and sensitivity of this antibody-antigen interactions, label-dependent techniques are most commonly implemented in CTC enrichment.[138] The first and only FDA-approved system is from CellSearch, which employs anti-EpCAM coated magnetic beads to fish out CTCs from the blood then analyzed with fluorescence-based detection methods.[143] Despite the pioneering development of this technique, the difficulty in CTC release and relatively low capture efficiency are still challenging for the follow-up research. Nevertheless, its standardized and reproducible approach has made it a reference method for CTC isolation in various EpCAM-positive cancer types. In order to breakthrough the limitations in terms of individual physical or biological approaches, researchers have been working intensively on the combination of those and novel technologies. For example, adapting from CellSearch methods, different kinds of immunomagnetic materials were designed, including magnetic rods, pillars, nanoparticles with cleavable coatings and so on.[144] 2D surfaces with appropriate coating were also developed with low cost, high viability and easy release features. Yu et al. designed a surface with hierarchically arranged rough surface to enhance the cell adhesion on polymer coated glass chip, CTCs showed high affinity to anti-EpCAM-conjugated rough surfaces and can be released via boronic acid dynamic chemical bond with high viability.[145] Further more, more and more 2D methods were brought into microfluidic systems with higher sensitivity and control to achieve better performance. Microfluidics offers precise control and manipulation of small volumes of fluids, where not only fluid dynamic forces but also external forces like magnetic, electric field forces can be applied to sort out CTCs from blood samples.[131,146] So-called CTC-chips can bring advantages such as high-throughput processing, reduced sample volumes, enhanced sensitivity, and the ability to create customized environments for cell studies. The channels in the microfluidic chip were modified with gold nanoparticles then conjugated with molecular markers to achieve efficient capture, they can separate viable CTCs directly from the blood samples then release them by ligand exchange with gold nanoparticles.[147] In a more sophisticated system, Lee et al. achieved on-chip capture and characterization of CTCs by magnetic field gradient and

immunofluorescence in a integrated microfluidic system, where up to eight distinct subtypes of heterogenic CTCs can be recognized.[148] Overall, the incorporation of microfluidic technology into CTC research has led to a more efficient capture and analysis. These devices contribute significantly to advancing our knowledge of CTC biology, facilitating early cancer diagnosis, and pushing forward to personalized medicine and treatment management.

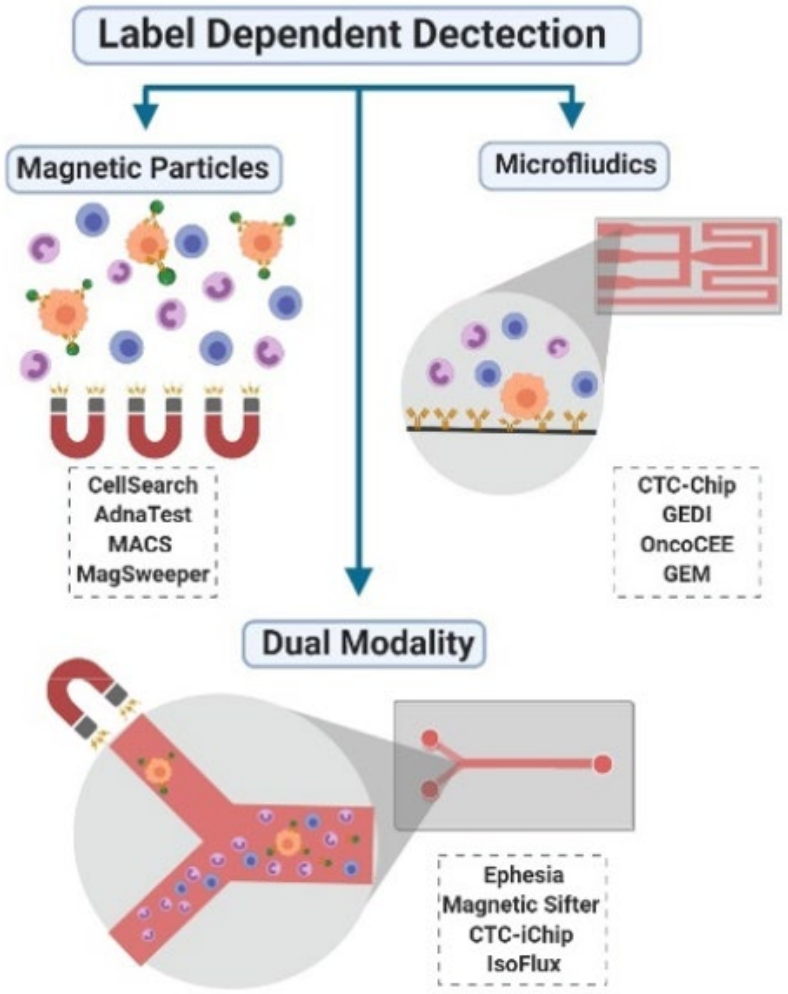

Figure 11: Summary of different label-dependent techniques for CTC isolation and enumeration. Reprinted with permission from ref. [139] Copyright 2020 MDPI.

2.3.2 Multicellular Tumor Spheroids

Cell culture is a widely used technique in biological research which involves the growth and maintenance of cells outside their natural environment, typically within a controlled laboratory setting. The cell culture system provides cells with suitable conditions for proliferation and survival, in which cellular processes can be studied, allowing the development of medical, pharmaceutical and biotechnological applications.[4] Two dimensional (2D) cell culture has been implemented since early 1900s, and in recent decades,

it is extensively used in laboratories worldwide.[149] In a traditional 2D cell culture system, cells are grown on a flat support e.g. polystyrene surfaces, to monolayer. Notably, this still remains the most commonly used system for screening anti-cancer therapeutics and related oncological researches.[150] However, the simple 2D culture models cannot mimic the complicated physiological conditions in tumor microenvironment (TME), including the tumor cellular organization and proliferation kinetics. The lack of spatial conformation in 2D monolayer cells results in the inability of creating a realistic model of *in vivo* solid tumor mimics, the diffusion-limited distribution of oxygen, nutrients, metabolites and signaling molecules cannot be precisely represented *in vitro*, making the screening of anti-cancer drug unreliable and ineffective (Figure 12). Therefore, a growing interest in the 3D *in vitro* models emerged in recent years, attributing to their enhanced capacity to mimic the intricate features of the TME.[6,7] A well established 3D *in vitro* model can bridge the gap between conventional 2D cell studies and *in vivo* model, reducing animal use, and recapitulating tumors histologically and genetically.

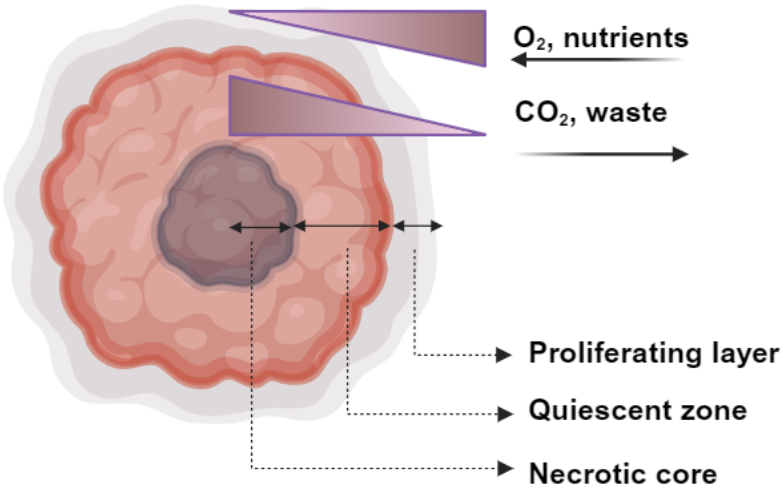

Figure 12: The characteristics of a tumor spheroid.

Various 3D models were developed for more advanced oncological studies, among which, multicellular tumor spheroid (MCTS) model grown with 3D culture systems stands out with relative ease of assembly and reproducibility.[153] MCTS with sphere-like structures are typically grown from individual cell suspensions in non-adherent conditions. These cells normally originated from cancer cell lines, including breast, colon, pancreas and lung cancer

cell lines, rarely from cells derived from tumor tissues. Whether MCTSs can be formed and their morphologies are heavily dependent on the cell types.[151,152]

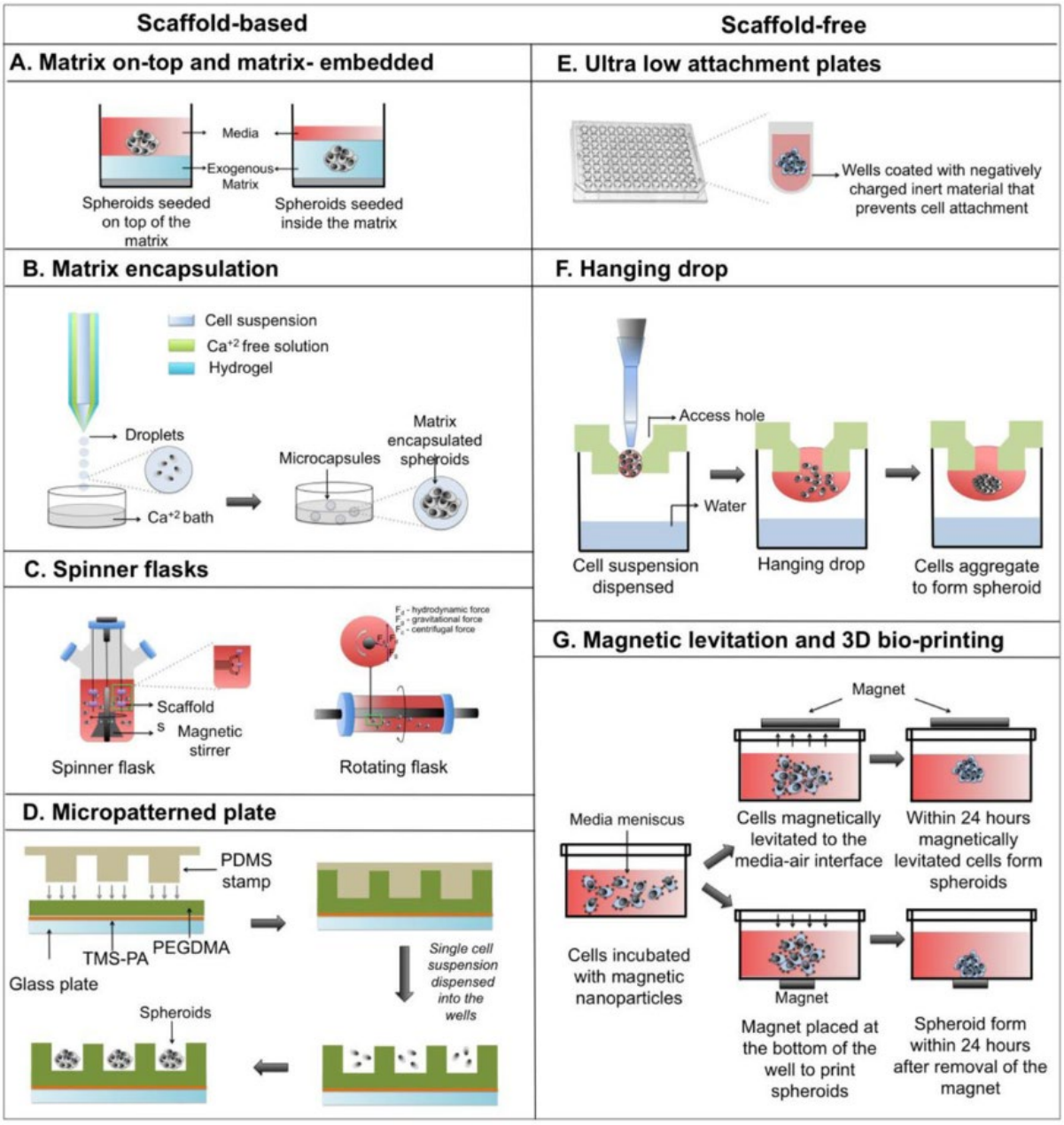

Figure 13: Overview of different technologies for MCTS formation. Reprinted with permission from ref. [154] Copyright 2016 Elsevier.

The key principle of various methodologies for MCTS formation is to provide single cells in suspension with suitable conditions, where the cell-cell adhesion is predominant comparing to cell-substrate adhesion, preventing the adhesion of cells onto the substrate as in traditionally 2D culture systems, but promoting cell aggregation into spherical structure

(Figure 13). Non-adherent conditions can be achieved with substrate-dependent methods (e.g. forced-floating or hanging drop techniques), where ultra-low attachment plates are employed for cell seeding. In this method, the plate are typically superhydrophobic such as poly(2-hydroxy(etheyl methacrylate)[155], or multi-well plates coated with agarose[156]. Depending on the cell type and seeding density, MCTS can be harvested after 1 to 7 days of culture. Apart from the static culture, dynamic technologies utilizing stirring or rotating systems use mechanical forces to keep cell suspension in non-adherent condition. For example, spinner flasks with stirring blades or gyratory shakers can generate dynamic flow to prevent unwanted adhesion.[157] Despite the advantages of dynamic culture in effective and mass production of MCTSs, the size and morphology are hard to control, which leads to problematic and inconsistent responses to downstream anti-tumor analyses. Hence, researchers also combined static and dynamic methods by seeding cells using hanging droplet technique to preform uniform spheroids, then transfer them into a microfluidic system for evaluating fluid dynamics.[158]

Tumor generation *in vivo* heavily relies on their surrounding environment, extracellular matrix (ECM), which provides structural support and signaling functions. As mentioned in the previous chapter, replicating ECM *in vitro* can regulate the behavior of cells in laboratory conditions, thus promoting cells to form MCTS. As in natural ECM mimetics, collagen,[159] gelatin,[160] decellularized matrix,[161] chitosan,[162] and Matrigel[163] were used (Figure 12). Their outstanding biocompatibility and ability to recapitulate cell-ECM interactions allow them to form MCTS efficiently. However, due to the complexity of natural materials, it is difficult to control their physical and biological properties, leading to batch-to-batch differences. On the other hand, synthetic ECM alternatives, such as PEG or PG-based hydrogels or microgels are structurally and chemically defined with tunable properties.[149] They can also be combined with natural materials to achieve a better performance. As an example, Pradhan et al. reported PEG-fibrinogen hydrogel microspheres for long-term 3D culture of MCTS, where emulsion technique was utilized for cancer cell encapsulation. The uniformity in size and morphology is well-controlled and extended cell types were proven to be valid in this well-established tumor microsphere model.[164]

3. Scientific goals

Utilizing the biocompatible and multifunctional properties of polyglycerol family, we aim to unveil more complicated cellular behaviors in the region of the interfaces between cells and materials. By doing this, we took cues from nature, functionalize and decorate the synthetic polymer with desired structures and functions, using it to achieve some simple mimetics of natural environment. This simple mimick of nature offers us insights into cell adhesion, proliferation, and differentiation; bringing us closer to a better understanding of these mysterious cellular processes; pushing beyond the development of technologies that can solve various biomedical problems.

In the first project, I investigated the mussel-inspired polyglycerol (MI-PG) coating materials, in order to understand the effects of functionalities and molecular structures on the adhesive performance and coating characteristics. By solely varying the coating polymers and keep the coating conditions consistent, substrates with different coating characteristics can be obtained. Based on that, we aimed to find suitable applications for this well-tunable coating. Herein, the cell adhesion behavior on substrates with different topographies was addressed, and the potential of MI-PG coatings, serving as potential supporting materials in biointerfaces, was investigated.

Moving from 2D to 3D, my objective for the second project was to develop a system that integrated the state-of-the-art technology in circulating tumor cell studies in our own methods, where the efficient isolation combined with 3D culture for further down-streaming analyses. We aim to tackle the difficulties in the traditional cancer diagnosis and therapy, in which the treatment is invasive and inefficient. By evaluating the CTCs from the patient's blood, an optimal personalized treatment was to be provided with the help of the system.

In order to deepen the understanding of three-dimensional cell cultures, our goal was to design a versatile hydrogel platform with tunable features that could host various types of cancer cell lines, inducing them to grow into multicellular tumor spheroids. These MCTSs are especially valuable in current oncological studies to bridge the insufficient conventional 2D cell culture system and inappropriate *in vivo* animal experiments.

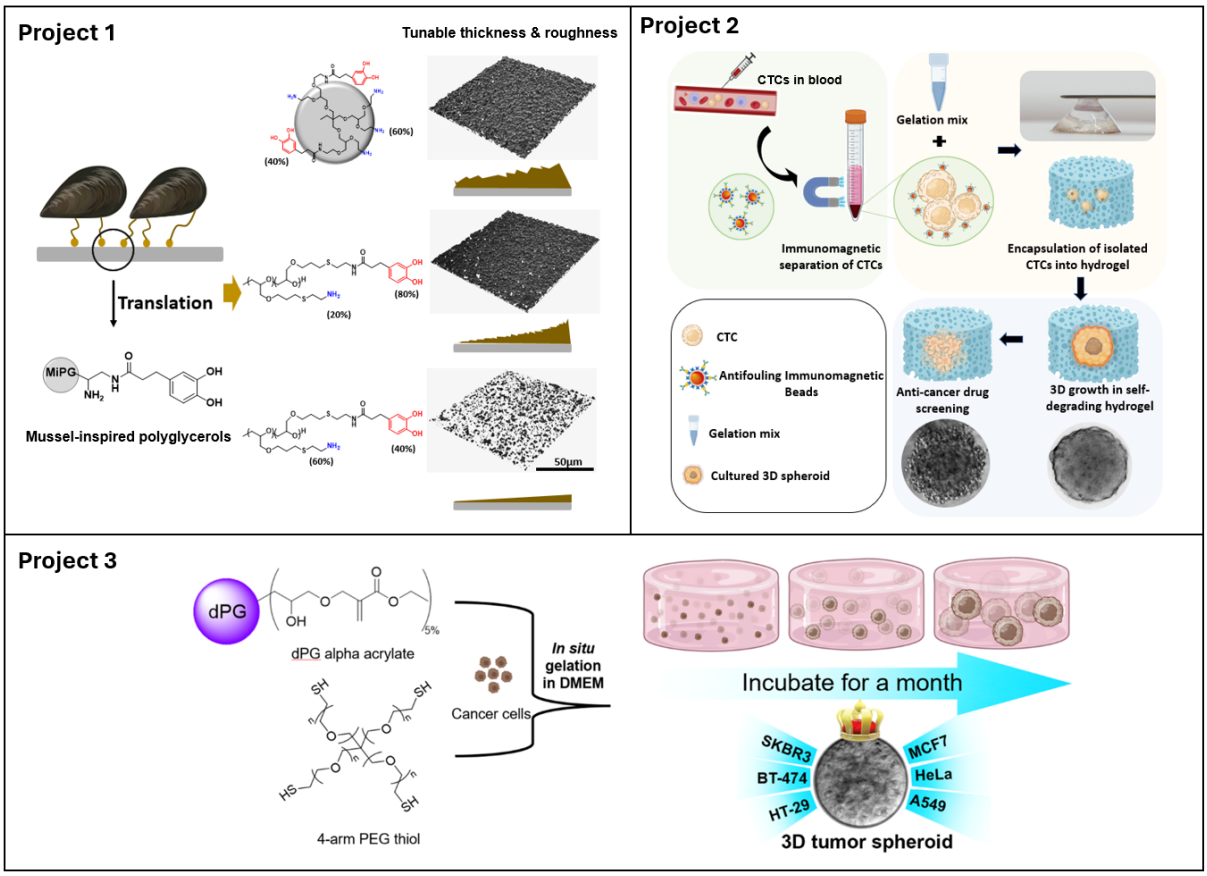

Figure 14: Overview of the projects covered in this thesis. 1) Mussel-inspired polyglycerol coatings for surface modification with tunable architecture. 2) Polyglycerol-based biomedical matrix for immunomagnetic circulating tumor cell isolation and their expansion into tumor spheroids for drug screening. 3) Polyglycerol-based hydrogel as versatile support matrix for 3D multicellular tumor spheroid formation.

4. Publications and manuscripts

In the following section, the published papers are listed and the author contributions are specified.

4.1 Mussel-Inspired Polyglycerol Coatings for Surface Modification with Tunable Architecture

Peng Tang, Guoxin Ma, Philip Nickl, Chuanxiong Nie, Leixiao Yu*, and Rainer Haag*

Advanced Materials and Interfaces **2023**, *10*, 2300165.

https://doi.org/10.1002/admi.202300165

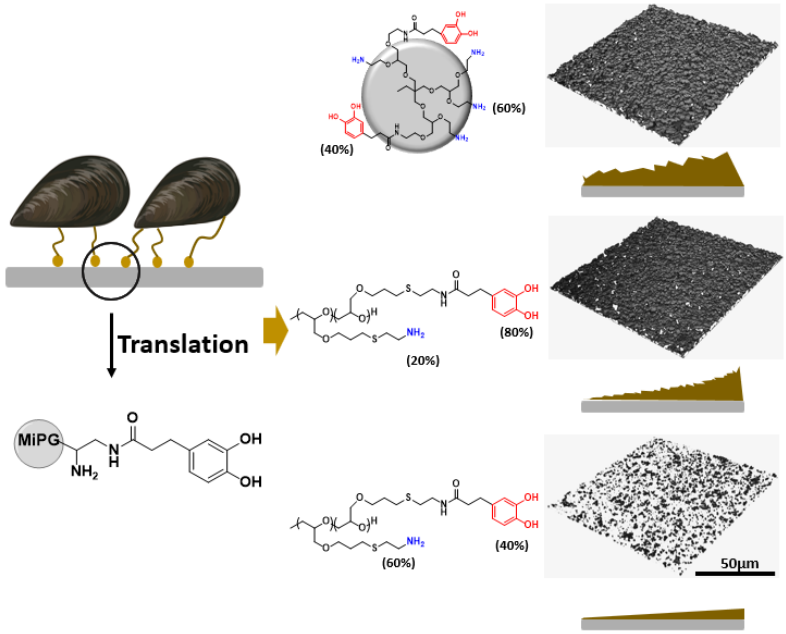

Figure 15: Graphical abstract of project 1. Reprinted with permission from ref.[165]. Copyright 2023 Wiley-VCH.

Contributions of authors: In this publication, Peng Tang performed most of the synthesis and characterizations, wrote the manuscript, and took charge of all revision procedures. Guoxin Ma helped with the functionalization of MiPG. Philip Nickl measured XPS for the samples and Chuanxiong Nie helped with the measurement of confocal microscopy. Leixiao Yu and Rainer Haag supervised the project, offered scientific ideas and suggestions as well as proofread the manuscript.

ADVANCED MATERIALS INTERFACES
Open Access
www.advmatinterfaces.de

Mussel-Inspired Polyglycerol Coatings for Surface Modification with Tunable Architecture

Peng Tang, Guoxin Ma, Philip Nickl, Chuanxiong Nie, Leixiao Yu, and Rainer Haag**

Mussel-inspired coatings, known for their outstanding substrate-independent adhesive capabilities, have numerous potential applications in materials science and biomedical fields. To improve the understanding of how these polymers' molecular structure and chemical composition affect their coating mechanisms and resulting coating properties, herein three mussel-inspired polymers are developed: dendritic polyglycerol with 40% catechol groups and 60% amines (dPG40), linear polyglycerol with 80% catechols and 20% amines (lPG80), and finally lPG40 with 40% catechols and 60% amines. After a series of characterizations, it is found that chemical surface modification with a monolayer coating can be easily achieved with lPG40, and that robust and well-defined nano- to micro-structural surface coatings are possible with lPG80 and dPG40. Tunable properties are found to include not only coating speed, but coating thickness, roughness, and surficial topography. This diverse suite of controllable attributes enables mussel-inspired polyglycerol (MiPG) coatings to satisfy a wide-range of applications on multiple materials.

1. Introduction

In the past decades, many surface modification techniques, including chemical vapor deposition (CAD),[1] self-assembly of monolayer coating (SAM),[2] spin-coating,[3] surface grafting to/from chemistry,[4] have been developed and successfully used to endow materials with different chemical, physical and biological properties to extend their application.[5] Compared to traditional chemical modification, increasing evidence suggests that the construction of well-defined nanostructures and/or microstructures on the surface of biomaterials and biomedical devices, such as dental implants,[6] orthopaedic implants,[7] and artificial hips,[8] can play a vital role in regulating cell activities and functions, particularly in the domain of tissue engineering. The native extracellular matrix (ECM) is a macromolecular network complex that possesses a microscale and nanoscale hierarchical structure to mediate many aspects of cell behavior including cell adhesion, growth, proliferation, differentiation, and immune response.[9] In that sense, ECM-mimicking biomaterials with nanostructural or microstructural surfaces are exceptionally appealing in cellular studies. Hou et al. engineered hydrogels with different stiffness and roughness to investigate the cellular mechano-response of stem cells and induce osteogenesis of MSC.[10] Evidence shows that the tailored nano-structural surface coatings can also greatly enhance the capture efficiency of biochips toward circulating cancer cells.[11] Clinically, micro- to nanoscale topographies on dental implants were extensively used to improve osseointegration.[6] Therefore, versatile methods, e.g. stereolithography (SLA),[12,13] chemical etching,[14] electrospinning,[15] and polymer coatings,[16] were developed to engineer various micro/nano-structures, including nanorods,[17] nanopillars,[18] and nanofibers,[19] to meet the requirements of different applications. However, SLA and chemical etching face the problems of multiple-step processes and strict conditions. Moreover, most polymer coatings require reactive moieties between the biomedical devices and polymers, limiting both the choice and applications of biomaterials use. Developing a method that is simple and substrate-independent is therefore especially intriguing and promising.

Benefiting from the abundant amine groups (lysine) and catechol groups (3,4-dihydroxyl-L-phenylalanine, in the mussel foot proteins (mfps, e.g. 15% mol% for mfps-1 and 28% mol% for mpfs-5[20]), mussels can adhere and quickly form strong surface-adherent protein films on virtually any material's surface through their mfp-rich byssus.[21] Dopamine, containing both the catechol and amino groups, was used as the first generation of mussel-inspired building blocks for surface coating. The resulting polydopamine (PDA) films were found capable of adhering to almost all kinds of solid surfaces.[22] However, the coating process took up to tens of hours to achieve a very thin PDA layer (≈50 nm

P. Tang, G. Ma, P. Nickl, C. Nie, R. Haag
Institute for Chemistry and Biochemistry
Freie Universität Berlin
Takustraße 3, 14195 Berlin, Germany
E-mail: haag@chemie.fu-berlin.de
L. Yu
State Key Laboratory of Oral Diseases
West China Hospital of Stomatology
Sichuan University
Chengdu, Sichuan 610041, China
E-mail: leixiaoyu@scu.edu.cn

The ORCID identification number(s) for the author(s) of this article can be found under https://doi.org/10.1002/admi.202300165

DOI: 10.1002/admi.202300165

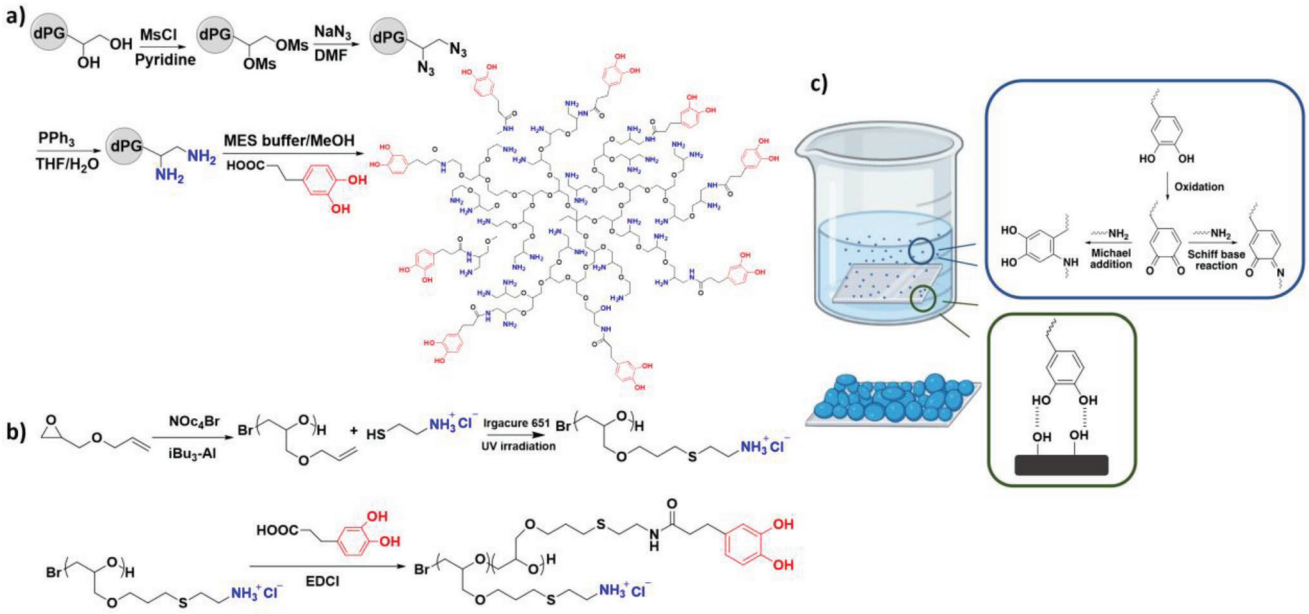

Figure 1. Mussel-inspired polyglycerol polymers. a) Structure of dPG40 with 40% catechol and 60% amino groups. b) Structure of catecholic lPG polymers. c) MiPG coating is achieved by dip-coating method under basic conditions. Polymer aggregates adsorb to substrates and bond tightly via hydrogen bond (with glass substrates). Possible reactions involved in the process of MiPG coating are indicated in the box.

in thickness) with limited surface structures. To accelerate the self-polymerization of dopamine, many methods, for example oxidants,[23] catalysts,[24] UV irradiation,[25] and microwave,[22] were used to promote the involved reaction kinetics including Michael addition, Schiff base reaction, and oxidative coupling.[26] In spite of improved coating processes, it is still hard to obtain well-defined surface structures, especially microstructures via polydopamine coatings. Mimicking the molecular structure of mussel foot proteins, we previously developed several heteromultivalent catecholic polymers.[11,16] Many coatings and surficial structures have been thereby achieved through those building blocks. However, the relationship between the polymeric molecular structures and the resulting nano-/microscale coating structures had not yet been fully understood, which is essential for the design of coating polymers and fabrication of topographical structures.

Herein, three MiPGs with different polymer conformation and catechol functionality, i.e., mussel-inspired dendritic polyglycerol with 40% catechol groups (dPG40), and mussel-inspired linear polyglycerol with 80% and 40% of catechol groups (lPG80 and lPG40) were synthesized to understand the underlying reaction processes and establish relationship between the molecular structure and chemical composition of a coating polymer with the obtained surficial topographic structures. By tuning various parameters, the toolbox that we offer here, consisting of mussel-inspired polyglycerol building blocks, can be developed further to study surface coatings with well-defined structures from nanoscale to microscale. This can extend the scope of their biomedical applications, e.g. implant surface modification, medical device surface design, and pre-surgery treatment, as well as potential application in regenerative medicine.

2. Results & Discussion

2.1. Mussel-Inspired Polyglycerol Coating Polymers

To explore how the catechol/amine content and the polymer chain conformation affect the coating process and the obtained coating surficial structures, three mussel-inspired polyglycerol coating polymers (MiPGs), i.e., dendritic polyglycerol with 40% catechol and 60% amino groups (dPG40), linear polyglycerol with 80% catechol and 20% amino groups (lPG80), and linear polyglycerol with 40% catechol and 60% amino groups (lPG40) were prepared based on our previous synthesis protocols.[11,27] The dPG40 was obtained by modifying dendritic polyglycerol (M_n = 5180 g mol^{-1}, M_w = 7120 g mol^{-1}, D = 1.37), through amination and amide coupling with 3-(3,4-dihydroxyphenyl)-2-hydroxypropanoic acid (DHHA) under acidic condition, nearly 40% catechol groups functionalization were achieved, with 60% free amines (**Figure 1**a). To prepare the lPG80 and lPG40, poly(allyl glycidyl ether) (PAGE) was first synthesized via ring opening anionic polymerization, followed respectively by thiol-ene and amide coupling reactions (Figure 1b). The degree of catechol grafting densities was controlled by tuning the equivalent relation between DHHA and amino groups from the polymer chain. The obtained lPG40 was characterized by FTIR and NMR (Figure S2, Supporting Information). The adsorption peak at the wavelength of 1518 (cm^{-2}) on the FTIR diagram was assigned to the amide bond, which suggests the successful coupling of catechol groups (Figure S1, Supporting Information). The ^{1}H NMR characteristic peak for the aromatic ring of catechol confirms the successful functionalization. Moreover, the integrals of peaks for catechol and cysteamine allowed us to calculate the functionalization of catechol groups (47% and 83%

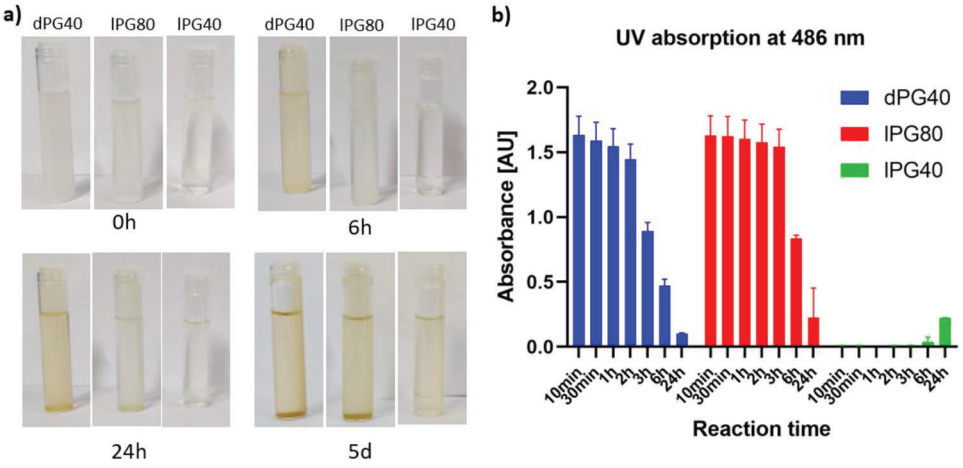

Figure 2. a) Photos of coating solutions after different incubation times (from left to right: dPG40, lPG80, and lPG40). b) UV absorption of coating solutions at wavelength of 486 nm.

of catechol functionalization in lPG40 and lPG80 was achieved, respectively, Figures S2 and S3, Supporting Information).

In mussel adhesion, the catechol group serves as the anchoring domain while amines offer sites for intra- or intermolecular crosslinking. The interplay of catecholic oxidation and amine-induced crosslinking forms a stable and robust network, which contributes to strong adhesion.[28] Under basic conditions, MiPG polymers may undergo vigorous oxidation and covalent crosslinking. Investigation of the reaction rate or coating kinetic guides us to a better understanding of our three MiPG polymers. All three polymers were pre-dissolved in methanol (20 mg polymer in 15 mL, 1.3 mg mL^{-1}), and then 5 mL base aqueous buffer (MOPS buffer, pH = 8.5) was added to form the coating polymer solution (1 mg mL^{-1} in methanol/MOPS buffer solution). The dPG40 and lPG80 solutions immediately turned cloudy after the base buffer addition. However, for lPG40, no obvious change was observed (**Figure 2**a). Meanwhile, due to the exothermic manner of catechol oxidation,[28] dPG40 displayed the most heat release, accompanied by air bubbles in solution. For lPG80 the heat release was less intense, while for lPG40 only extremely small temperature changes were detected. In the coating solution (methanol/MOPS buffer, 3v/1v), the catechol groups underwent immediate oxidation to quinone. Nucleophilic addition then occurred between the amine and quinone, forming quinone-amine adducts. In the meantime, a Schiff-base reaction took place between amine and quinone to yield imine. These reactions contributed to the crosslinking of the polymer.[26,29] The obtained highly crosslinked polymer microgel-like aggregates were insoluble in the coating solution and subsequently precipitated. In the case of dPG40 and lPG80, these aggregates grew larger and then bonded tightly to the bottom of the vials with incubation. After the thorough consumption of polymer, the solution was clarified again, and a thick polymer layer was found at the bottom of the vial (Figure 2). For lPG40, the polymer solution remained clear for days, as expected for this significantly milder reaction. UV–vis spectra were performed to analyze the reactions. The absorption at the wavelength of 486 nm was ascribed to the polymer aggregates formed in the solution. The change in the absorbance at 486 nm allowed us to investigate the reaction kinetics of these coating polymers under base condition. In Figure 2b, both dPG40 and lPG80 showed strong absorption because of the immediate occurrence of the aggregates (≈1.78 AU), while no obvious absorption was observed for lPG40. Besides, a drastic decrease at 3 h for dPG40 (from 1.78 to 0.96 AU) suggests the rapid precipitation of polymer aggregates from solution, indicating a faster reaction rate than lPG80. After 24 h, both dPG40 and lPG80 solution became clear and showed very low UV–vis absorption, while an increase in lPG40 was found (up to 0.22 AU), proving that the slow reaction of lPG40 under the same condition.

2.2. MiPG Coating with Well-Defined Surface Structures

Mussel-inspired coating polymers are well-known as universal coatings that can form stable coating layers on various substrates, such as TiO_2, PS (polystyrene), and glass, via coordinative and/or hydrogen bonding depending on the substrate (Figure 1c).[30] Here we used glass substrates (1 cm × 1 cm), on which MiPG coatings were formed via simple dip-coating method at room temperature.

As mentioned before, insoluble polymer aggregates formed after incubation under basic conditions, then precipitated and attached to the substrate to achieve a coating layer. These aggregates adhered tightly to the surfaces of glass slides via hydrogen bonding. By controlling the coating time, these three different polymers formed coatings with different thickness and topographical features. As seen in **Figure 3**a, a thin and translucent layer was quickly formed on the glass slides, and a yellow and opaque layer was observed with increasing incubation time. Shorter times taken to form a thick opaque coating indicated faster coating kinetic. The transmittance of the resulting coatings was measured by UV–vis spectrometry. A drastic decrease in the transmittance of the dPG40 coating surface was observed within one hour of dip-coating. In comparison, for lPG80 transmittance dropped below 10% after 3 h. No significant decrease was observed for lPG40, even after 48 h (Figure 3b). This result agreed with our observations of the polymer solution and suggests that dPG40 was more reactive and formed a coating more

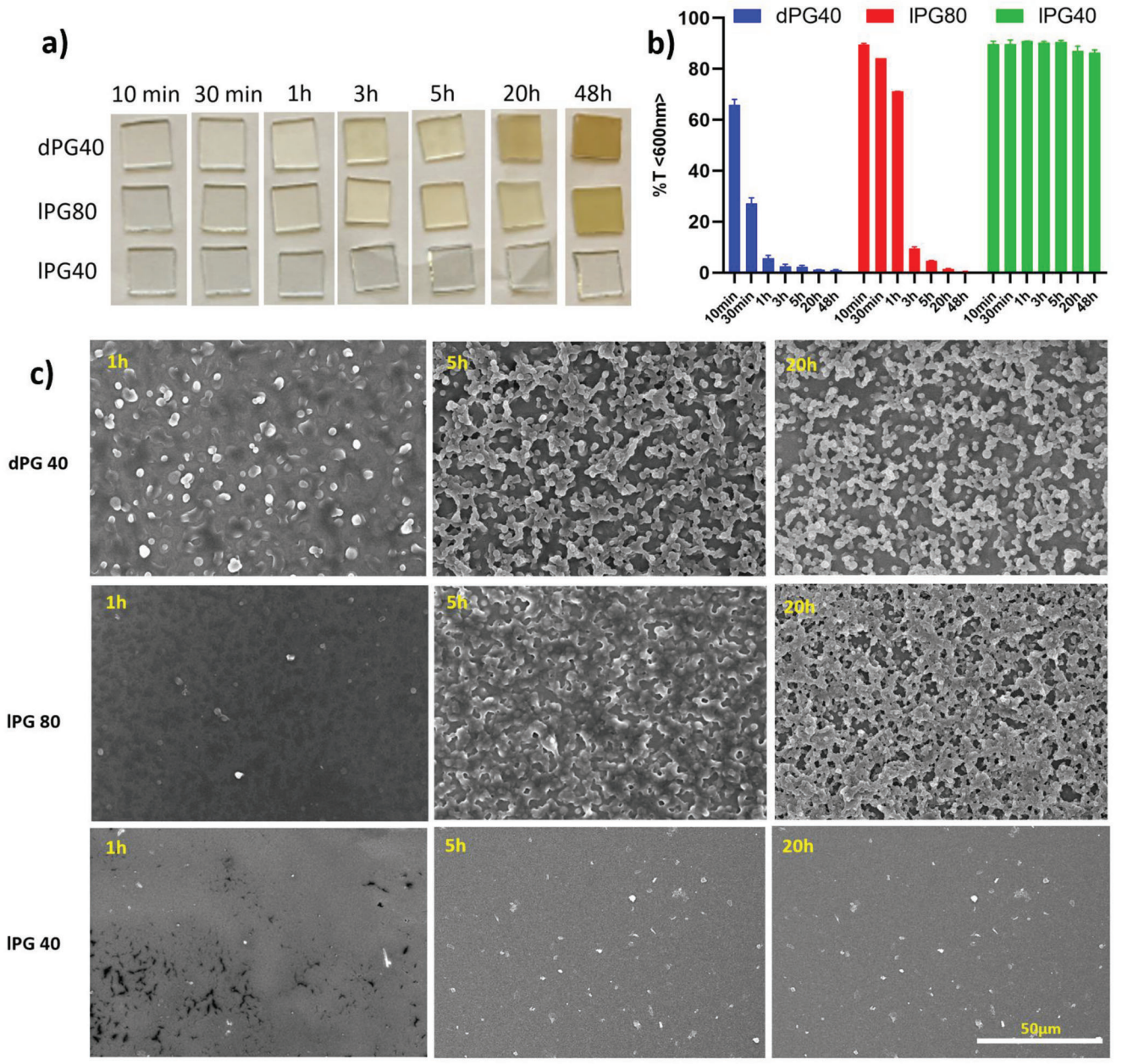

Figure 3. a) Pictures of dPG40, lPG80, and lPG40 coatings on glass substrates with different incubation times. b) Transmittance of dPG40, lPG80, and lPG40 coated glass substrates measured by UV–vis spectrometry. c) SEM images of dPG40, lPG80, and lPG40 coatings with different incubation time. The scale bar indicates 50 μm.

rapidly than the other two polymers. In comparison, lPG80 displayed similar results to dPG40 with a relatively longer incubation time, while lPG40 showed barely any evidence of thick coating layers. The dendritic structure is renowned for its potential to provide a multivalent adhesion system, thus providing multiple sites for crosslinking and greatly enhancing reaction efficiency as compared to the linear structure. On the other hand, owing to the manner of the reaction mechanism, the oxidation of catechol groups is the main factor in determining reaction speed, because only the presence of oxidized catechols can effectively crosslink the quinones and amines. Hence, a higher content of catechol groups results in a faster coating process. Despite the higher catechol content in lPG80, dPG40 still showed a faster coating process. This can be attributed to the linear chain structure of lPG80. In a linear polymer solution, one would expect a greater degree of possible entanglement and a larger hydrodynamic volume, both of which would hinder reactivity during the coating process.

After formation of aggregates in a coating solution, aggregates would accumulate on the substrate, resulting in certain architectures on the coating surfaces. The surface topology is supposedly determined by the size of aggregates and how they come together to form the coating layer. The surface structures of the coatings

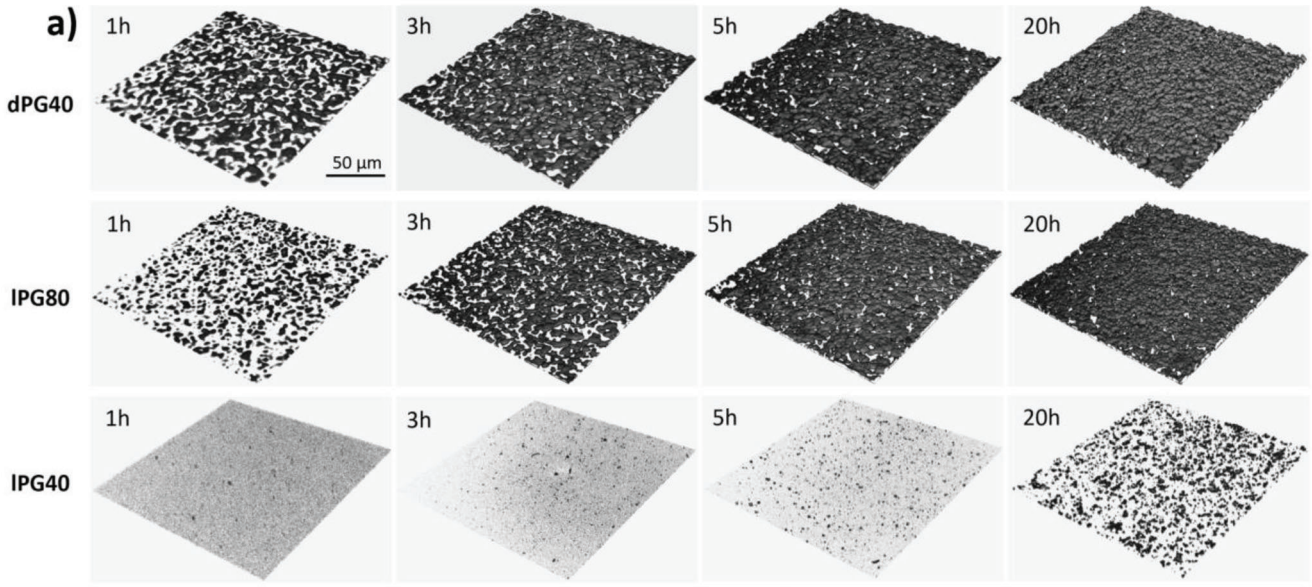

b)

Coating time	Thickness (μm)			Roughness (Rq in μm)		
	dPG40	lPG80	lPG40	dPG40	lPG80	lPG40
3h	4.75 ± 0.39	3.73 ± 0.40	0.55 ± 0.07	1.62 ± 0.12	1.54 ± 0.14	0.02 ± 0.01
5h	5.83 ± 0.42	4.74 ± 0.47	1.00 ± 0.14	1.89 ± 0.23	2.64 ± 0.16	0.04 ± 0.01
20h	7.08 ± 0.61	6.75 ± 0.29	1.87 ± 0.29	2.87 ± 0.18	3.18 ± 0.25	0.32 ± 0.03

Figure 4. a) 3D-model of MiPG coating layer detected by CLSM. b) Summary of the thickness and roughness (Rq, root mean square) of dPG40, lPG80, and lPG40 coating surfaces.

were detected by SEM. As shown in Figure 3c, the biggest aggregates were found in dPG40-coated samples. The size of the generated aggregates decreased from 2.84 ± 0.82 μm (1 h) to 2.41 ± 0.57 μm (5 h), then reached 2.17 ± 0.63 μm (20 h). The decrease in size with incubation time is explained by the consumption of the polymers in solution as the polymer concentration decreases with time. While smaller sizes of aggregates formed on lPG80, which decrease from 1.77 ± 0.33 μm (5 h) to 1.51 ± 0.25 μm (20 h). As results indicated above, dPG40 is the most reactive coating polymer compared with the other two. Under basic conditions, it is prone to a fast oxidation and crosslinking reaction, quickly generating aggregates in the solution, depositing onto the substrate surface and self-growing from the substrate surface. Because of the entanglement polymer conformation, the less reactive lPG40 slowly crosslinked and formed a comparatively smooth monolayer coating with smaller surficial structures.

Due to the detection limitation of AFM (atomic force microscope), it was very challenging to image a surface structure with high roughness (Rq > 1.5 μm).[31] Therefore, confocal laser scanning microscope (CLSM) was used to analyze topographical structures of these coating surfaces. CLSM can be implemented as an alternative to AFM benefiting from the autofluorescent nature of the eumelanin structure on MiPG coating surface.[32] 3D models of the coating layer were reconstructed by z-stacking scanning (Figure S8, Supporting Information). The coating thickness was measured from the z-stacking of the 3D models and the surface roughness was analysed and calculated through ImageJ with the RoughnessCalculation Plugin. The resulting roughness values were presented as root mean square (Rq in μm). As shown in **Figure 4**b, dPG40 yielded thicker coating in a relatively short time (4.75 μm at 3 h to 7.08 μm at 20 h). While lPG80 needed more time to form comparable thickness (3.73 μm at 3 h to 6.75 μm at 20 h) compared to dPG40. Moreover, the dPG40 surfaces were rougher than lPG80 (1.62 μm and 1.54 μm, respectively) due to the faster formation of the coating layer. However, as the coating process continued, the roughness of the lPG80 layer (Rq = 2.64 μm at 5 h) surpassed that of dPG40 (Rq = 1.89 μm), reaching 3.18 μm after 20 h in comparison to and 2.87 μm for dPG40. As discussed before, smaller aggregates are formed when the polymer concentration is lower in lPG80, the piling up of smaller aggregates increased the gap between peaks and valleys the roughness profile, yielding higher roughness parameter value. As for lPG40, the thickness and roughness were difficult to be measured using this method since only very thin layers of polymer films can be formed, causing barely no changes on the glass surface.

Wettability of a surface is dependent not only on the surficial chemical composition but also on the physical structures. Roughness plays an important role in surface static contact angle.[33] In the measurements, although the MiPG polymer is hydrophilic, higher contact angle values were obtained with the increase of the roughness parameters (**Figure 5**). The water contact angle of lPG80 increased from 31° ± 1.7° (10 min) to 52.3° ± 2.3° (5 h). We assume water droplets wetted the surfaces as predicted by

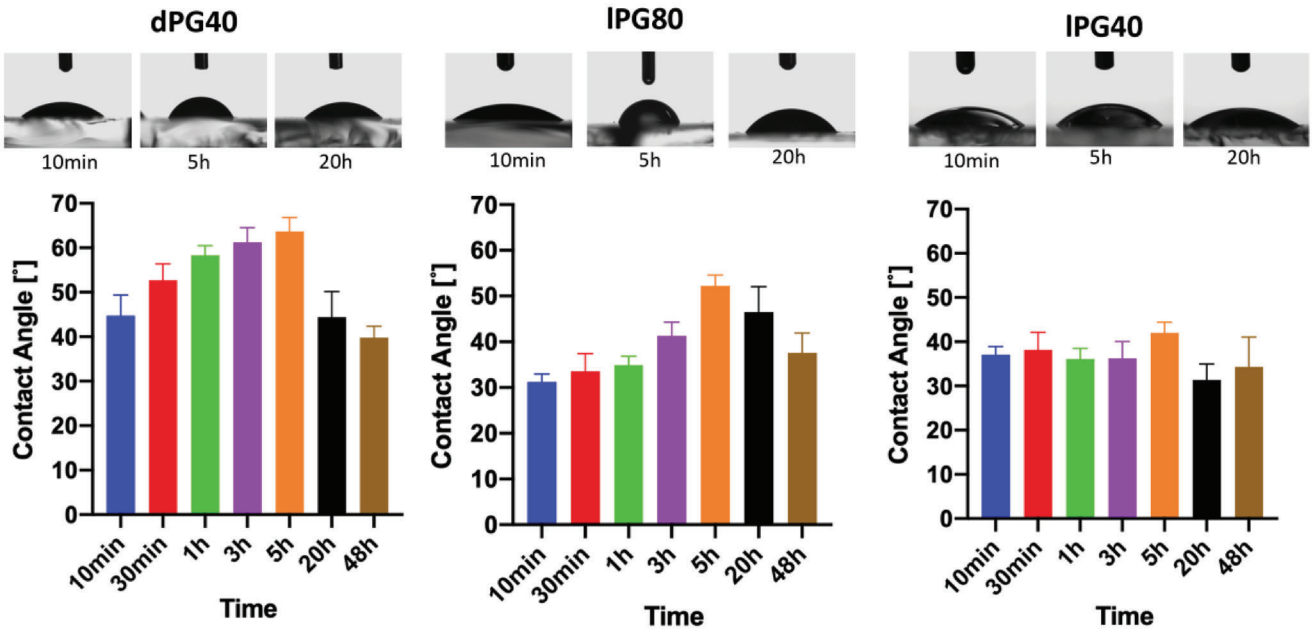

Figure 5. Wettability of dPG40, lPG80, and lPG40 coating surfaces.

the Cassie-Baxter model, where higher roughness contributes to higher hydrophobicity, as more air can be trapped in the grooves during inhomogeneous wetting.[34] However, a decrease in contact angle values was observed in both dPG40 and lPG80 (20 h and 48 h). This can be explained by the fact that after the roughness exceeds a certain value, the grooves become big enough and the water molecules can easily spread within the surficial structures, resulting in lower contact angle values (37.6° ± 4.3° for lPG80, 48 h and 39.8° ± 2.5° for dPG40, 48 h).

XPS was used to characterize the chemical compositions of the MiPG coated surface. In the deconvoluted C-1s spectra, similar chemical compositions were observed for all materials, confirming the successful surface coating with MiPG polymer (**Figure 6**). The chemical composition of the surface coating remained unchanged even after a long period of incubation in the coating solution, demonstrating the stability of this coating surface in aqueous solution. Besides, the chemical compositions of the surface coatings, also the elemental compositions were studied (Figure S7, Supporting Information). The absence of sulphur in dPG40 and the presence of that in lPG80 and lPG40 are explained by the addition of cysteamine during synthesis, some residue of sulphur in dPG40_20 h could be explained by the long incubation time in coating solution which containing MOPS buffer. In contrast to confocal microscopy, where no coating with lPG40 was apparent, the successful chemical functoinalization of glass substrates with lPG40 could be confirmed by XPS, where highly resolved C1s spectrum revealed the chemical composition of the polymer.

2.3. Cell Adhesion on Nanostructured Coated Surfaces

It has been proven that specific nanostructures can enhance cell adhesion as the nanostructured surfaces offer ECM-mimicking morphology, promoting the formation of cellular focal adhesions (FA) and filopodia.[35,11] Controlled interaction between cell and nanostructured substrates enables applications such as control of cell adhesion and detachment, rare cell detection, and regulating stem cell specification.[36,37,9a,b] MiPG polymers have the advantage of forming a well-defined coating with customizable roughness, making it facile to find an optimized structure for cell adhesion.

In this study, we chose human breast cancer cells (MCF-7) as a model cell line to study cell-substrate interaction. As shown in **Figure 7**a and Figure 7b, MCF-7 cells preferentially adhere on the dPG40 surface with roughness at ≈2 µm in Rq, as compared to surfaces with lower or higher surficial roughness values. A similar phenomenon was observed on lPG80 surfaces. However, after optimal surface roughness was reached, substrates with higher roughness impeded the adhesion and spreading of MCF-7 cells. This result was further confirmed by single-cell imaging with SEM. After 3 h of incubation, the adhered cells were fixed and observed. A larger cell spreading area indicated better cell adhesion behavior.[38] The result from SEM was in line with the conclusion we drew from fluorescence microscopy (Figure 7c). A given cell line, due to its particular size and shape, will display a surface-structure-dependent behavior toward the MiPG coated surfaces, which indicates the potential of our coating materials with tunable architectures in biomedical applications.

3. Conclusion

To realize simple and versatile solid surface functionalization with defined nano- and micro-structures for biomedical applications, we designed three mussel-inspired polyglycerol-based coatings with different molecular structures and chemical composition. We then studied their polymer solution, coating processes, and corresponding coated surfaces. It was found that dPG40 can

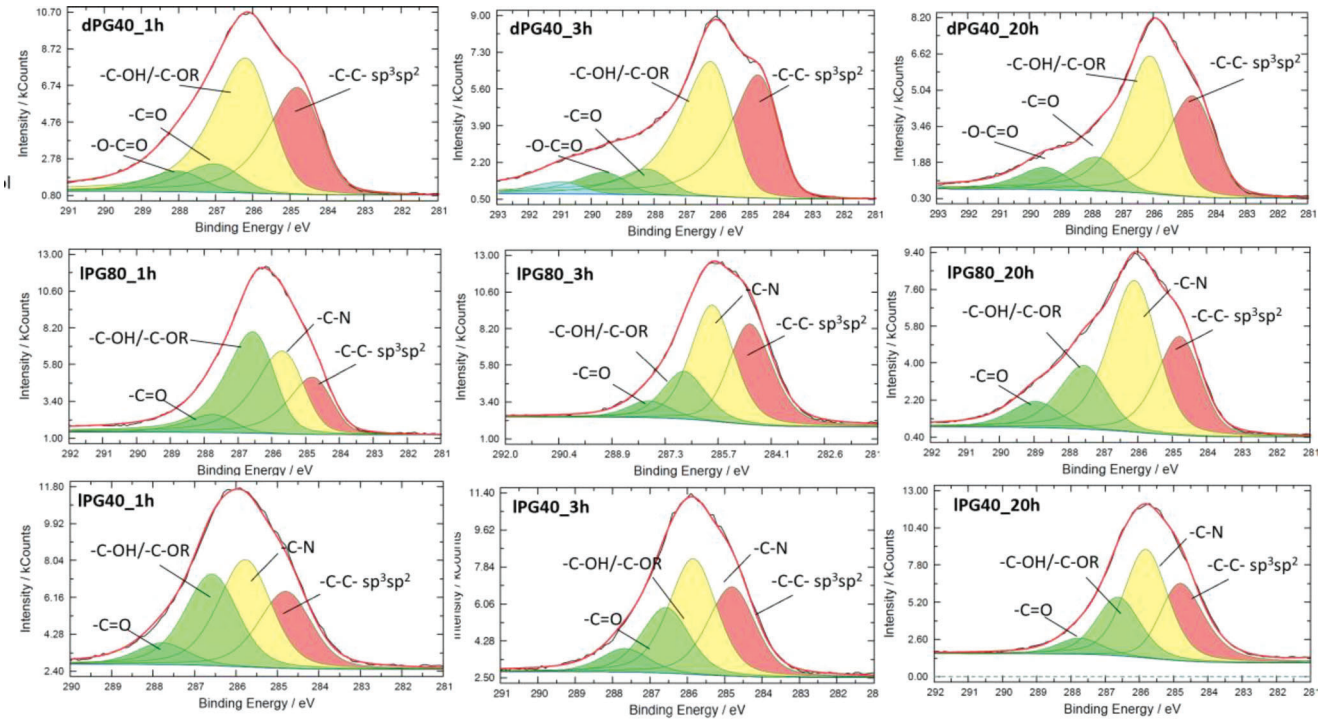

Figure 6. The deconvoluted highly resolved C1s XP spectra of the resulting dPG40, lPG80, and lPG40 coating surfaces.

achieve effective thick coating within one hour despite lower catecholic content in its polymeric chain, yielding a robust, stable hydrogel-like coating layer with a thickness of up to 7 microns. In comparison, the linear structure of lPG80 slowed the reaction due to molecular chain entanglements and a larger hydrodynamic diameter. This decelerated coating process made the resultant coating more controllable than dPG40. Owing to its slower coating process, lPG80 can form coatings with a wider range of roughness (1.54 – 3.18 µm, Rq). This type of coating polymer is therefore especially suitable for fabricating nano and micro-structured surfaces and for application to cell study. Last but not least, although lPG40 could not easily form a measurably thick coating layer, monolayer functionalization was confirmed by XPS. Suggested applications for lPG40 might therefore include only chemical functionalization for further modification, rather than topographical alternation. We investigated the versatility of mussel-inspired polyglycerol coating and demonstrated examples of biological application, and the potential of this type of coating polymer can be suitable for cellular biointerfaces.

4. Experimental Section

Materials and Methods: All chemicals and solvents were used directly without any further purification unless pointed out individually. Dialysis was done in benzoylated cellulose tubes (molecular weight cut-off 2000 g mol^{-1}, Sigma-Aldrich). ^{1}H-NMR spectra were recorded on a Bruker AC 400 under 400 MHz. Analytes were dissolved corresponding deuterated solvents at concentration of ≈20 mg mL^{-1}. Gel permeation chromatography (GPC) measurements were performed on Agilent 1250 series instrument. Molecular weight and distribution were determined by the calibration with standards.

Synthesis of Mussel-Inspired Polyglycerol 40 (dPG40): Dendritic polymer was synthesized according to previous protocol with some modifications.[27a] In brief, dendritic polyglycerol (dPG-OH, M_n = 3816 g mol^{-1}, M_w = 5813 g mol^{-1}, D = 1.52) was functionalized through mesylation, azidation, and reduction. Unlike the previous reported method, where the catechol groups were protected by acetal then deprotected after coupling,[27a] the process was simplified by directly amide coupling with amine and 3-(3,4-dihydroxyphenyl)-2-hydroxypropanoic acid (DHHA) under acidic condition (2-(N-morpholino)ethanesulfonic acid buffer, pH = 5). ^{1}H-NMR (400 MHz, Methanol-d3) δ = 6.65 – 6.46 (m, Ar), 4.02 – 3.05 (m, PG-backbone), 2.72 (m, -COCH$_2$CH$_2$C-), 2.41 (m, -COCH$_2$CH$_2$-).

Synthesis of Poly(allyl glycidyl ether) (PAGE): The PAGE was synthesized through anionic polymerization reaction under argon atmosphere and exclusion of moisture. A Schlenk flask was completely dried, then tetra-n-octylammonium bromide (NOc_4Br 1 g, 1.92 mmol) was added to the flask and dried at in 120 °C for 3 h under vacuum to remove the trace of water. After cooling down to room temperature, dry toluene (30 mL) was added to dissolve the initiator. Afterwards, allyl glycidyl ether (10 mL, 84 mmol) was added, followed by the slow addition of catalyst triisobutylaluminum (6.97 mL, 7.6 mmol) under 0 °C with ice/water bath and then the mixture was stirred overnight. 1 mL of H_2O was added to quench the reaction. The solvent was dried with sodium sulfate then evaporated by rotary distillation. Later diethylene ether was added to precipitate the initiator residues and catalyst and the solvent was removed by evaporation. Further purification was performed by dialysis in dichloromethane (DCM) for 2 days. M_n = 5796 g mol^{-1} ^{1}H-NMR (400 MHz, Chloroform-d) δ = 5.98 – 5.77 (1H, CH_2-O-CH_2-CH = CH_2), 5.32 – 5.05 (2H, CH_2-O-CH_2-CH = CH_2), 3.97 (2H, CH_2-O-CH_2-CH = CH_2), 3.77 – 3.34 (7H, PG-backbone). IR: ν (cm^{-1}) = 3357, 2871, 2101, 1646, 1456, 1350, 1264, 1066, 921, 875.

Thiol-Ene Reaction of PAGE: PAGE was dissolved in THF/MeOH (1:1). Then cysteamine hydrochloride (4 g, 35 mmol, 4 eq. to allyl groups) and 2-2-dimethoxy-2-phenylacetophenone (Irgacure 651, 0.045 g, 2% eqv. to allyl groups) were added to the mixture. The reaction was carried out under UV radiation (≈1.2 mW cm^{-2}, λ = 365 nm) at room temperature. The reaction

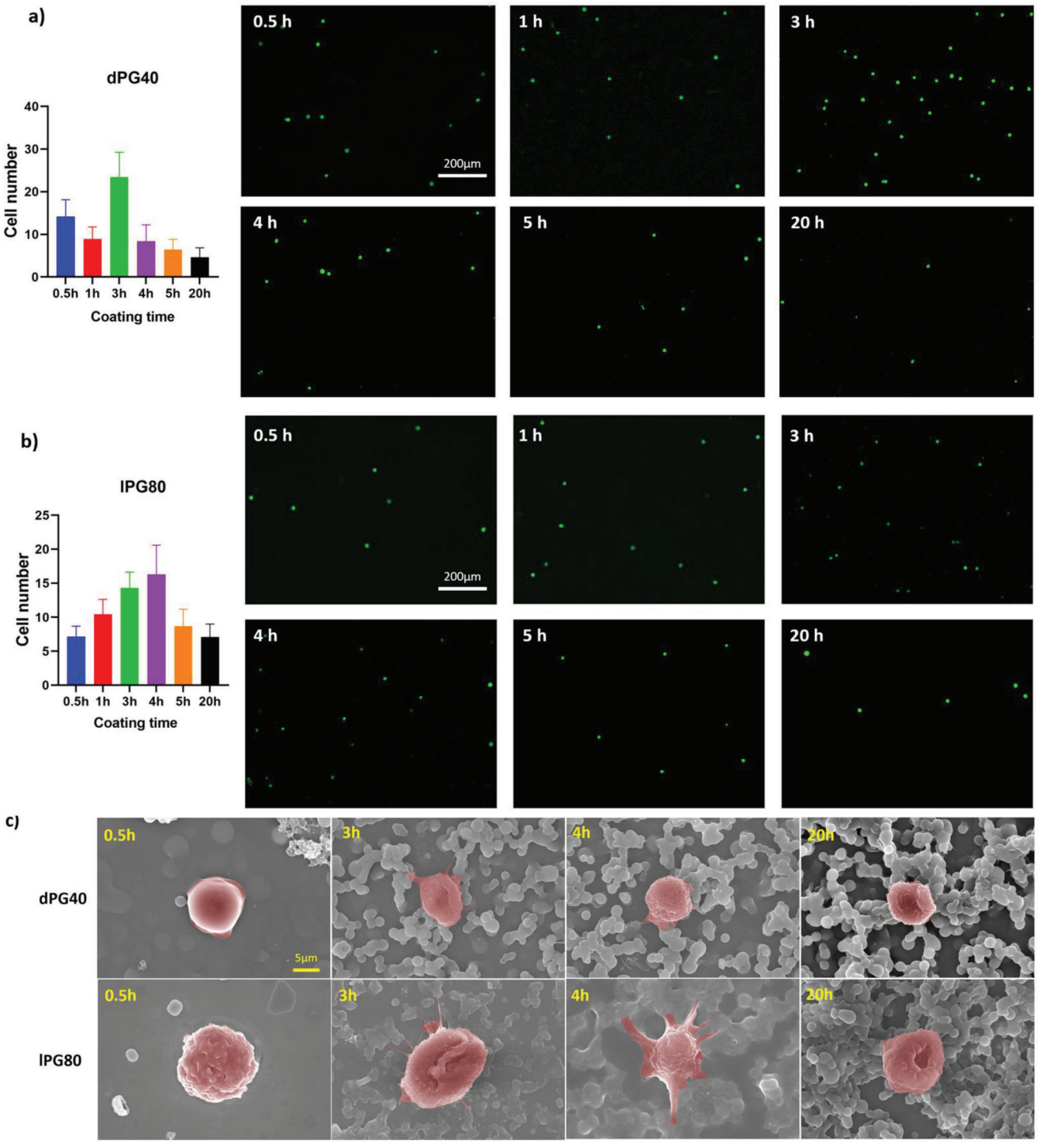

Figure 7. Cell adhesion on MiPG coating surfaces. a) Cells spiked on dPG40 surface; b) Cells spiked on IPG80 surface. MCF-7 cells were spiked and incubated for 3 h before washing with PBS buffer. The remaining stained cells were counted with ImageJ. c) Single-cell morphology characterized by SEM, with larger cell spreading area indicating better cell-substrate interaction.

was monitored by ^{1}H-NMR and finished in around 10 hours. Afterwards, the product was purified by dialysis in methanol.

^{1}H-NMR (400 MHz, Deuterium Oxide) δ = 3.87 – 3.49 (8H, PG-backbone), 3.24 (2H, CH_2-S-CH_2-CH_2-N), 2.88 (2H, CH_2-S-CH_2-CH_2-N), 2.68 (2H, CH_2-O-CH_2-CH_2-CH_2-S), 1.91 (2H, CH_2-O-CH_2-CH_2-CH_2-S). IR: ν (cm^{-1}) = 3410, 2862, 2008, 1599, 1479, 1374, 1261, 1108, 932, 887.

Synthesis of Mussel-Inspired Linear Polyglycerol 40 and 80 (lPG40 and lPG80): The catecholic coating polymers were prepared by coupling amino groups from polymer and carboxyl groups from 3,4-dihydroxyhydrocinnamic acid (DHHA). Polymer and 1-Ethyl-3-(3-dimethylaminopropyl) carbodiimide hydrochloride (EDCI, 6 eq. to amino groups) were dissolved into pH 5 MES buffer/methanol (1/1, v/v) mixture solvent. Afterwards, 3,4-dihdroxyhydrocinnamic acid (1.2 eq. to amino groups) was added into the mixture and gently stirred overnight at room temperature. Purification was conducted by dialysis in methanol. ^{1}H-NMR (400 MHz, Methanol-d4) δ = 6.73 – 6.45 (1H, Ar-H), 3.83 – 3.38 (10H, PG-backbone), 3.01 – 2.69 (3H, S-CH_2-CH_2-N), 2.68 – 2.46 (3H, O-CH_2-CH_2-CH_2-S), 1.94-1.66 (2H, O-CH_2-CH_2-CH_2-S). IR: ν (cm^{-1}) = 3133, 2922, 1666, 1602, 1518, 1441,1281, 952, 821

Coating Preparation: Freshly cleaned glass slides were immersed in polymer solution (1 mg mL^{-1} in MeOH/3-(N-morpholino)propanesulfonic acid (MOPS) buffer (pH = 8.5), 3v/1v) for pre-set time points. Afterwards, slides were thoroughly rinsed with methanol, Milli Q water, then dried with nitrogen gas flow. All the slides were further dried in oven (60 °C) overnight before use.

UV–Vis Absorption and Transmission: UV–vis absorption was conducted on Agilent Cary 8454 UV-vis spectrometer, using half-micro quartz cuvettes. Polymers were dissolved in methanol at the concentration of 1 mg mL^{-1}. Upon the addition of MOPS buffer (pH = 8.5), samples were measured at the different time point (10 min, 30 min, 1 h, 2 h, and 3 h, respectively). Methanol/MOPS mixture was employed as background. UV-transmission of the polymer coated slides was measured on Agilent Cary 854 UV–vis spectrometer. Transmittance at the wavelength of 600 nm was used for data analysis.

Scanning Electron Microscopy (SEM): All pre-dried samples were sputtered with a thin layer of gold nanoparticles (≈8–10 nm) under high vacuum using sputter coater (Emscope SC 500, Quorum Technologies, UK). Surface morphology or single cell on substrates were investigated with scanning electron microscope (Hitachi SU8030, Japan, at high voltage of 15 kV, with working distance of 8.3 mm).

Single Cell Imaging with SEM: Spiked cells were incubated for 3 h in RPMI 1640 medium, then gently rinsed with DPBS. Afterwards, cells were fixed with glutaraldehyde solution (2.5 wt.% in DPBS) for 1 h at room temperature, followed by dehydration with ethanol/DPBS gradient solution (30/70, 50/50, 70/30, 90/10, 95/5, 100/0, v/v, 30 min for each time). Critical-point dry was done by Hexamethyldisilazane (HMDS)/ethanol solution (50/50, 100/0, v/v, 30 min for each time). Samples were dried in well-ventilated hood overnight at room temperature before measured with SEM.

Confocal Laser Scanning Microscopy (CLSM): Coated substrates were put on microscope cover glasses (bottom side up, fixed with glycerine), then imaged with confocal laser scanning microscope (Leica SP8). The surface roughness of the coatings was analysed and calculated by ImageJ.

Water Contact Angle (WCA): Water contact angle measurements were carried out on a contact angle goniometer (DataPhysics Instruments, Germany) with sessile drop method. Mean values of several measurements of each sample were taken.

X-Ray Photoelectron Spectroscopy: X-ray photoelectron spectroscopy (XPS) spectra were recorded on a Kratos (Manchester, UKAxis Ultra DLD spectrometer), equipped with a monochromatic Al Kα X-ray source. The spectra were measured in normal emission, and a source-to-sample angle 60° was used. All spectra were recorded utilizing the fixed analyzer transmission (FAT) mode. The binding energy scale of the instrument was calibrated, following a technical procedure provided by Kratos Analytical Ltd (calibration was performed according to ISO 15 472). The spectra were recorded utilizing the instrument's slot and hybrid lens modes. An analysis area of ≈300 µm x 700 µm was investigated; charge neutralization was applied. For quantification, the survey spectra were measured with a pass energy of 80 electron Volt (eV), and the spectra were quantified utilizing the empirical sensitivity factors that were provided by KRATOS (the sensitivity factors were corrected with the transmission function of the spectrometer). The high-resolution XPS spectra were measured with a pass energy of 20 eV, and the respective data were processed using UNIFIT 2020 spectrum processing software. For peak fitting, a Shirley background and a Gaussian/Lorentzian sum function were applied. If not denoted otherwise, the L-G mixing component was set to 0.35 for all peaks. All binding energies were calibrated to the signal observed for the C sp^2/sp^3 component (observed at 284.8 eV).

Cell Culture and Cell Adhesion Analysis: Human breast cancer cell lines (MCF7) were obtained from the American Type Culture Collection (ATCC). Roswell Park Memorial Institute RPMI-1640 culture medium (Gibco) was supplemented with 10% (v/v) fetal bovine serum (FBS) (Gibco) and 1% (v/v) of penicillin-streptomycin solution (Gibco). All the cancer cell lines were cultured at 37 °C with 5% CO_2 in culture flask.

MCF-7 cells were first dissociated by trypsin solution (Gibco) for 2 min. Then the cells were pre-stained with CellTrace™ Violet dye (Thermo Fisher Scientific, Waltham, MA, USA) for 20 min according to standard protocol from the manufacturer. Stained cells were spiked in serum-free RPMI-1640 medium with a concentration of 5000 cells mL^{-1}. Samples were incubated in 1 mL of prepared cell suspension for 3 h at 37 °C. Afterwards, all samples were gently rinsed with DPBS for 3 times to remove the excess cells then observed and photographed under fluorescence microscope (Zeiss Axio Observer Z1).

Supporting Information

Supporting Information is available from the Wiley Online Library or from the author.

Acknowledgements

The authors acknowledge the financial support of Dahlem research school (DRS) and Collaborative Research Center "Dynamic Hydrogels at Biological Interfaces"(CRC 1449) funded by the Deutsche Forschungsgemeinschaft (DFG, German Research Foundation) – Project ID 431232613 – SFB 1449. The authors would like to thank Cathleen Hudziak for providing the starting polymer dendritic polyglycerol (dPG) and Core Facility BioSupraMol (Freie Universität Berlin, Germany) for the support in SEM and CLSM measurements. Yannic Kerkhoff is thanked for offering help with ImageJ analysis of confocal 3D image. The authors also thank Benjamin Allen for polishing the manuscript. The authors want to thank Gary Chinga and Bob Dougherty for the development of RoughnessCalculation Plugin. [Correction added on 22 August 2023, after first online publication: Projekt Deal funding statement has been added.]

Open access funding enabled and organized by Projekt DEAL.

Conflict of Interest

The authors declare no conflict of interest.

Data Availability Statement

The data that support the findings of this study are available in the Supporting Information of this article.

Keywords

biointerfaces, cell adhesion, mussel-inspired polyglycerols, surface functionalization

Received: February 24, 2023
Revised: April 25, 2023
Published online: May 28, 2023

[1] J.-O. Carlsson, P. M. Martin, in *Handbook of Deposition Technologies for films and coatings*, Elsevier, New York **2010**, p. 314.
[2] J. C. Love, L. A. Estroff, J. K. Kriebel, R. G. Nuzzo, G. M. Whitesides, *Chem. Rev.* **2005**, *105*, 1103.
[3] N. Sahu, B. Parija, S. Panigrahi, *Indian J. Phys.* **2009**, *83*, 493.
[4] S. Minko, in *Polymer surfaces and interfaces*, Springer, New York **2008**, p. 215.
[5] E. Luong-Van, I. Rodriguez, H. Y. Low, N. Elmouelhi, B. Lowenhaupt, S. Natarajan, C. T. Lim, R. Prajapati, M. Vyakarnam, K. Cooper, *J. Mater. Res.* **2013**, *28*, 165.
[6] R. Smeets, B. Stadlinger, F. Schwarz, B. Beck-Broichsitter, O. Jung, C. Precht, F. Kloss, A. Gröbe, M. Heiland, T. Ebker, *Biomed Res. Int.* **2016**, *2016*, 3943481.
[7] S. B. Goodman, Z. Yao, M. Keeney, F. Yang, *Biomaterials* **2013**, *34*, 3174.
[8] D. Choudhury, M. Vrbka, A. B. Mamat, I. Stavness, C. K. Roy, R. Mootanah, I. Krupka, *J. Mech. Behav. Biomed. Mater.* **2017**, *72*, 192.
[9] a) J. Dong, J. F. Chen, M. Smalley, M. Zhao, Z. Ke, Y. Zhu, H. R. Tseng, *Adv. Mater.* **2020**, *32*, 1903663; b) A. Singh, M. Ferri, M. Tamplenizza, F. Borghi, G. Divitini, C. Ducati, C. Lenardi, C. Piazzoni, M. Merlini, A. Podestà, *Nanotechnology* **2012**, *23*, 475101; c) M. J. Dalby, N. Gadegaard, R. O. Oreffo, *Nat. Mater.* **2014**, *13*, 558; d) J. Li, X. Jiang, H. Li, M. Gelinsky, Z. Gu, *Adv. Mater.* **2021**, *33*, 2004172.
[10] Y. Hou, W. Xie, L. Yu, L. C. Camacho, C. Nie, M. Zhang, R. Haag, Q. Wei, *Small* **2020**, *16*, 1905422.
[11] L. Yu, P. Tang, C. Nie, Y. Hou, R. Haag, *Adv. Healthcare Mater.* **2021**, *10*, 2002202.
[12] D. Qin, Y. Xia, G. M. Whitesides, *Nat. Protoc.* **2010**, *5*, 491.
[13] Y. Lei, S. Yang, M. Wu, G. Wilde, *Chem. Soc. Rev.* **2011**, *40*, 1247.
[14] K. Q. Peng, Y. J. Yan, S. P. Gao, J. Zhu, *Adv. Mater.* **2002**, *14*, 1164.
[15] B. Sun, Y. Long, H. Zhang, M. Li, J. Duvail, X. Jiang, H. Yin, *Prog. Polym. Sci.* **2014**, *39*, 862.
[16] Q. Wei, R. Haag, *Mater. Horiz.* **2015**, *2*, 567.
[17] N. Sun, X. Li, Z. Wang, R. Zhang, J. Wang, K. Wang, R. Pei, *ACS Appl. Mater. Interfaces* **2016**, *8*, 12638.
[18] S. Hou, J.-F. Chen, M. Song, Y. Zhu, Y. J. Jan, S. H. Chen, T.-H. Weng, D.-A. Ling, S.-F. Chen, T. Ro, *ACS Nano* **2017**, *11*, 8167.
[19] L. Zhao, Y. T. Lu, F. Li, K. Wu, S. Hou, J. Yu, Q. Shen, D. Wu, M. Song, W. H. OuYang, *Adv. Mater.* **2013**, *25*, 2897.
[20] H. G. Silverman, F. F. Roberto, *Mar. Biotechnol.* **2007**, *9*, 661.
[21] H. Lee, S. M. Dellatore, W. M. Miller, P. B. Messersmith, *Science* **2007**, *318*, 426.
[22] M. Lee, S. H. Lee, I. K. Oh, H. Lee, *Small* **2017**, *13*, 1600443.
[23] Q. Wei, F. Zhang, J. Li, B. Li, C. Zhao, *Polym. Chem.* **2010**, *1*, 1430.
[24] Y. Tan, W. Deng, Y. Li, Z. Huang, Y. Meng, Q. Xie, M. Ma, S. Yao, *J. Phys. Chem. B* **2010**, *114*, 5016.
[25] W. Sheng, B. Li, X. Wang, B. Dai, B. Yu, X. Jia, F. Zhou, *Chem. Sci.* **2015**, *6*, 2068.
[26] J. Yang, C. Stuart, *Chem Soc Rev* **2014**, *43*, 8271.
[27] a) Q. Wei, K. Achazi, H. Liebe, A. Schulz, P. L. M. Noeske, I. Grunwald, R. Haag, *Angew. Chem., Int. Ed.* **2014**, *53*, 11650; b) C. Schlaich, L. C. Camacho, L. Yu, K. Achazi, Q. Wei, R. Haag, *ACS Appl. Mater. Interfaces* **2016**, *8*, 29117.
[28] H. Lee, N. F. Scherer, P. B. Messersmith, *Proc. Natl. Acad. Sci. USA* **2006**, *103*, 12999.
[29] B. K. Ahn, *J. Am. Chem. Soc.* **2017**, *139*, 10166.
[30] M. l. W. Kulka, I. S. Donskyi, N. Wurzler, D. Salz, O. z. Özcan, W. E. Unger, R. Haag, *ACS Appl Bio Mater* **2019**, *2*, 5749.
[31] S. S. Ray, *Clay-containing polymer nanocomposites* **2013**, *39*, 1112.
[32] P. Meredith, B. J. Powell, J. Riesz, S. P. Nighswander-Rempel, M. R. Pederson, E. G. Moore, *Soft Matter* **2006**, *2*, 37.
[33] R. N. Wenzel, *J. Phys. Chem.* **1949**, *53*, 1466.
[34] S. Giljean, M. Bigerelle, K. Anselme, H. Haidara, *Appl. Surf. Sci.* **2011**, *257*, 9631.
[35] L. Wang, W. Asghar, U. Demirci, Y. Wan, *Nano Today* **2013**, *8*, 374.
[36] W. Zhou, X. Zhong, X. Wu, L. Yuan, Z. Zhao, H. Wang, Y. Xia, Y. Feng, J. He, W. Chen, *Surf. Coat. Technol.* **2006**, *200*, 6155.
[37] W. Chen, S. Weng, F. Zhang, S. Allen, X. Li, L. Bao, R. H. Lam, J. A. Macoska, S. D. Merajver, J. Fu, *ACS Nano* **2013**, *7*, 566.
[38] K. Anselme, L. Ploux, A. Ponche, *J. Adhes. Sci. Technol.* **2010**, *24*, 831.

ADVANCED MATERIALS INTERFACES
Open Access

Supporting Information

for *Adv. Mater. Interfaces*, DOI 10.1002/admi.202300165

Mussel-Inspired Polyglycerol Coatings for Surface Modification with Tunable Architecture

Peng Tang, Guoxin Ma, Philip Nickl, Chuanxiong Nie, Leixiao Yu and Rainer Haag**

Supporting Information

Mussel-inspired Polyglycerol Coatings for Surface Modification with Tunable Roughness

Peng Tang,[a] *Guoxin Ma* [a], *Philip Nickl,*[a] *Chuanxiong Nie,*[a] *Leixiao Yu,*[b,*] *Rainer Haag*[a,*]

[a] Institute for Chemistry and Biochemistry, Freie Universität Berlin, Takustraße 3, 14195 Berlin, Germany

E-mail: haag@chemie.fu-berlin.de

[b] State Key Laboratory of Oral Diseases, West China Hospital of Stomatology, Sichuan University, Chengdu, Sichuan 610041, China

E-mail: leixiaoyu@scu.edu.cn;

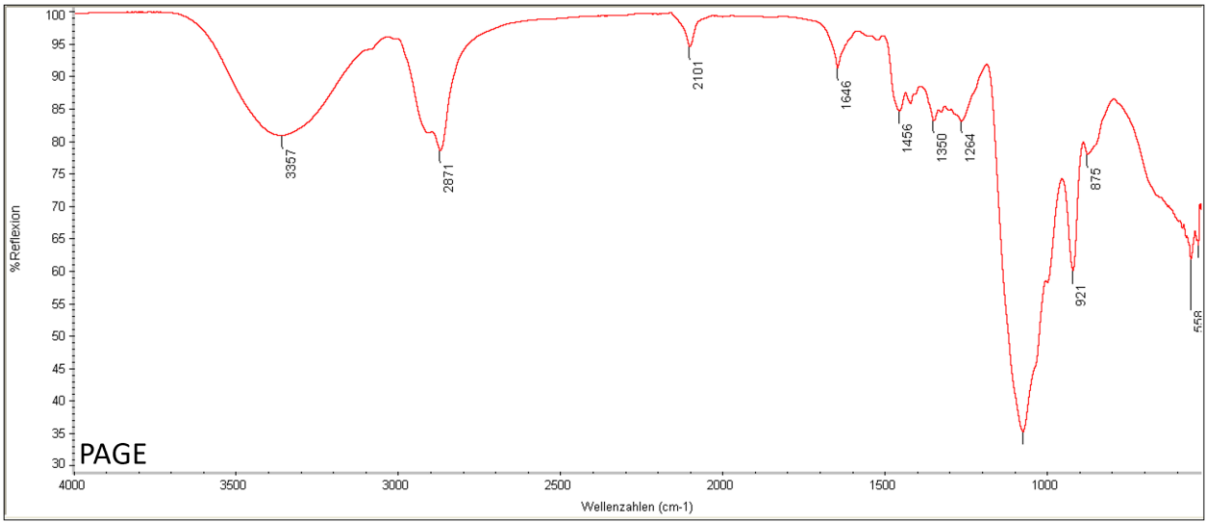

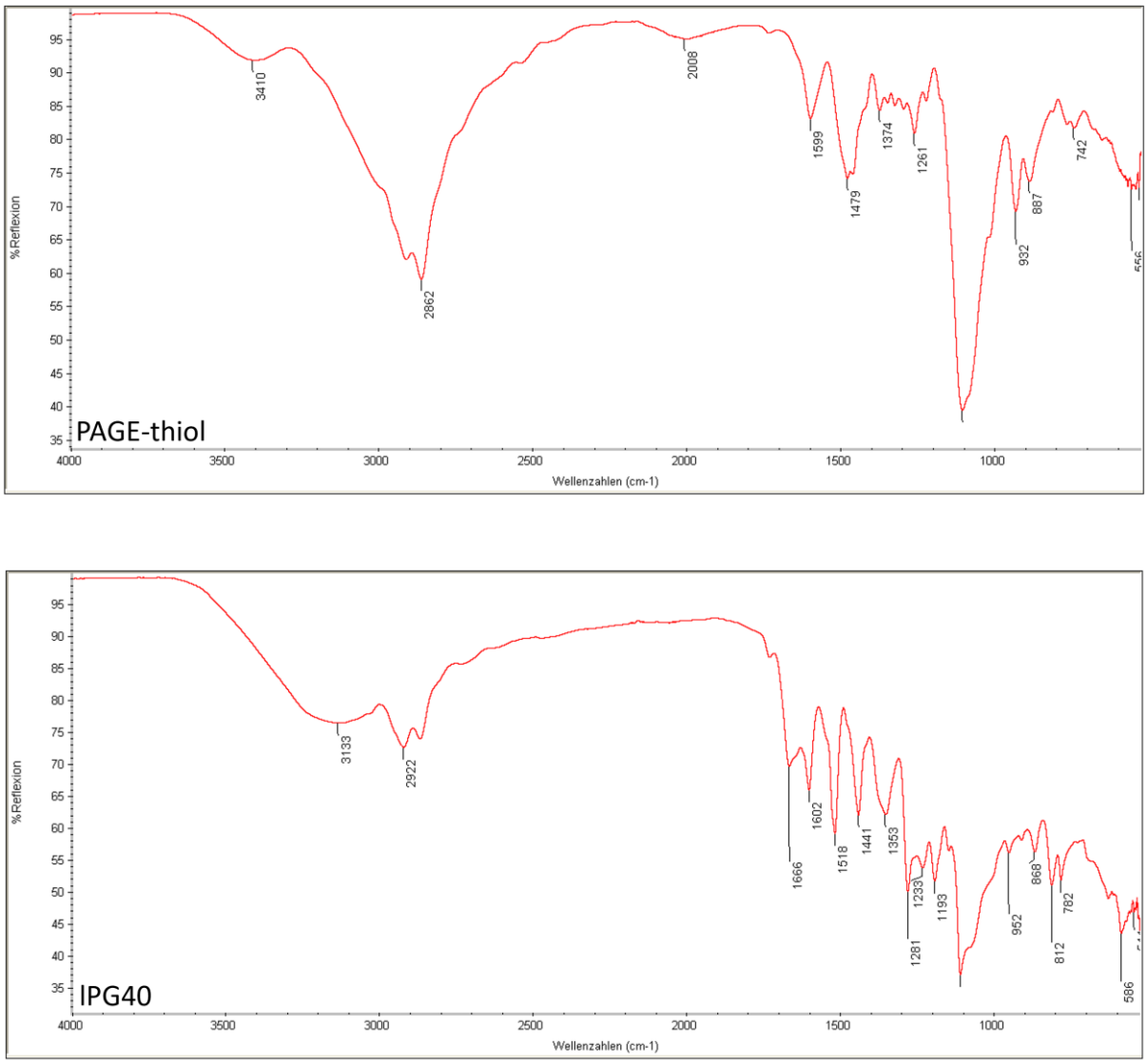

Figure S1. FTIR spectra of PAGE, PAGE-thiol and lPG40

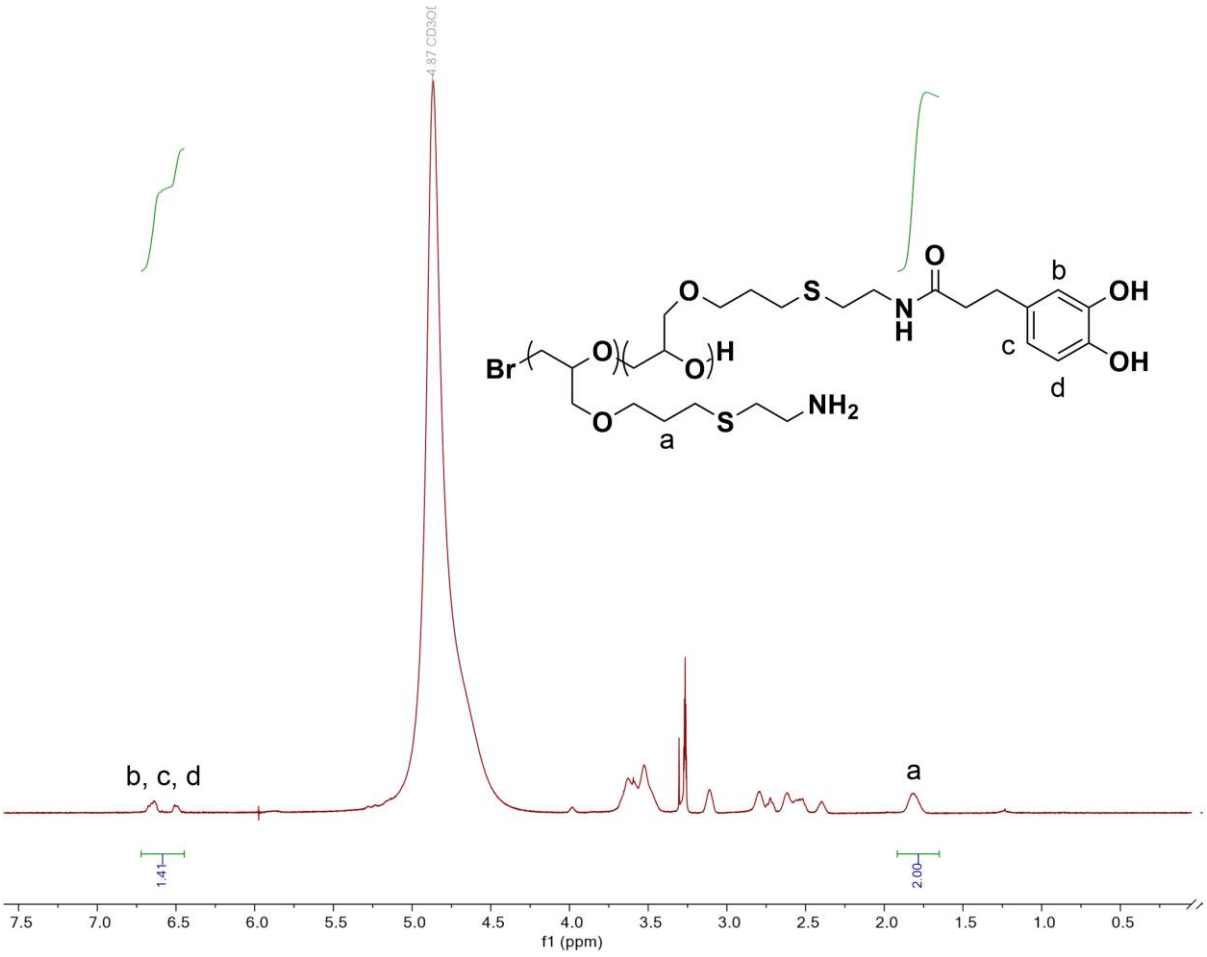

Figure S2. ^{1}H NMR spectrum of lPG40

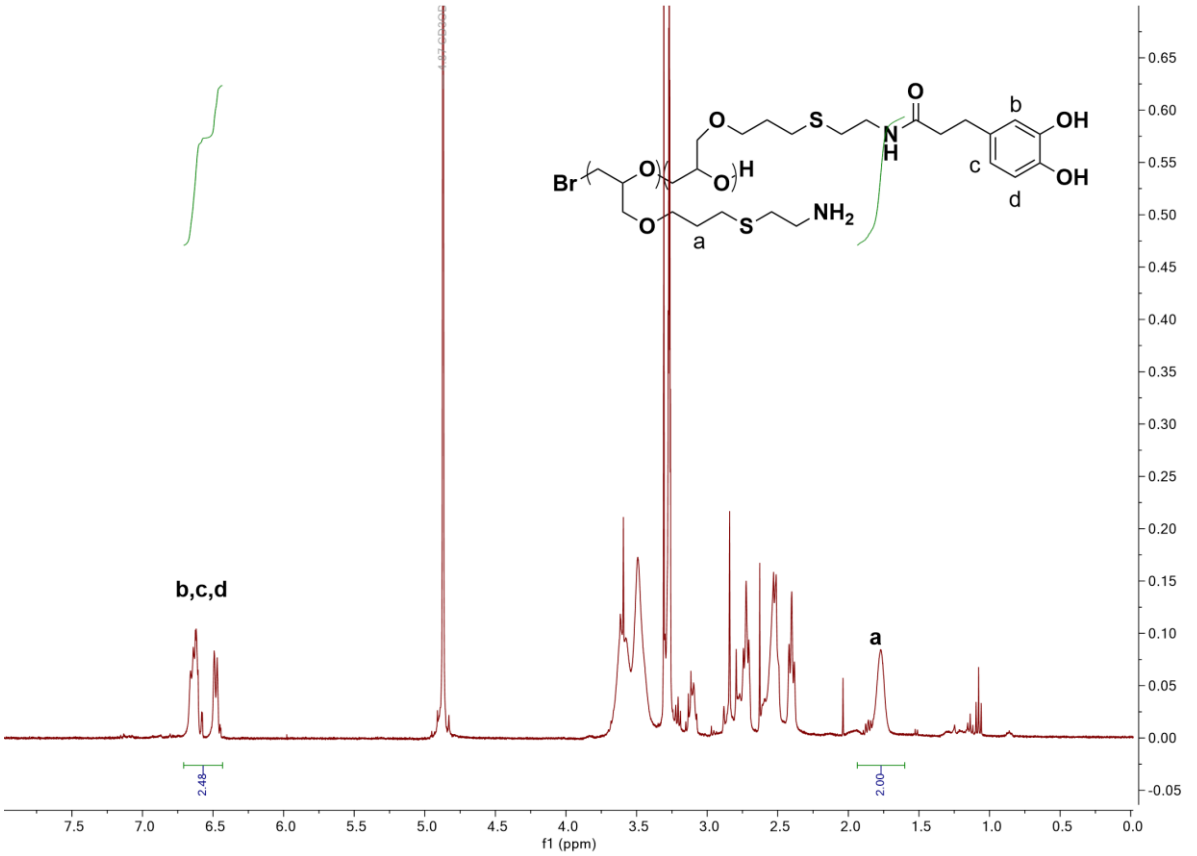

Figure S3. ^{1}H NMR spectrum of lPG80

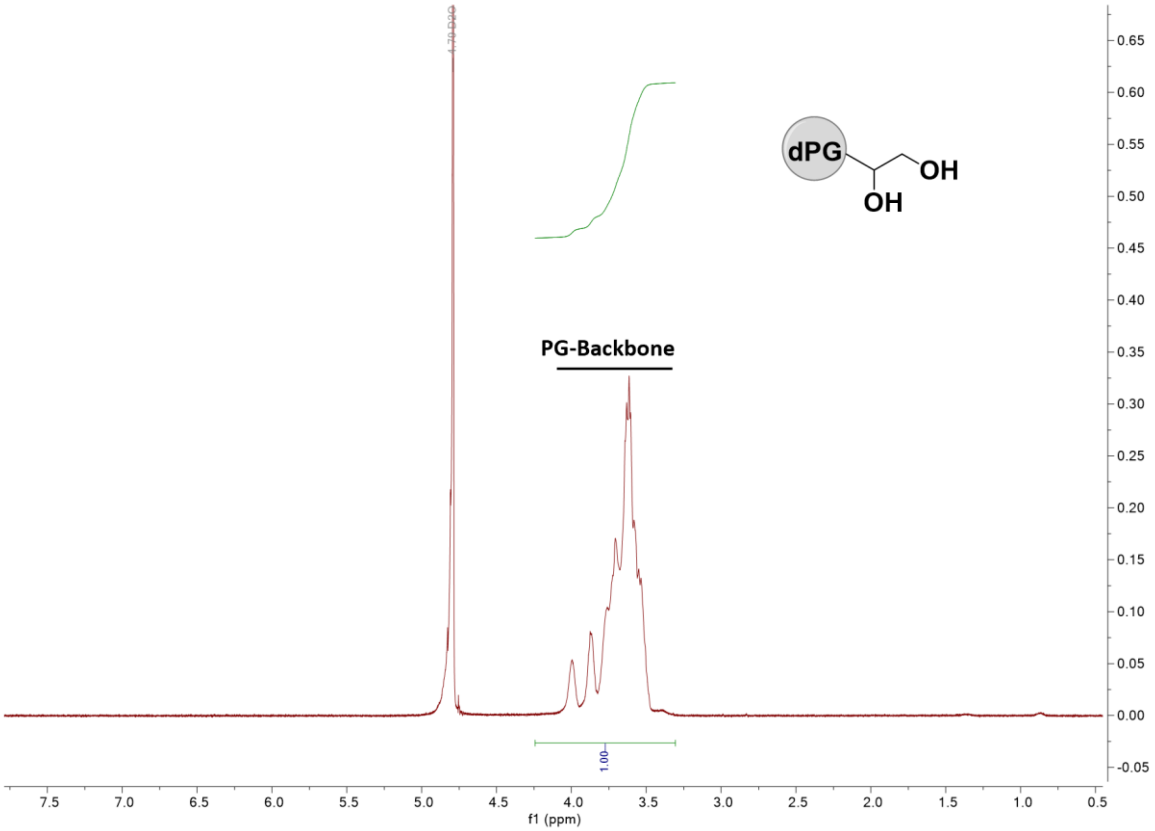

Figure S4. ^{1}H NMR spectrum of dPG-OH

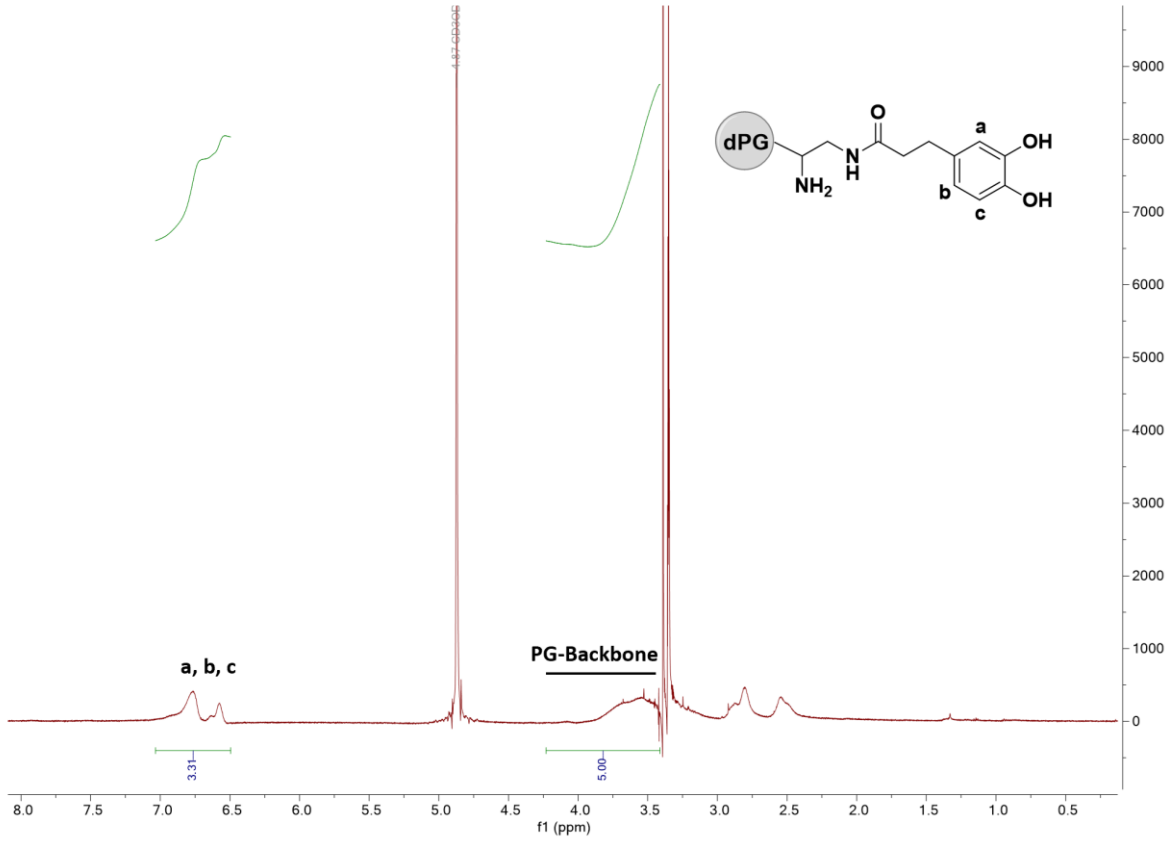

Figure S5. ^{1}H NMR spectrum of dPG40

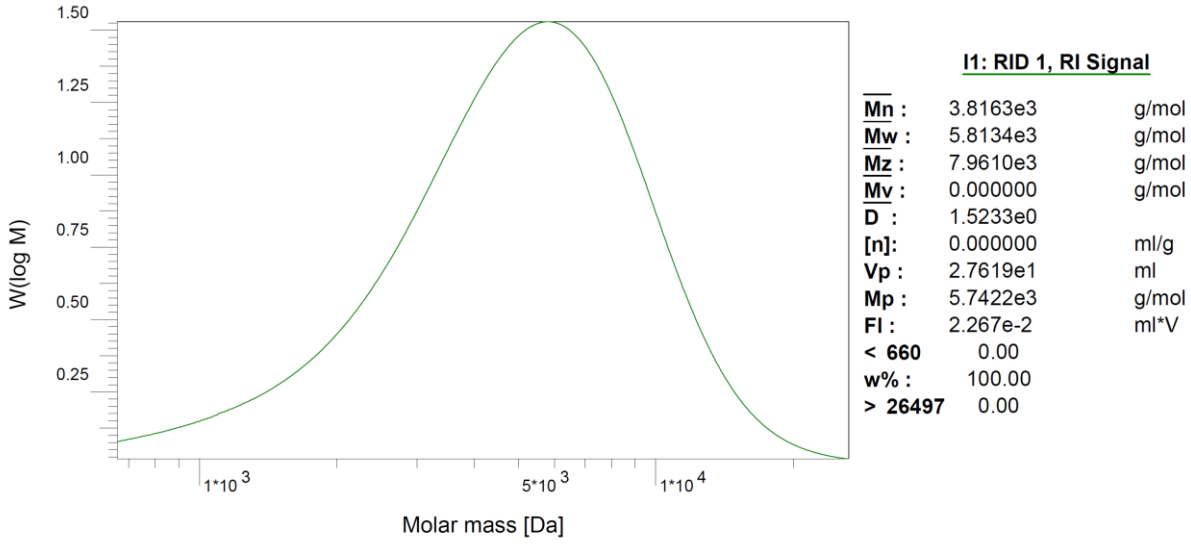

Figure S6: GPC result of the dPG-OH, the starting material of dPG40.

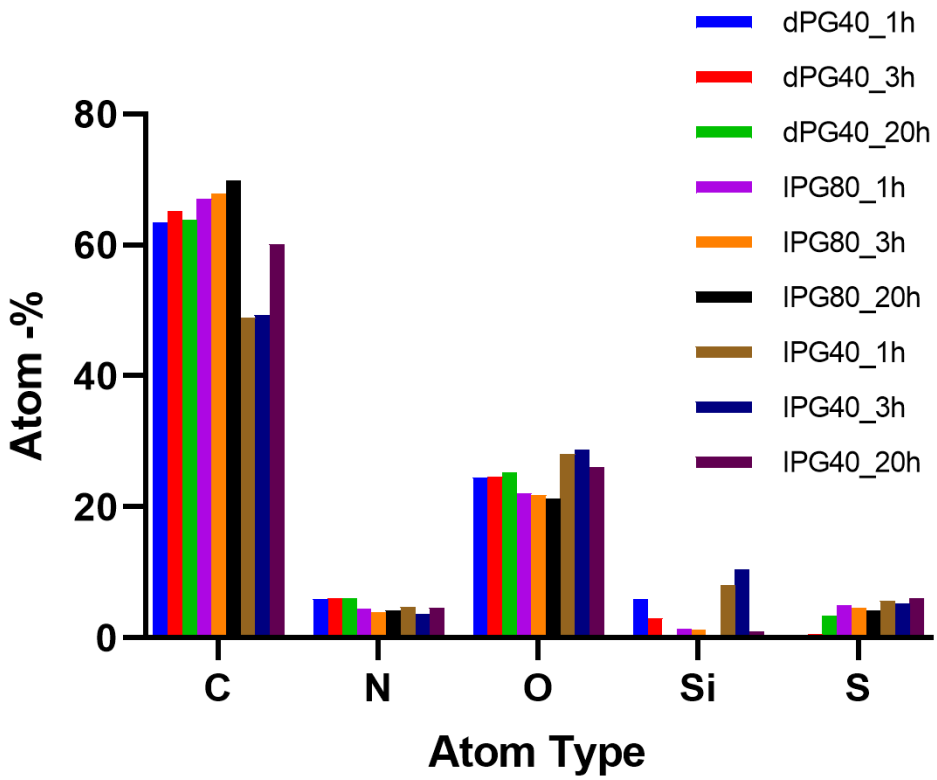

Figure S7. Elemental composition obtained from quantified XP survey spectra.

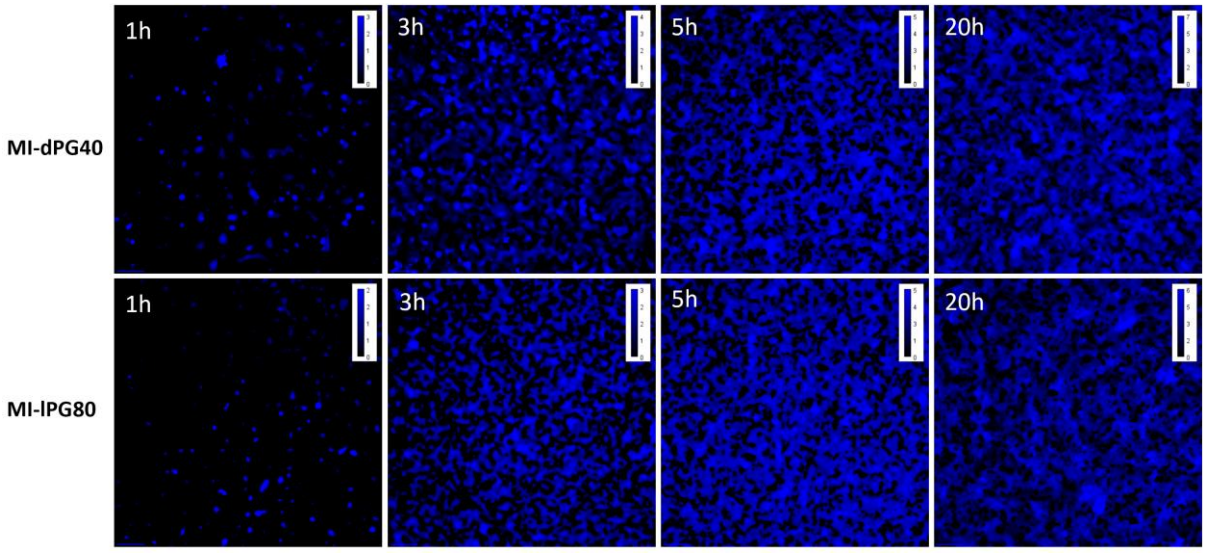

Figure S8. Phase images of MiPG coated surfaces from CLSM, stacked and processed by ImageJ.

4.2 Polyglycerol-Based Biomedical Matrix for Immunomagnetic Circulating Tumor Cell Isolation and Their Expansion into Tumor Spheroids for Drug Screening

Peng Tang, Boonya Thongrom, Smriti Arora*, Rainer Haag*

Advanced Healthcare Materials **2023,** *12*, 2300842

https://doi.org/10.1002/adhm.202300842

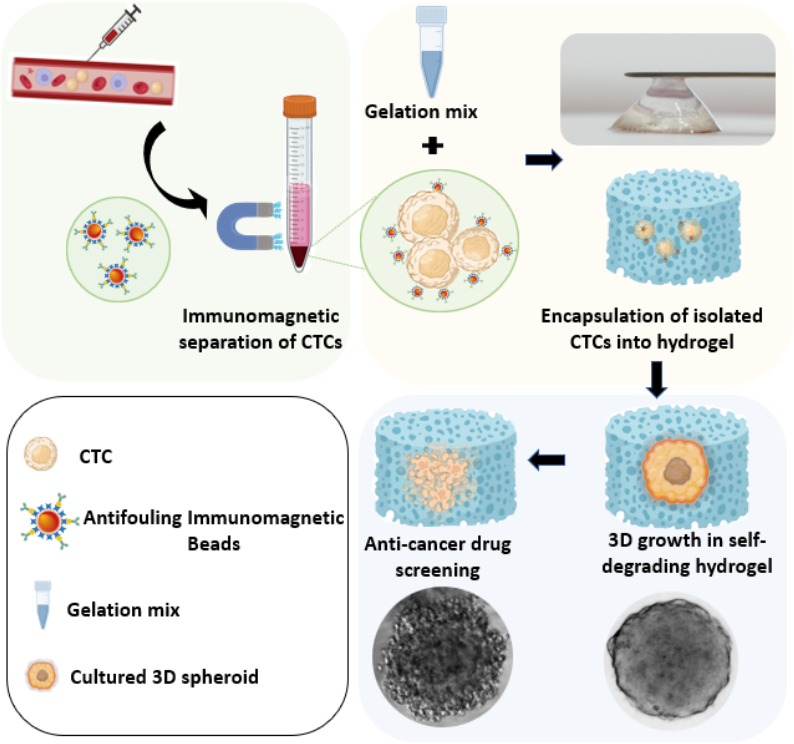

Figure 16: Graphical abstract of project 2. Reprinted with permission from ref. [166]. Copyright 2023 Wiley-VCH

Contributions of authors: In this publication, Peng Tang performed the biological experiments including the CTC capture, culture, characterizations and data processing, wrote parts of the manuscript, and took over most parts of the revision process. Boonya Thongrom synthesized all the gel components and characterized the chemical and physical properties of the hydrogels. Smriti Arora synthesized and functionalized the immunomagnetic beads, provided scientific guidance and helped with the proofreading of the manuscript. Rainer Haag supervised the whole project, provided valuable suggestions and proofread the manuscript.

ADVANCED HEALTHCARE MATERIALS
www.advhealthmat.de

Polyglycerol-Based Biomedical Matrix for Immunomagnetic Circulating Tumor Cell Isolation and Their Expansion into Tumor Spheroids for Drug Screening

Peng Tang, Boonya Thongrom, Smriti Arora, and Rainer Haag**

Circulating tumor cells (CTCs) are established as distinct cancer biomarkers for diagnosis, as preclinical models, and therapeutic targets. Their use as preclinical models is limited owing to low purity after isolation and the lack of effective techniques to create 3D cultures that accurately mimic in vivo conditions. Herein, a two-component system for detecting, isolating, and expanding CTCs to generate multicellular tumor spheroids that mimic the physiology and microenvironment of the diseased organ is proposed. First, an antifouling biointerface on magnetic beads is fabricated by adding a bioinert polymer layer and conjugation of biospecific ligands to isolate cancer cells, dramatically enhancing the selectivity and purity of the isolated cancer cells. Next, the isolated cells are encapsulated into self-degradable hydrogels synthesized using a thiol-click approach. The hydrogels are mechanochemically tuned to enable tumor spheroid growth to a size greater than 300 µm and to further release the grown spheroids while retaining their tumor-like characteristics. In addition, drug treatment highlights the need for 3D culture environments rather than conventional 2D culture. The designed biomedical matrix shows potential as a universal method to ensure mimicry of in vivo tumor characteristics in individual patients and to improve the predictability of preclinical screening of personalized therapeutics.

1. Introduction

Cancer metastasis is a multistep process involving dynamic changes in mutational and phenotypic landscapes.[1] These properties necessitate the constant monitoring of cancer patients to provide the most efficient care. However, the readily available primary tumor biopsies do not reflect the wide heterogeneity of tumors; in fact, they may only reveal signatures specific to local tumors, lacking the aberrant genomic changes that occur during the metastatic course. Thus, it becomes extremely challenging to devise a common treatment strategy to target different metastatic populations.[2] To achieve favorable long-term clinical outcomes, it is imperative to establish focused therapeutic treatments that are customized to each patient.[3] In this context, circulating tumor cells (CTCs) have been clinically validated as the first real-time, cellular, liquid biopsy cancer biomarkers that could enable highly precise and personalized cancer treatment.[4] Isolating and expanding CTCs from distinct treatment stages may therefore illuminate the evolution of specific tumor characteristics that can guide therapeutic decisions.[5]

Numerous strategies have been developed to isolate and culture CTCs among a billion normal blood cells, taking advantage of their unique biological and physical properties. Existing CTC isolation techniques include functionalized nanostructured surfaces based on cell-substrate affinity,[6] microfluidic devices that promote cell–surface contact,[7] immunomagnetic beads immobilized with capture biomolecules,[8] and microfilter devices for isolating tumor cells based on their varying size.[9,4b] Furthermore, these methods can be integrated with 3D expansion models, like spheroids, organoids, and xenografts, that are becoming increasingly vital for high-throughput drug screening and for studying metastases.[10] Such systems have clinical applicability to human malignancies as they can accurately replicate the key elements of the 3D architecture of the tumor microenvironment that results from altered cellular morphology, motility, and polarity. Although the personalized patient-derived xenograft is a very promising model, this technique is typically expensive, low-throughput, and very challenging to scale up.[11] These challenges have inspired the transition to 3D gel-based matrices like collagen and Matrigel[12] to better reflect the functional pathophysiology of in vivo tumors and simulate the interactions between cells and the extracellular matrix (ECM). These matrices comprise a crosslinked polymer network that can be adjusted to customize the stiffness and viscoelasticity of soft tissues.[13] In addition, hydrogels can offer a wide range of biochemical and biophysical cues for in vitro cell growth by using natural

P. Tang, B. Thongrom, S. Arora, R. Haag
Institute for Chemistry and Biochemistry
Freie Universität Berlin
Takustr. 3, 14195 Berlin, Germany
E-mail: smriti@zedat.fu-berlin.de; haag@chemie.fu-berlin.de

The ORCID identification number(s) for the author(s) of this article can be found under https://doi.org/10.1002/adhm.202300842

DOI: 10.1002/adhm.202300842

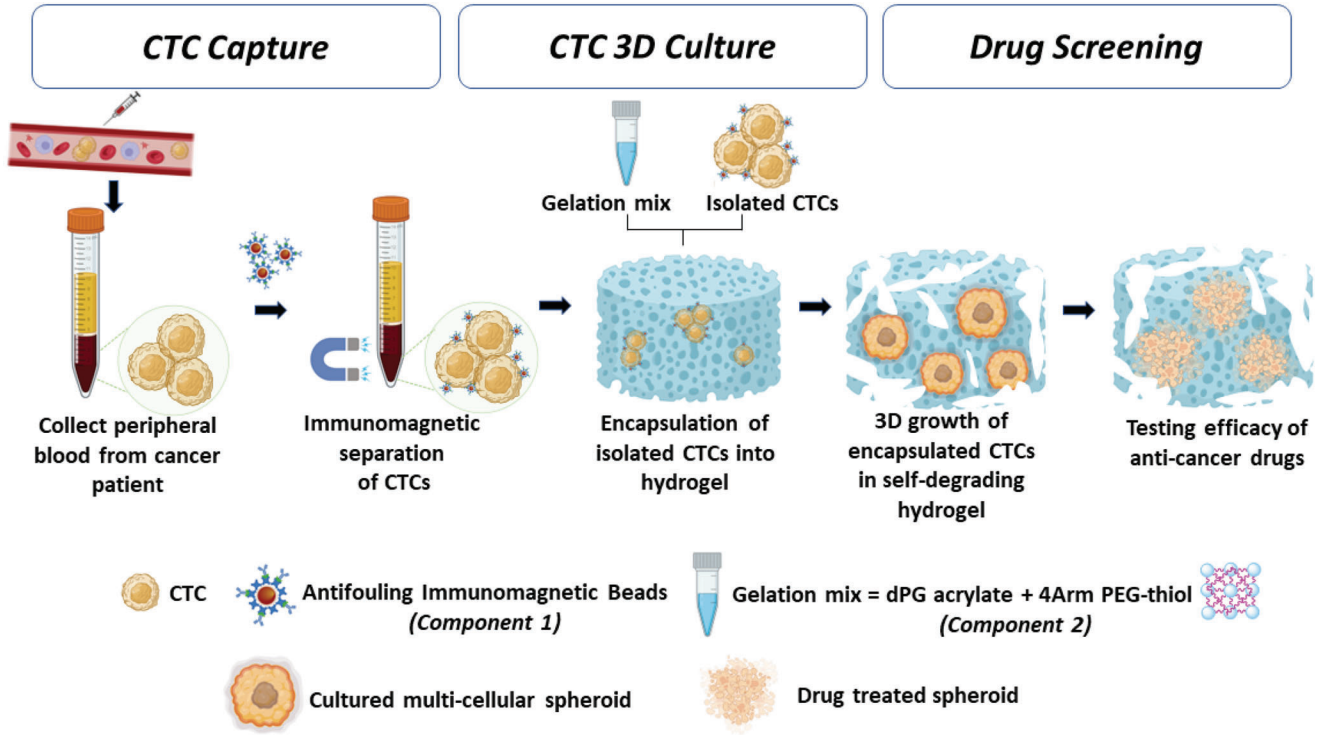

Figure 1. Schematic illustration of the polyglycerol-based biomatrix designed for detecting, isolating, and expanding CTCs from cancer patients' blood to monitor early-stage cancer and determine the potency and efficacy of anticancer drugs for individual cancer patients.

ECM molecules or synthetic materials modified by cell adhesion receptors, making them suitable for the challenge of culturing primary cancer cells.[11a,14] Matrigel-based and synthetic hydrogels have been used for expanding CTCs from cancer patients while preserving the expression of epithelial-cell adhesion molecule (EpCAM) and β-catenin.[15] However, the advantage of using synthetic hydrogels is the flexibility to include desired levels of modifications along biological or physical parameters, such as biodegradability, porosity, growth factors, and cleavage sites. A combinatorial two-step approach has been proposed by Liao et al., integrating a negative-selection CTC isolation and subsequent spheroid cell culture to test for potential cancer metastasis and thus the prognosis for disease.[16] However, negative CTC isolation techniques often have lower capture selectivity, purity, and viability, limitations which could restrict their use for cell proliferation and downstream analysis at clinical levels.

To address these issues, we present a two-component system that can detect, isolate, and culture CTC tumor spheroids from cancer patients' blood at various treatment stages. This system could be used to monitor early-stage cancer and assess the potency and efficacy of anticancer drugs for individual cancer patients (**Figure 1**). The first component involves immunomagnetic beads fabricated with dendritic polyglycerol (dPG)-catechol, an anti-biofouling coating, and functionalized with anti-EpCAM antibodies to isolate EpCAM-overexpressing CTCs (in this case, MCF-7) with high efficiency, selectivity, and viability. The dPG-based polymeric coating acts as a potent antifouling backdrop to fend off nonspecific blood cells' and proteins' adherence (red blood cells, white blood cells, proteins, etc.). These immunomagnetically isolated cells were embedded inside a synthetic degradable hydrogel composed of dPG and four-arm polyethylene glycol (PEG) to grow 3D spheroids. By simply adjusting the concentration and the ratio of two gel components, an optimal ECM-mimicking environment can be provided to grow multicellular tumor spheroids (MCTSs). Such a 3D matrix facilitates better intercellular communication and encourages self-assembly to generate structures that better resemble in vivo organization. Furthermore, the cultured tumor spheroids in 3D were screened for dose-dependent effects with the chemotherapeutic drug candidates doxorubicin and paclitaxel.

2. Results and Discussion

2.1. Antifouling Immunomagnetic Beads

dPG is considered an excellent alternative to PEG for its extraordinary performance and functionality. It has been used as a bioinert and biocompatible surface coating polymer, as described by earlier studies from our group.[17] Now, we fabricate magnetic iron nanoparticles (FeNPs) with a multifunctional dPG coating (**Figure 2**i). First we synthesized homogenous magnetic nanoparticles of ≈20 nm in size, functionalized with oleic acid using a known protocol.[18] Furthermore, oleic acid was replaced with dopamine to add water solubility and reactive amino groups. Then, the amino groups were coupled with succinic acid-functionalized dPG (dPG-SA). The average molecular weight of the dPG coating polymer is about 19 kDa, with 60% acidic functionalities, and an estimated 81 groups of succinic acid per dPG molecule as quantified by ^{1}H NMR end-group analysis. Transmission electron microscopy (TEM) imagery clearly depicts the

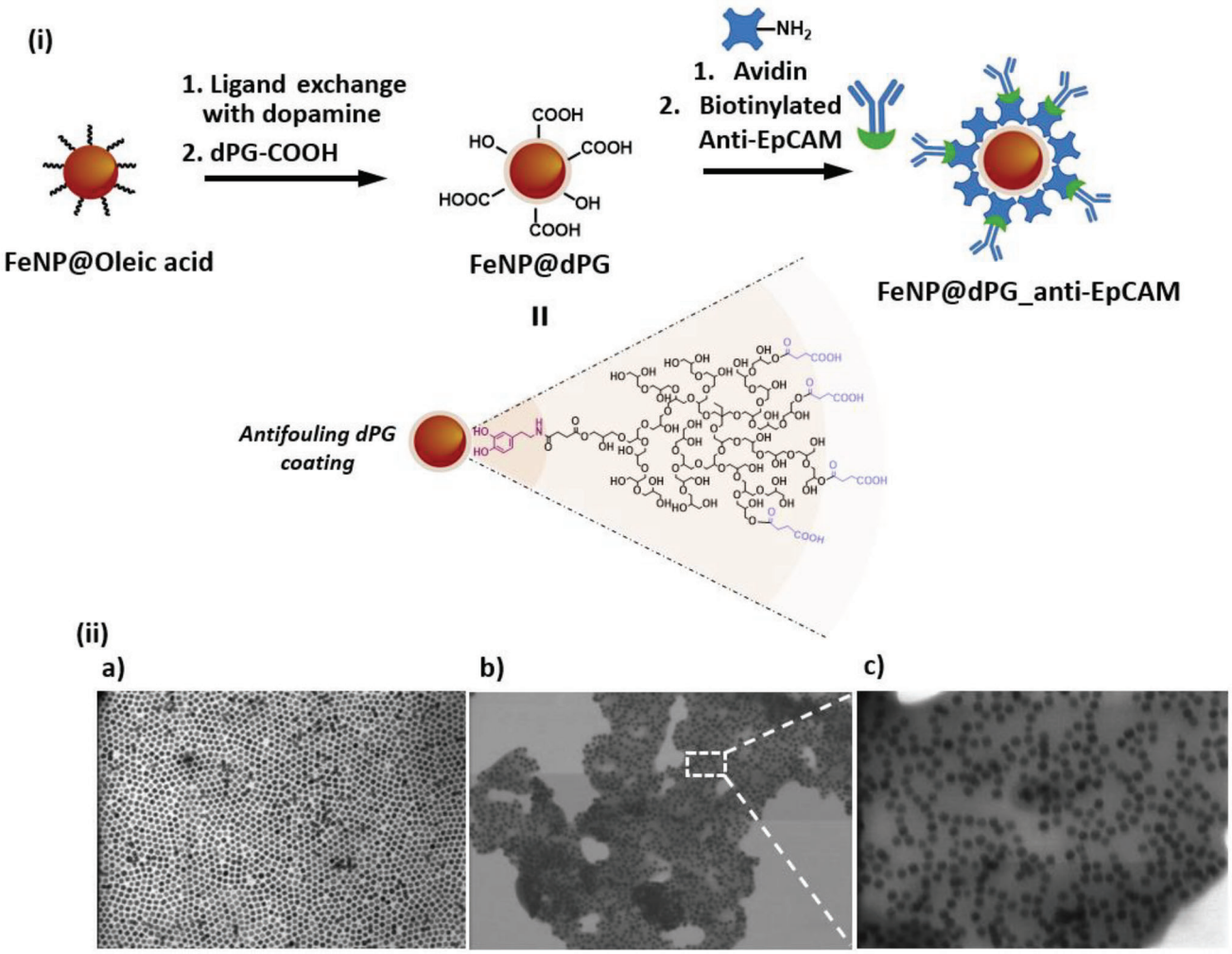

Figure 2. i) Schematic representation of the synthesis of anti-EpCAM antibody-functionalized dPG-coated FeNPs; ii) SEM images of FeNPs with an average particle size of ≈20 nm and different surface coatings: a) oleic acid coating on FeNPs. Scale = 200 nm, b,c) dPG coating on FeNPs. Scale = 250 nm, and the corresponding zoomed-in image, Scale = 100 nm.

change of the patterned arrangement of the particles to a polymeric coating when the ligand is switched from oleic acid to dPG (Figure 2ii). Here, the catechol groups and their oxidized derivatives serve as an anchoring domain that forms coordinate bonds with the FeNP surface to secure the coating of the dPG layer on the FeNPs.[19] The dPG backbone, once hydrated by the water molecule, acts as a hydrophilic domain that can significantly inhibit cell adhesion and the absorption of nonspecific proteins.[20] This strong bioinert scaffold helps prevent blood cells and nonspecific protein absorption from interfering with CTC isolation. A prominent CTC biomarker is EpCAM (epithelial cell adhesion molecule), which is overexpressed in most adenocarcinoma CTCs but negatively expressed in healthy blood cells.[21] As a result, the bioactive anti-EpCAM antibody-based CTC separation approaches have been used extensively.[22] Hence, to specifically capture CTCs, we used biotin ligand to further immobilize the biospecific anti-EpCAM antibody onto the dPG coating. This functionalization was performed using an avidin biolinker and was based on the non-covalent interaction between biotin and avidin, which is the one of the strongest noncovalent interactions in nature (the dissociation constant of avidin and biotin is 10^{-15} M).[23] In addition, since biotin is a small molecule and is biorthogonal to the conjugated antibodies, it does not impair the bioactivity of the conjugated antibodies.[24] Along with its antifouling properties and hydrophilicity, the multivalent nature of dPG allows high antibody functionalization. The resulting biointerfaces are termed as FeNP@dPG_anti-EpCAM.

2.2. Cell Capture Efficiency of the Antifouling Immunomagnetic Beads

Immunomagnetic iron nanoparticles equipped with anti-EpCAM antibodies can specifically recognize and capture $EpCAM^+$ cancer cells. In this study, the MCF-7 cell line was used as the model cancer cell line, while the HeLa cell line, which is $EpCAM^-$, was used as the negative control. The capture efficiencies under different conditions were investigated using

flow cytometry. MCF-7 cells were marked with violet fluorescent dye, genetically modified HeLa cells expressed green fluorescent protein, and the iron nanoparticles were conjugated with red fluorescent marker. The captured cells would be isolated by magnetic separation and would show both violet/red fluorescence for MCF-7 cells and green/red fluorescence for HeLa cells, respectively. In **Figure 3**i, microscopic images show the binding of iron nanoparticles with cells, and it is assumed that the iron nanoparticles could result in aggregation of cells.[8b]

To quantify the capture efficiency, we used flow cytometry, which is demonstrated in Figure 3ii. The population of the captured MCF-7 cells is represented with high violet (stained cancer cells) and red fluorescence (stained immunomagnetic beads). The capture methodology was optimized by investigating the concentration of immunomagnetic beads (FeNP@dPG_anti-EpCAM) and their incubation time at 100 000 cells mL^{-1}. As the concentration of the immunomagnetic beads rose from 0.05 to 0.4 mg mL^{-1}, capture efficiency increased from 84.2% to 99.6% (Figure 3iii a). Higher immunomagnetic bead concentrations, however, can result in severe aggregation, which could squander particles and further influence the hydrogel behavior in the subsequent cell-encapsulated hydrogel formation, ultimately impairing future cell growth. Even though the antibody/antigen contact happens extremely quickly, a longer incubation period with gentle mechanical mixing promotes the conjugation of cells with iron nanoparticles. Around 89.0% of capture efficiency was already attained after only 5 min of incubation, increasing to 93.6% after 40 min. After 90 min, however, the capture efficiency decreased to 85.4% (Figure 3iii b). This decline could be related to the loss of cell activity after longer periods of mixing in Dulbecco's buffered saline (DPBS) solution. As a result, 0.1 mg mL^{-1} of FeNP@dPG_anti-EpCAM and 40 min of incubation were used as a standard condition for MCF-7 cell capture, with 93.6% capture efficiency. As mentioned above, the specific recognition and capture were done by anti-EpCAM. High EpCAM expressing cell lines, MCF-7 and SKBR3, were captured with efficiency of 93.56% and 90.04%, respectively. The low EpCAM expressing cell line, A549 was captured with 67.304% efficiency while the negative EpCAM expressing cell line was captured with an efficiency of 2.63% (Figure 3iii c). When we attempted to individually capture HeLa cells with FeNP@dPG_anti-EpCAM, only 2.6% capture efficiency was reached, rising to 4.3% when spiked together with MCF-7 cells; in this case, the capture efficiency of MCF-7 remained at 92.4% (Figure 3iii d). Furthermore, the specificity was proven by FeNP@dPG without anti-EpCAM, with only 11.1% capture efficiency in comparison with 93.6% achieved with FeNP@dPG_anti-EpCAM (Figure 3iii e). The dPG coating layer on the outer shell of nanoparticles also prevented nonspecific binding with cells or proteins. The capture sensitivity of immunomagnetic beads was identified by spiking cells from as low as 1 to 1000 cells mL^{-1} (Figure 3iii f). The capture efficiency remained around 90% at all spiked cell counts. In order to mimic clinical conditions, we spiked cancer cells in DPBS, human serum, and healthy human blood, respectively. In serum, cancer cells were captured with 82.7% efficiency, and in healthy human blood, it was found to remain at 76.6% (Figure 3iii g). The presence of different proteins, cells, and other blood components had an impact on the capture efficiency to a great extent. Although capture efficiency decreased slightly, it is still viable for 3D culture. The outstanding antifouling property of the dPG layer and the specificity of anti-EpCAM validates the high performance of FeNP@dPG_anti-EpCAM in capturing $EpCAM^+$ cancer cells like MCF-7 cells. Besides, the easy separation of the cells using immunomagnetic iron nanoparticles facilitates their direct encapsulation in hydrogels.

2.3. Synthesis of Gel Precursors, Hydrogel Formation, and Rheological Characterization

The follow-up tumor spheroid formation demands a simple and fast hydrogel matrix in aqueous solution with no release of toxic by-products. In light of these requirements, thiol-click chemistry is preferred because it produces no by-products and reacts quickly at physiological pH. The resulting hydrogel is also self-degradable, making it possible to extract formed spheroids for further morphological analysis and anticancer drug testing. Among olefinic acceptors, acrylate has proven to be a good candidate for thiol-click coupling to fabricate hydrogel, which can be gradually degraded when incubated at 37 °C.[25] Herein, we used dPG and four-arm polyethylene glycol (four-arm PEG) as the precursors for gelation. dPG, employed as mentioned as a coating polymer on FeNPs, was also used as the main component in hydrogel formation, owing to its efficient functionality and bioinertness.

Four-arm PEG-thiol was synthesized in accordance with the literature with a slight modification (Figure S3).[25] It was functionalized with thiol group by using thiourea. The thiolation and hydrolysis were carried out at 80 °C after introducing a mesyl group. After purification, a pale yellowish precipitate was obtained in a high yield. The final product was characterized by ^{1}H NMR and the functionalized thiol groups were quantified by the Ellman test, which showed ≈3.4 groups per molecule (Figure S6, Supporting Information). On the other hand, we functionalized dPG with acrylate via acrylation reaction using acryloyl chloride (**Figure 4**i). After the dialysis purification, the dPG-acrylate was obtained and kept as an aqueous stock solution. We quantified the acrylate groups according to the literature[25] by ^{1}H NMR end-group analysis, showing roughly 5% functionalization or seven groups per molecule (Figure S2, Supporting Information).

The formation of the hydrogel involved simply mixing an aqueous solution of dPG-acylate and four-arm PEG-thiol in phosphate buffer saline (PBS) (Figure 4i). In order to encapsulate the cells, we replaced PBS buffer with cell culture media (RPMI-1640), and the cells were encapsulated in situ during gelation. Furthermore, we investigated to optimize the cell–cell and cell–gel interactions and so determine the recipe for the best hydrogel for tumor spheroid formation after encapsulation. In general, the viscoelasticity of hydrogels plays a crucial role in growing tumoroids, as the hydrogel must mimic the proper viscoelastic stiffness of natural ECM.[11a,13] With appropriate stiffness and support from the hydrogel's 3D structure, cancer cells can expand to form tumor spheroids. As a result, we used the dilution approach to change the stiffness of our hydrogels from 10% to 5% to 3% (w/v) (Table S1, Supporting Information). To further evaluate rheological properties over time in the presence of MCF-7 cells, we prepared in situ cell-encapsulated hydrogel in a 48-well plate with various gel concentrations, adding the cell

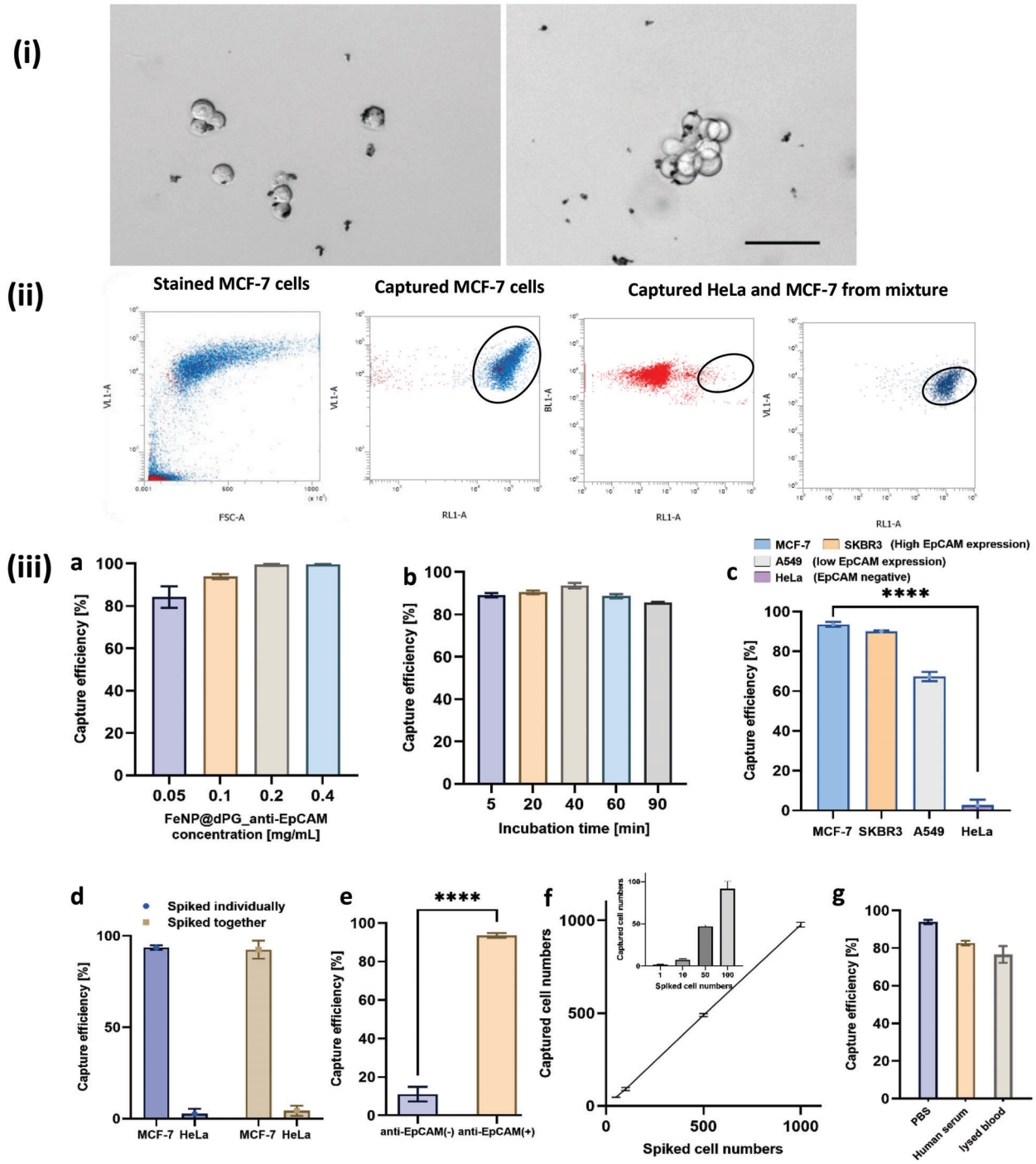

Figure 3. i) Bright-field images of single and clustered MCF-7 cells captured using anti-EpCAM antibody-modified dPG-coated FeNPs (FeNP@dPG_anti-EpCAM). Scale bar = 50 µm; ii) representative flow cytometry images for stained MCF-7 cells before and after capture and a mixture of MCF-7 and HeLa cells. The circled population indicates where the cells are using FeNP@dPG_anti-EpCAM; iii) representative capture efficiency (determined by flow cytometry) using: a) different concentrations of FeNP@dPG_anti-EpCAM particles (0.05, 0.1, 0.2, and 0.4 mg mL^{-1}), capture time = 40 min; b) different incubation times (5, 20, 40, 60, and 90 min) with 0.1 mg mL^{-1} of FeNP@dPG_anti-EpCAM particles; c) different cell lines (MCF-7, SKBR3, A549, HeLa) with different EpCAM expression; d) different cancer cell lines with varied EpCAM expressions (MCF-7 ($EpCAM^+$), HeLa ($EpCAM^-$); MCF-7 cells mixed with HeLa cells in serum-free cell culture medium), capture time = 40 min; e) different particles (FeNP@dPG and FeNP@dPG_anti-EpCAM at 0.1 mg mL^{-1}), capture time = 40 min; f) different numbers of spiked MCF-7 cells (100, 500, and 1000 cells mL^{-1}) in cell culture media, capture time = 40 min. The inset indicates the capture performance for low concentrations of cancer cells (1, 10, 50, and 100 cells mL^{-1}) spiked in cell culture media. g) Different incubation media (DPBS, human serum, lysed blood), capture time = 40 min; data are presented as mean ± standard deviation, $n = 3$. Statistical analysis was performed by using a one-way ANOVA test. *$p < 0.05$; **$p < 0.01$; ***$p < 0.001$; ****$p < 0.0001$. N.S. denotes not significant at $p > 0.05$.

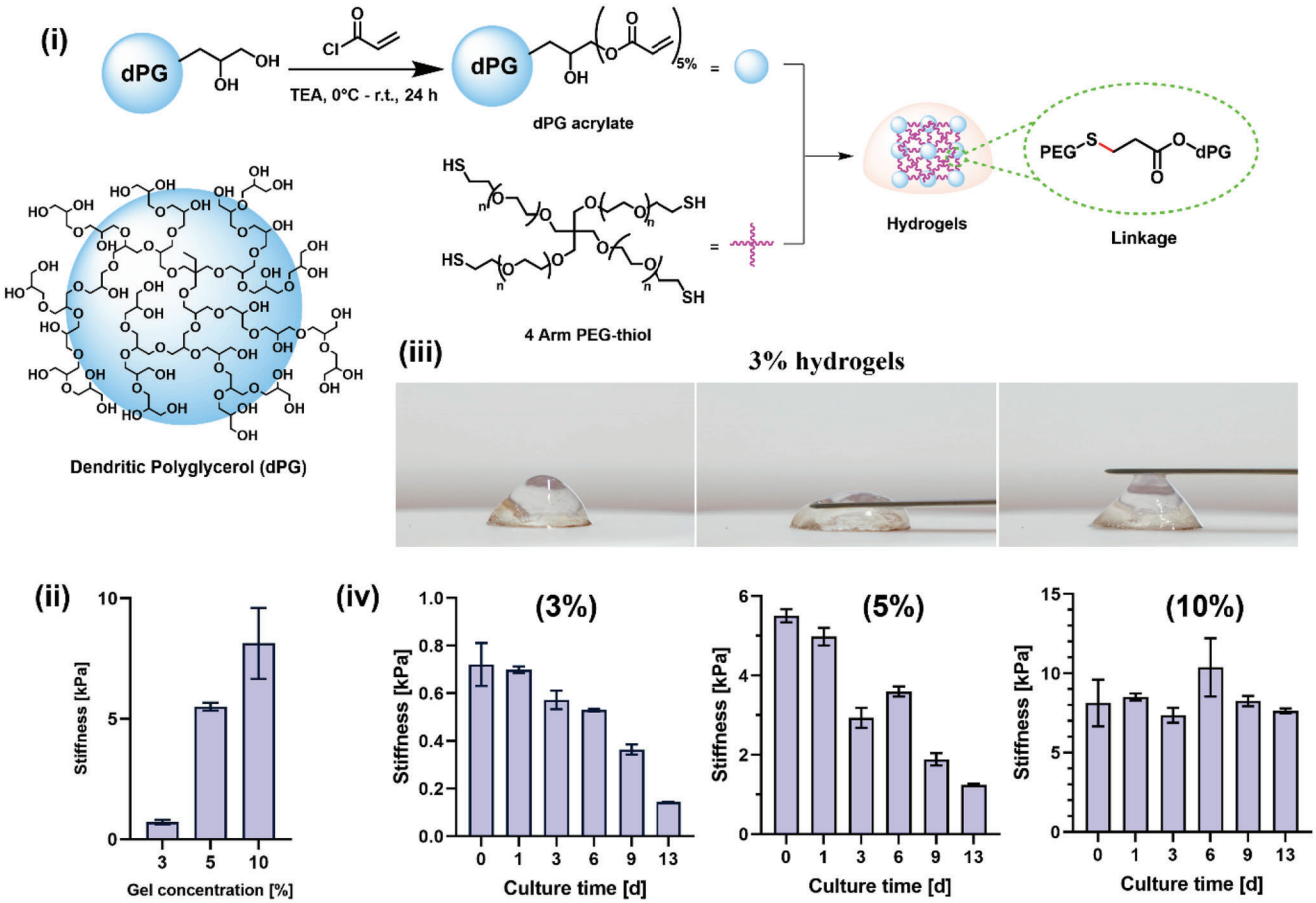

Figure 4. i) Synthesis of dPG-acrylate, followed by hydrogel fabrication between dPG-acrylate and four-arm PEG-thiol, for expansion of immunomagnetically isolated MCF-7 cells into tumor spheroids. Idealized structure of dendritic polyglycerol (dPG); ii) representative change in stiffness (kPa) with variation in hydrogel concentration; iii) motion images of 3% hydrogel; iv) stiffness measurements over a period of 13 d for 3%, 5%, and 10% acrylate-functionalized dendritic polyglycerol-based hydrogel fabricated in the presence of MCF-7 cells.

culture media after complete gelation. The hydrogels' stiffness was measured by rheometer at different times during incubation. The hydrogels were characterized by oscillatory shear on frequency sweep at a constant strain, resulting in a shear modulus graph that shows storage modulus (G') and loss modulus (G''). G' represents the material's solid behavior, while G'' represents its liquid behavior. After the rheological measurement, the G' and G'' values were plotted over the frequency range from 0.5 to 10 Hz, as shown in Figures S9–S11 (Supporting Information). The shear modulus graphs of the hydrogels at three different concentrations show that G' is evidently predominant over G'', indicating that all gel samples have higher energy storage than energy dissipation. This proves the successful formation of a chemically crosslinked network in the hydrogels.

In order to simplify the shear modulus graphs while examining the degradability of the gels, we chose the G' value at 1 Hz, which is directly related to the stiffness of the hydrogel. First, we compared the stiffness of three different gel concentrations at day 0, as seen in Figure 4ii. The 10% gel appears rigid and stiff, while the 5% gel is soft and elastic (Figure S8, Supporting Information), and the 3% hydrogel is the softest, behaving like slime (Figure 4iii). We determined the degradability of the hydrogel sample as it softened over time by comparing the hydrogel's stiffness at various incubation times. At 10% gel concentration, there was no discernible reduction in stiffness even after a prolonged incubation period (Figure 4iv). In contrast, from day 0 to day 13, the 5% and 3% hydrogel samples became progressively less stiff, showing a distinct decline of G' in both cases: from 5.5 to 1.2 kPa for the 5% gel, and from 0.7 to 0.1 kPa for the 3% gel, respectively (Figure 4iv). Thus, it is evident that hydrogel samples at 5% and 3% show dynamic softening over time due to ester bond degradation of the acrylate group.

2.4. Multicellular Tumor Spheroid Formation from Immunomagnetically Separated MCF-7 Cells and Anticancer Drug Screening

Following a detailed analysis of the chemical and rheological characteristics of hydrogels in relation to their effects on cell development, we found that the soft and slimy gels of 3% gel concentration permitted homogenous tumoroids to form, while no spheroid growth was seen with the 5% and 10% gels (Figure S12, Supporting Information). Soft hydrogels with viscoelastic,

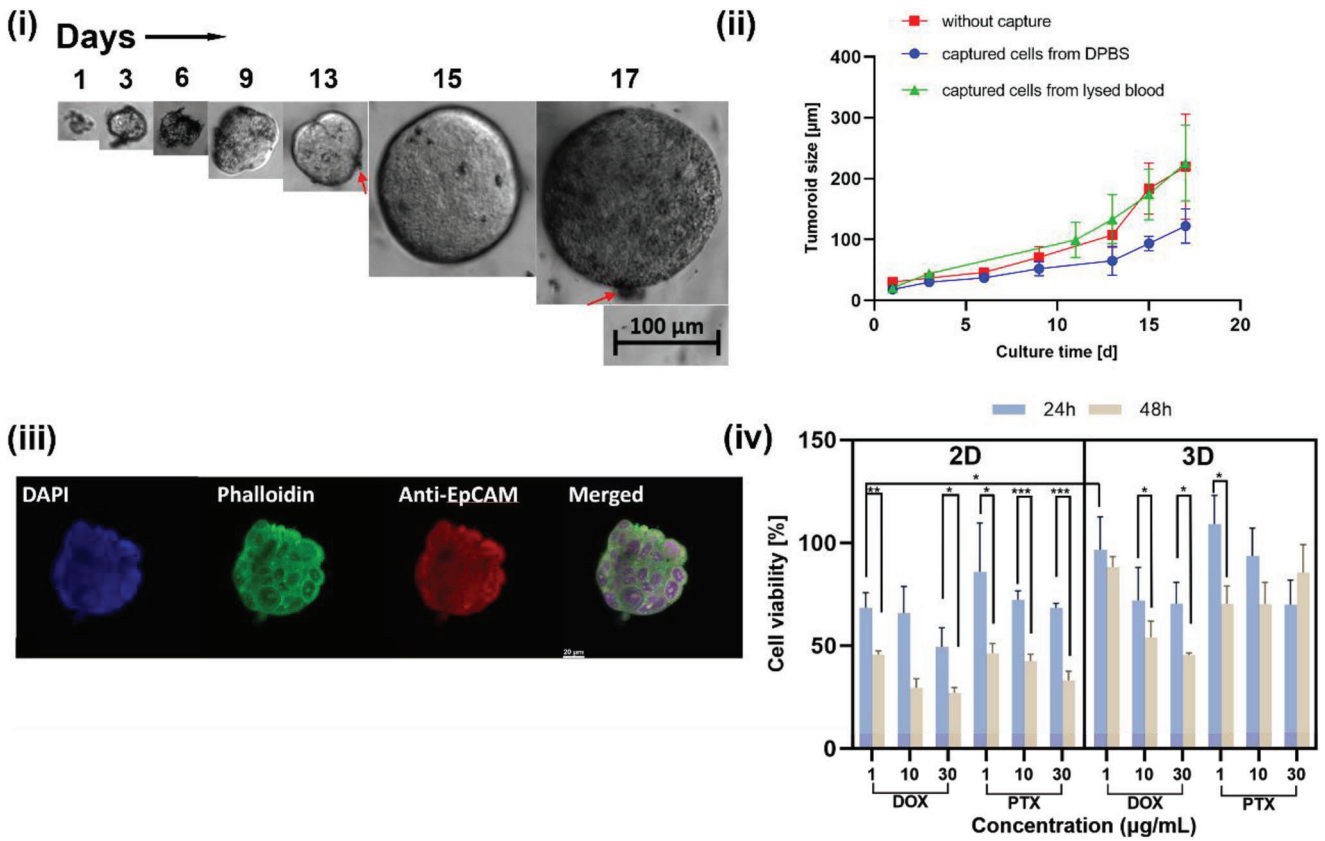

Figure 5. i) Bright-field images illustrating the expansion of immunomagnetically isolated cancer cell into a 3D tumor spheroid when incubated in 3% hydrogel (dPG-acrylate based). Scale bar = 100 µm; ii) comparative size change of 3D tumor spheroid from MCF-7 cells captured from PBS or lysed blood over a span of 17 d with and without immunomagnetic isolation. Data are presented as mean ± standard deviation, $n = 6$; iii) confocal microscopy images of 3D tumor spheroids cultured from MCF-7 cells captured in lysed blood for 15 d, stained with DAPI (nuclei), Phalloidin Fluoro594 (cellular cytoskeleton), and anti-EpCAM Fluoro488 (EpCAM surface protein). Scale bar = 20 µm; iv) the dose-dependent effects of the anticancer drugs doxorubicin (DOX) and paclitaxel (PTX) on the cultured tumor spheroids, with dPG-based hydrogel as a growth matrix. The tumor spheroid growth from immunomagnetically isolated MCF-7 cells within the hydrogel was tracked for 15 d prior to drug exposure. On day 15, the spheroids were exposed to three different drug concentrations ((i) 1, (ii) 10, (iii) 30 µg mL^{-1}), and the effect of the drugs was studied for 24 and 48 h of exposure. $n = 6$, two sample *t*-test, $*p < 0.05$, $**p < 0.01$, $***p < 0.001$, mean ± SD.

dynamically softening environments (from 0.7 to 0.1 kPa in stiffness measure) facilitated the formation of tumoroids. By contrast, stiffer gels constrained cell proliferation due to their rigid network and the resulting reduced mobility in their environment. We therefore chose 3% gel concentration as the ideal setting for MCTS formation in dPG-acrylate based hydrogel.

After cells were homogenously combined and encapsulated in 3% gel, we observed the development of tumor spheroids under a microscope. MCF-7 cells typically have a diameter of 19 µm,[26] but under standard incubation conditions (37 °C, 5% CO_2), the cells expanded to 70.71 µm on day 9 and 219.54 µm on day 17 of growth (Figure S14, Supporting Information). The tumoroids' morphologies were consistent across different sites within the gel (Figures S12, Supporting Information), and Figure S15 (Supporting Information) shows a confocal laser scanning microscopy (CLSM) image of the structure of a single tumor spheroid. Comparing the culture times with the rheology measurements of the hydrogels, it is assumed that the expansion of single cells to spheroids can be attributed to the 3D support of the gel matrix. The chemistry and stiffness of the customized gel match the extracellular matrix (ECM) environment, facilitating 3D spheroid growth. In addition, the ester-based hydrogel's degradation trend is consistent with tumor spheroids' growth in size, since softer gels are expected to have loose network density, allowing easy expansion for tumor spheroids. To further substantiate the claim that cancer cells can be used for downstream analysis and that the 3D culture does not alter their fundamental characteristics, we used CLSM to examine EpCAM, which MCF-7 cells overexpress. As seen in **Figure 5**iii, the resulting imagery confirmed the presence of EpCAM protein on the tumoroid surface. EpCAM serves as a well-established biomarker for cancer cells and their tumor initiating properties. In addition, it also serves as an adhesion molecule and as a promoter of cell proliferation. Therefore, EpCAM overexpression in 3D spheroids confirms their metastatic and stable proliferation nature. This is some of the most significant evidence for the viability and proliferation of EpCAM-expressing cancer cells.

According to several described methods for tumoroid formation, e.g., the inverse drop method, magnetic levitation,[27] tumoroids can form easily when a group of single cells aggregates

together. However, tumoroid formation from a small number of cells is challenging due to the scarcity of CTCs isolated from blood samples. To prove that our gel matrix is viable with low seeding numbers of cells, we seeded 10, 100, 500, and 1000 cells to 100 µL of hydrogels (3%), observing the formation of tumor spheroids at each seeding concentration. Even when starting with just ten cells at the beginning of 3D culture in hydrogel, the tumor spheroid grew to 300 µm on day 13 of culture (Figure S16, Supporting Information). Our gel matrix validates the growth of tumoroids from a low number of cells while preserving the vital cell characteristics for further applications.

After tuning the hydrogel to optimize tumor spheroid growth, we also seeded immunomagnetically isolated cells in the optimized hydrogel candidates. In general, we observed a similar trend of growth in the presence of FeNP@dPG_anti-EpCAM: single cells grew to 52.15 µm on day 9 and 122.33 µm on day 17 of culture (Figure 5i–iii). Explanations for the smaller sizes of these spheroids could be the restriction of iron nanoparticles and the slight change in hydrogel properties due to the presence of these particles. In spite of the downsizing, tumoroids still formed homogeneously throughout the hydrogels (Figure S13, Supporting Information). The hydrogels were found to be degraded after ≈15 d; this degradation not only coordinates the growth of tumoroids but also permits the grown tumoroids' release.

The grown tumor spheroids were directly evaluated in drug screening experiments as candidates for downstream applications. We cultured cells in 2D well plates to serve as control in investigating the drugs' effectiveness. Doxorubicin (DOX) and Paclitaxel (PTX) are the most commonly used anticancer drugs. We exposed 2D and 3D cultured MCF-7 cells to DOX and PTX at different concentrations (1, 10, and 30 µg mL^{-1}) for 24 and 48 h, then used the Celltiter-Glo luminescence assay to determine cell viability. The results show that DOX has a better effect than PTX in general, leaving only 27.02% living cells after 48 h incubation at high concentration, i.e., 30 µg mL^{-1}. Comparing the 2D and 3D models, an increased resistance to both drugs was clearly seen in 3D tumor spheroids (Figure 5iv). This observed behavior may be explained by the tumor developing cytostasis (a stage at which the drug treatment no longer causes cell death), which may have been facilitated by the hypoxic conditions present within the cultured MCTSs. These conditions are known to exist in in vivo solid tumors, contributing to drug resistance mechanisms.[28] The densely packed tumor spheroids exhibit considerable resistance, making it difficult for drug molecules to penetrate them and demonstrating that the tumor microenvironment significantly affects the drug screening process. As a result, 3D tumor models that imitate ECM are significantly more effective than 2D models at simulating in vivo tumors and would help us understand underlying multidrug resistance mechanism, a crucial hurdle in the development of anticancer drugs, especially against CTCs.

3. Conclusion

Here, we have presented a straightforward and effective method for the capture and 3D growth of CTCs. A dual-component polyglycerol-based biomatrix was developed to immunomagnetically isolate CTCs with high purity and specificity and to further expand these cells into multicellular tumor spheroids. The first component consists of magnetic iron nanoparticles fabricated with an additional bio-inert antifouling dPG coating and subsequently conjugated to anti-EpCAM antibodies in order to extract CTCs. The designed FeNP@dPG_anti-EpCAM particles displayed a capture efficiency of 93.6% for the MCF-7 cell line; these cells were further used for expansion into MCTSs.

Furthermore, the immunomagnetically separated captured cells were directly encapsulated into a hydrogel, which was composed of dendritic polyglycerol and four-arm polyethylene glycol, crosslinked by thiol-Michael click reaction. We tuned the stiffness of the hydrogels and found that 3% gel concentration gave a perfectly suitable consistency for MCF-7 cells to grow into MCTSs, which could then be easily extracted after the complete degradation of the gel. This behavior results from degradable ester bonds within the gel matrix, which lead to the dynamic softening of hydrogels over time (from 0.7 kPa at day 0 to 0.1 kPa at day 13). These rheological characteristics substantially encourage the growth of tumor spheroids of up to 300 µm in size. Moreover, the immunomagnetic separation followed by immediate 3D culture did not impede tumor development. By establishing the presence of the surface marker EpCAM, which the MCF-7 cell line overexpressed, we further demonstrated that the growing MCTSs retain the cancer cell characteristics. We also anticipated that MCTSs can offer a wealth of therapeutically pertinent data for planning and researching drug resistance mechanisms and the effects of anti-cancer medications on individual patients. We therefore explored the impact of generic anticancer drugs on MCTSs. The drug screening results showed higher apparent drug resistance in the 3D model than in 2D culture, showing that tumor spheroids can provide critical insights in future drug testing.

Our technique can connect liquid biopsy, oncological research, and cancer treatment, providing the next step for personalized therapeutic management.

Supporting Information

Supporting Information is available from the Wiley Online Library or from the author.

Acknowledgements

The authors acknowledge the financial support of Dahlem Research School (DRS) and Collaborative Research Center "Dynamic Hydrogels at Biological Interfaces" (CRC 1449) funded by the Deutsche Forschungsgemeinschaft (DFG, German Research Foundation) (Project ID 431232613 – SFB 1449). The authors would like to thank Cathleen Hudziak for providing the starting polymer hyperbranched polyglycerol (hPG) and Core Facility BioSupraMol (Freie Universität Berlin, Germany) for the support in TEM and CLSM measurements. The authors also thank Benjamin Allen for polishing the paper.

Open access funding enabled and organized by Projekt DEAL.

Conflict of Interest

The authors declare no conflict of interest.

Data Availability Statement

The data that support the findings of this study are available in the supplementary material of this article.

Keywords

3D hydrogels, biomaterials, circulating tumor cells, drug screening, multicellular tumor spheroids, polyglycerol biointerfaces

Received: March 22, 2023
Revised: June 8, 2023
Published online: July 21, 2023

[1] a) D. X. Nguyen, P. D. Bos, J. Massagué, *Nat. Rev. Cancer* **2009**, *9*, 274; b) A. W. Lambert, D. R. Pattabiraman, R. A. Weinberg, *Cell* **2017**, *168*, 274.
[2] J. Liu, J. Lian, Y. Chen, X. Zhao, C. Du, Y. Xu, H. Hu, H. Rao, X. Hong, *Front. Genet.* **2021**, *12*, 734595.
[3] a) N. McGranahan, C. Swanton, *Cell* **2017**, *168*, 613; b) K. W. Hunter, R. Amin, S. Deasy, N.-H. Ha, L. Wakefield, *Nat. Rev. Cancer* **2018**, *18*, 211.
[4] a) G. Siravegna, S. Marsoni, S. Siena, A. Bardelli, *Nat. Rev. Clin. Oncol.* **2017**, *14*, 531; b) B. Singh, S. Arora, A. D'Souza, N. Kale, G. Aland, A. Bharde, M. Quadir, M. Calderón, P. Chaturvedi, J. Khandare, *J. Mater. Chem. B* **2021**, *9*, 2946; c) S. Nagrath, L. V. Sequist, S. Maheswaran, D. W. Bell, D. Irimia, L. Ulkus, M. R. Smith, E. L. Kwak, S. Digumarthy, A. Muzikansky, P. Ryan, U. J. Balis, R. G. Tompkins, D. A. Haber, M. Toner, *Nature* **2007**, *450*, 1235.
[5] B. Rupp, H. Ball, F. Wuchu, D. Nagrath, S. Nagrath, *Trends Pharmacol. Sci.* **2022**, *43*, 378.
[6] a) L. Yu, P. Tang, C. Nie, Y. Hou, R. Haag, *Adv. Healthcare Mater.* **2021**, *10*, 2002202; b) J. Chen, L. Yu, Y. Li, J. L. Cuellar-Camacho, Y. Chai, D. Li, Y. Li, H. Liu, L. Ou, W. Li, R. Haag, *Adv. Funct. Mater.* **2019**, *29*, 1808961.
[7] a) J. Zhou, A. Kulasinghe, A. Bogseth, K. O'Byrne, C. Punyadeera, I. Papautsky, *Microsyst. Nanoeng.* **2019**, *5*, 8; b) H. Chen, Y. Li, Z. Zhang, S. Wang, *Biomicrofluidics* **2020**, *14*, 041502.
[8] a) Z.-m. Chang, R. Zhang, C. Yang, D. Shao, Y. Tang, W.-f. Dong, Z. Wang, *Nanoscale* **2020**, *12*, 19121; b) P. Liu, P. Jonkheijm, L. W. M. M. Terstappen, M. Stevens, *Cancers* **2020**, *12*, 3525.
[9] a) S. Ribeiro-Samy, M. I. Oliveira, T. Pereira-Veiga, L. Muinelo-Romay, S. Carvalho, J. Gaspar, P. P. Freitas, R. López-López, C. Costa, L. Diéguez, *Sci. Rep.* **2019**, *9*, 8032; b) K. Morita, N. Sawabata, S. Tatsumi, T. Fujii, T. Nishikawa, T. Kawaguchi, T. Arakane, Y. Tominaga, H. Sakaguchi, T. Kobayashi, S. Hontsu, Y. Yamamoto, N. Fujioka, N. Ouji-Sageshima, T. Ito, C. Ohbayashi, *Anticancer Res.* **2022**, *42*, 4305.
[10] a) A. M. K. Law, L. Rodriguez de la Fuente, T. J. Grundy, G. Fang, F. Valdes-Mora, D. Gallego-Ortega, *Front Oncol* **2021**, *11*, 782766; b) M. Tellez, D. Cochonneau, M. Cade, C. Jubellin, M.-F. Heymann, D. Heymann, *Cancers* **2018**, *11*, 19; c) E. A. Kwizera, W. Ou, S. Lee, S. Stewart, J. G. Shamul, J. Xu, N. Tait, K. H. R. Tkaczuk, X. He, *ACS Nano* **2022**, *16*, 11374; d) S. Arora, A. D'Souza, G. Aland, N. Kale, B. Jadhav, T. Kad, P. Chaturvedi, B. Singh, J. Khandare, *Lab Chip* **2022**, *22*, 1519; e) S. Sharma, R. Zhuang, M. Long, M. Pavlovic, Y. Kang, A. Ilyas, W. Asghar, *Biotechnol. Adv.* **2018**, *36*, 1063.
[11] a) Y. Li, E. Kumacheva, *Sci. Adv.* **2018**, *4*, eaas8998; b) S. J. Weroha, M. A. Becker, S. Enderica-Gonzalez, S. C. Harrington, A. L. Oberg, M. J. Maurer, S. E. Perkins, M. AlHilli, K. A. Butler, S. McKinstry, S. Fink, R. B. Jenkins, X. Hou, K. R. Kalli, K. M. Goodman, J. N. Sarkaria, B. Y. Karlan, A. Kumar, S. H. Kaufmann, L. C. Hartmann, P. Haluska, *Clin. Cancer Res.* **2014**, *20*, 1288; c) C. Scott, M. Becker, P. Haluska, G. Samimi, *Front. Oncol.* **2013**, *3*, 295.
[12] N. Chaicharoenaudomrung, P. Kunhorm, P. Noisa, *World J. Stem Cells* **2019**, *11*, 1065.
[13] Y. Jia, Z. Wei, S. Zhang, B. Yang, Y. Li, *Adv. Healthcare Mater.* **2022**, *11*, 2102479.
[14] a) A. D. Doyle, N. Carvajal, A. Jin, K. Matsumoto, K. M. Yamada, *Nat. Commun.* **2015**, *6*, 8720; b) A. W. Holle, J. L. Young, J. P. Spatz, *Adv. Drug Delivery Rev.* **2016**, *97*, 270.
[15] a) C.-L. Hu, Y.-J. Zhang, X.-F. Zhang, X. Fei, H. Zhang, C.-G. Li, B. Sun, *OncoTargets Ther.* **2021**, *14*, 2673; b) M. W. Tibbitt, K. S. Anseth, *Biotechnol. Bioeng.* **2009**, *103*, 655; c) S. A. Langhans, *Front Pharmacol* **2018**, *9*, 6; d) S. L. Ham, P. S. Thakuri, M. Plaster, J. Li, K. E. Luker, G. D. Luker, H. Tavana, *OncoTargets Ther.* **2017**, *9*, 249; e) J. Pape, M. Emberton, U. Cheema, *Frontiers in Bioengineering and Biotechnology* **2021**, *9*, 660502.
[16] C.-J. Liao, C.-H. Hsieh, H.-M. Wang, W.-P. Chou, T.-K. Chiu, J.-H. Chang, A. C. Chao, M.-H. Wu, *RSC Adv.* **2017**, *7*, 29339.
[17] a) M. W. Kulka, C. Nie, P. Nickl, Y. Kerkhoff, A. Garg, D. Salz, J. Radnik, I. Grunwald, R. Haag, *Adv. Mater. Interfaces* **2020**, *7*, 2000931; b) D. Braatz, M. Cherri, M. Tully, M. Dimde, G. Ma, E. Mohammadifar, F. Reisbeck, V. Ahmadi, M. Schirner, R. Haag, *Angew. Chem., Int. Ed.* **2022**, *61*, e202203942.
[18] J. Park, K. An, Y. Hwang, J.-G. Park, H.-J. Noh, J.-Y. Kim, J.-H. Park, N.-M. Hwang, T. Hyeon, *Nat. Mater.* **2004**, *3*, 891.
[19] W. Wei, J. Yu, C. Broomell, J. N. Israelachvili, J. H. Waite, *J. Am. Chem. Soc.* **2013**, *135*, 377.
[20] C. Siegers, M. Biesalski, R. Haag, *Chemistry* **2004**, *10*, 2831.
[21] M. Yu, A. Bardia, B. S. Wittner, S. L. Stott, M. E. Smas, D. T. Ting, S. J. Isakoff, J. C. Ciciliano, M. N. Wells, A. M. Shah, K. F. Concannon, M. C. Donaldson, L. V. Sequist, E. Brachtel, D. Sgroi, J. Baselga, S. Ramaswamy, M. Toner, D. A. Haber, S. Maheswaran, *Science* **2013**, *339*, 580.
[22] a) K. C. Andree, A. M. C. Barradas, A. T. Nguyen, A. Mentink, I. Stojanovic, J. Baggerman, J. van Dalum, C. J. M. van Rijn, L. W. M. M. Terstappen, *ACS Appl. Mater. Interfaces* **2016**, *8*, 14349; b) Z. Eslami-S, L. E. Cortés-Hernández, C. Alix-Panabières, *Cells* **2020**, *9*, 391; c) H.-W. Chien, J.-C. Wu, Y.-C. Chang, W.-B. Tsai, *Gels* **2022**, *8*, 391.
[23] U. Piran, W. J. Riordan, *J. Immunol. Methods* **1990**, *133*, 141.
[24] F. Rusmini, Z. Zhong, J. Feijen, *Biomacromolecules* **2007**, *8*, 1775.
[25] B. Thongrom, M. Dimde, U. Schedler, R. Haag, *Macromol. Chem. Phys.* **2023**, *224*, 2200271.
[26] A. Geltmeier, B. Rinner, D. Bade, K. Meditz, R. Witt, U. Bicker, C. Bludszuweit-Philipp, P. Maier, *PLoS One* **2015**, *10*, e0134999.
[27] A. Kamatar, G. Gunay, H. Acar, *Polymers* **2020**, *12*, 2506.
[28] a) A. S. Nunes, A. S. Barros, E. C. Costa, A. F. Moreira, I. J. Correia, *Biotechnol. Bioeng.* **2019**, *116*, 206; b) T. Tian, J. Ruan, J. Zhang, C.-X. Zhao, D. Chen, J. Shan, *J. Biomed. Nanotechnol.* **2022**, *18*, 660.

ADVANCED HEALTHCARE MATERIALS

Supporting Information

for *Adv. Healthcare Mater.*, DOI 10.1002/adhm.202300842

Polyglycerol-Based Biomedical Matrix for Immunomagnetic Circulating Tumor Cell Isolation and Their Expansion into Tumor Spheroids for Drug Screening

Peng Tang, Boonya Thongrom, Smriti Arora and Rainer Haag**

Supplementary Information

Polyglycerol-based biomedical matrix for immunomagnetic circulating tumor cell isolation and their expansion into tumor spheroids for drug screening

Peng Tang, Boonya Thongrom, Smriti Arora, Rainer Haag**

Institute for Chemistry and Biochemistry, Freie Universität Berlin, Takustr. 3, Berlin, 14195, Germany.

Email: haag@chemie.fu-berlin.de, smriti@zedat.fu-berlin.de

Experimental Part

Materials and Methods:

Chemicals and solvents are HPLC grade, purchased from Merck (Steinheim, Germany) and used directly without any purification unless stated otherwise. Dialysis was performed with benzoylated dialysis tubes (width: 32 mm, molecular weight cut-off 2000 g/mol) purchased from Merck (Steinheim, Germany). Diethyl ether (100%) was purchased from VWR chemicals. N, N-Dimethylformamide (99.8%) was purchased from Acros Organics. Potassium hydroxide, DCM (99%) were purchased from Thermo-Fischer Scientific. 4-arm PEG 10 kDa was purchased from JenKem Technology USA Inc. Tris(2-carboxyethyl)phosphine hydrochloride was purchased from TCI Deutschland GmbH. Invitrogen™ Fixative-Free Lysing Solution, High-Yield Lyse buffer was purchased from ThermoFischer Scientific. The absorption spectra and photoluminescence (PL) spectra were measured on a PerkinElmer Lambda 25 UV–vis absorption spectrophotometer and an Edinburgh F900 fluorescent spectrometer equipped with a xenon arc lamp, respectively. NMR spectra were measured on a Jeol ECX 400 or Jeol ECP 500 MHz and 100 MHz spectrometer. The determination of thiol group was performed by an Agilent Cary 8454 UV-visible spectrophotometer using disposable semi-micro UV-cuvette. Dendritic polyglycerol (dPG) with average weight molecular weight of 10 kDa was prepared as previously reported[1] using an enhanced approach.[2]

Synthesis of dPG-succinic acid (SA)

Dendritic polyglycerol (1 g, 0.01 mmol, 10KDa) was dissolved in pyridine (10 mL) followed by the addition of succinic anhydride (2 g, 2 mmol). The reaction mixture was stirred at room temperature for 18 h before the pyridine was removed under vacuum at 40 °C. The remaining solid was dissolved in CH_2Cl_2 (50 mL) and washed with cold 0.2 N HCl (100 mL, 3X) or until the aqueous phase remained at pH 1. The organic phase was evaporated, and the transparent gel was collected (95% yield) for further reaction. In this case, dPG acrylate contains 60% acrylate or an estimated 81 groups per dPG molecule.

Synthesis of FeNPs

Synthesis of iron-oleate complex[3]:

A mixture of iron chloride (10.8g, 40mmol), and sodium oleate (36.5g, 120mmol) was dissolved in ethanol (80 ml), distilled water (60 ml), and hexane (140 ml). The resulting solution was heated to 60 °C for 4 hours under a nitrogen atmosphere. Next, the mixture was cooled down to room temperature and the organic phase was separated and washed three times with deionized water. Finally, solvents were evaporated in rotavapor to give a wax-like compound.

Synthesis of magnetic nanoparticles[3]:

Iron oleate (1g, 1.1 mmol), oleic acid (0.3g, 1 mmol), and 5.15g of 1-octadecene was heated to 320 °C for 1 hour under an inert atmosphere. Then the mixture was cooled to room temperature and washed several times with ethanol: acetone (1:1, v/v) as precipitating agent, and subsequently centrifuged. Finally, the nanoparticles wee resuspended in toluene. The synthesized particles were visualized under TEM.

Coating of magnetic nanoparticles with dopamine: The hydrophobic ligands of synthesized magnetic nanoparticles were replaced with dopamine molecules via ligand exchange method with some modifications.[4] To the stock solution of magnetic nanoparticles (1.2g in 20 ml), 5 ml methanol was added, and the resultant was sonicated for 5 mins. Then the mixture was washed with toluene (3 ml) using magnet. Further, 1ml of 100 mg/ml dopamine hydrochloride was added and the resultant was sonicated for ~15 mins which resulted in precipitation of particles. The precipitated particles were separated using magnet and washed with methanol (3X), MQ (3X) to remove any unreacted dopamine hydrochloride. Finally, the particles were redispersed in 80 ml MQ and stored as it is.

dPG coating of FeNPs (FeNP@dPG):

dPG carboxylic acid (0.12 g) was allowed to dissolve in DMF (24 mL) overnight. The following day, reaction temperature was maintained at 0℃, with addition of DIPEA (1.15 ml) and stirring for 30 mins. Then EDC (0.5 g), HOBt (0.3 g) were added to the reaction mixture and stirred for ~60 mins. Further, dopamine functionalized particles (1.2 g in 80 ml MQ) were added, and the reaction was allowed to stir overnight. Finally, the particles were washed with MQ (3X) with the

help of a magnet to remove any unreacted dPG-carboxylic acid. The particles were resuspended in MQ (8 mL). The synthesized particles were visualized under TEM.

Biofunctionalization of dPG coated FeNPs (FeNP@dPG_anti-EpCAM):

FeNP@dPG (30 mg in 2ml) were first activated in presence of EDC (127 mg), NHS (127 mg) for 3-4 hours in DMF (4 ml). After completion, nanoparticles were washed with PBS pH 7.4 (4 ml, 3X) and then redissolved in PBS pH 7.4 (4 ml). Further, the reaction was cooled to 0 °C, avidin (2 mg) was added, and the reaction was stirred overnight at 0 °C. Finally, the next day, particles were purified by washing with PBS pH 7.4 (2 ml, 2X) using a magnet, redispersed in PBS (2 ml) and kept in fridge until further use. The avidin functionalization was confirmed by checking its binding with Biotin-Atto 520. FeNP@dPG_avidin (3 mg in 0.2 ml) was diluted to 1 ml and further treated with Biotin-Atto 520 (0.01 mg in 0.01 ml) for 1 hour. After completion, nanoparticles were washed until no further colour change was observed. The nanoparticles were then diluted (1:20) and fluorescence measurement was recorded at λ_{ex} = 480 nm. The λ_{em} = 540 nm confirmed the avidin-biotin conjugation was confirmed.

Further, the biofunctionalization with anti-EpCAM antibody was performed by treating FeNP@dPG_avidin (5 mg in 2 ml) with Biotin-anti-EpCAM (0.01 mg in 0.01 ml) overnight at 4 °C. The particles were purified by washing with PBS pH 7.4 (2 ml, 2X) using a magnet, redispersed in PBS (2 ml) and kept in fridge until further use.

Synthesis of dPG-acrylate

To the DMF solution (30 mL) of 10 kDa dPG (3 g, 0.3 mmol, 1 eq.) under dry condition was added triethylamine (TEA, 0.5 mL, 3.6 mmol, 12 eq.) and the reaction mixture was cooled down with ice bath. Acryloyl chloride (0.24 mL, 3mmol, 10 eq.) was added dropwise to the reaction flask. The reaction was stirred for 1 d and afterward, it was subjected to purification by the dialysis using a 2 kDa cutoff benzoylated cellulose dialysis tube in water for 2 d. Then, the aqueous solution of dPG acrylate was collected, concentrated, and kept in the fridge (82% isolated yield). ^{1}H NMR (500 MHz, D_2O, δ (ppm)): 0.88 (3H, broad s, initiator backbone), 3.44 - 4.30 (m, backbone repeating units), 6.03 (1H, broad s), 6.25 (1H, broad s) and 6.45 – 6.48 (1H, broad s). The number of acrylate functional groups was calculated following the literature.[5] In

this case, dPG acrylate contains 5% acrylate or an estimated 7 groups per dPG molecule. **Figure S2**.

Synthesis of 4-arm PEG mesylate

10 kDa dried 4-arm PEG OH (**Figure S**, 7 g, 0.7 mmol, 1 eq.) was dissolved in anhydrous dichloromethane (DCM, 50 mL) and TEA (0.97 mL, 7 mmol, 10 eq.) was added to the reaction flask. The mixture was then cooled with an ice bath followed by dropwise addition of methanesulfonyl chloride (0.43 mL, 5.6 mmol, 8 eq.), and the reaction was then run for 1 d. Afterward, the crude product was washed thrice with brine, dried with Na_2SO_4, and later concentrated by a rotary evaporator. The crude mixture was precipitated in cooled diethyl ether, collected, and dried overnight under a vacuum. The precipitate product was obtained as a white powder with an 85% isolated yield. ^{1}H NMR (500 MHz, $CDCl_3$, δ (ppm)): 3.08 (3H, s), 3.40 - 3.78 (m), 4.37-4.38 (2H, t). **Figure S5**.

Synthesis of 4-arm PEG thiol

4-arm PEG mesylate (4.33 g, 0.43 mmol, 1 eq.) and thiourea (0.66 g, 8.7 mmol, 20 eq.) were added to the reaction flask followed by 1-propanol (10 mL). The reaction was carried at 80 °C for 1 d to obtain 4-arm PEG isothiouronium intermediate. After removing 1-propanol, KOH (0.024 g, 0.43 mmol, 4 eq.) and water (40 mL) were added to the reaction flask and the solution was then heated to 80 °C for 1 d. Afterward, tris(2-carboxyethyl)phosphine (TCEP, 0.5 g, 1.7 mmol, 4 eq.) was added to the crude mixture which was stirred for 2 h. The purification step is then explained, first saturating the crude mixture with NaCl, second extracting the product with DCM thrice and drying it with Na_2SO_4, third concentrating the DCM layer, and finally precipitating it in cooled diethyl ether. Dried 4-arm PEG thiol as a pale yellowish powder was obtained with a 90% isolated yield. ^{1}H NMR (700 MHz, $CDCl_3$, δ (ppm)): 1.59 (1H, t), 2.68-2.71 (2H, quat), 3.41 - 3.74 (m). 4-arm PEG thiol was also characterized by Ellman essay following the procedure from Thermofisher Scientific company. The number of thiol groups was quantified using the standard calibration curve of cysteine which contains 1 thiol group. The result shows that the number of thiol group on 4-arm PEG thiol is approximately 3.4 groups of thiols. **Figure S6**.

Rheological Analysis:

The rheological data of all hydrogel samples were characterized by Malvern Instruments Kinexus equipped with a cone plate of 20 mm diameter and 1 ° angle. The rheological test was conducted at 25 °C by an oscillatory frequency sweep strain-controlled where the constant strain is set at 1% at the frequency range of 0.1 - 100 Hz. The report stiffness value was directly related to the storage modulus at 1 Hz.

Transmission electron microscopy (TEM):

The samples were prepared by dripping the nanoparticle solution onto a Formvar/Carbon 200 mesh copper grid (Merck). Images were obtained from TEM mode of Hitachi SU8030 at high voltage of 15 kV, with working distance of 8.3 mm.

Cell Culture

Cell culture: Human breast cancer cell lines (MCF-7) and human cervical cancer cell lines (HeLa) were obtained from the American Type Culture Collection (ATCC). GFP^+-HeLa cells, derived from the HeLa cell line (ATCC; CCl-2), were transfected with and expression unit for a destabilized enhanced green fluorescent protein (d2EGFP, Clontech, Palo Alto, USA). Roswell Park Memorial Institute RPMI-1640 culture medium (Gibco) was supplemented with 10 % (v/v) fetal bovine serum (FBS) (Gibco) and 1 % (v/v) of penicillin-streptomycin solution (Gibco). All the cancer cell lines were routinely cultured at 37 ℃ with 5 % CO_2 in culture flasks, and were used from the same passage number for the same set of experiments.

Blood Lysis

Healthy human blood was purchased from German Red Cross (DRK Blutspendedienst Nord-Ost), and it was lysed as per the protocol using the lysing buffer (Invitrogen™ Fixative-Free Lysing Solution, High-Yield Lyse). The lysed blood was collected and utilized further for cancer cell capture experiments.

Cell Capture

Cancer cell capture: MCF-7 cells were pre-stained with CellTrace^{TM} violet dye (Thermo Fisher Scientific, Waltham, MA, USA) according to the standard protocol and the iron nanoparticles were stained by conjugating with biotin-dye (Sulfo-Cyanin-5-PEG3-Biotin, Lumiprobe GmbH, Germany). Stained cells were divided into 1mL Eppendorf tubes, then incubate together with the FeNPs@dPG_anti-EpCAM for 40 minutes in the incubator under mild rotation (rotation speed: 10 rpm). Then the mixture was put to a strong magnet while the supernatant was carefully removed by pipetting. The remains were suspended again with DBPS/human serum/lysed blood and then analysed with Attune NxT Flow Cytometer (Thermo Fisher Scientific, Waltham, MA, USA). Cells and particles were sorted by flow cytometer according to different selection markers. Captured cells appeared with both violet and red fluorescence while the uncaptured cells expressed only violet fluorescence. (**See Figure S7**).

The capture efficiency was calculated by the equation:

$$Capture\ efficiency\ (\%) = \frac{Captured\ cell\ number}{Total\ cell\ number\ counted\ by\ FACS} \times 100\%$$

Cells or tumoroids were fixed with 4 % paraformaldehyde at room temperature for 30 min, then washed with DPBS for 3 times. The cell membranes were permeabilized with 0.25% (v/v) Triton-X 100 in DPBS for 15 min, followed by washing 3 times with DPBS. Next, Samples were treated with DAPI and Phalloidin-iFluro594 reagent (Abcam, Cambridge, United Kingdom) for 30 min, then washed with DPBS. Fluorescence images were acquired on a Zeiss Axio Observer Z1 microscope or a Leica SP8 confocal microscope.

Statistical Analysis:

All tests were performed in at least three independent sessions. The quantified data are expressed as mean ± standard deviation. GraphPad Prism software was used for statistical analysis in this study. Differences between several groups were analyzed using one-way ANOVA with the Tukey multiple comparison test, whereas difference between the two groups was analyzed through two-tailed unpaired t-tests. In the quantitative images, the differences with a probability value (p) < 0.05 were considered statistically significant, and ns indicated no statistical significance.

All the results are reported as mean ± SD. The differences among groups were determined using one-way ANOVA analysis and student's t-test; *p < 0.05, **p < 0.01, ***p < 0.001, ****p < 0.0001.

Immunofluorescence staining:

Cells or tumoroids were fixed with 4 % paraformaldehyde at room temperature for 30 min, then washed with DPBS for 3 times. The cell membranes were permeabilized with 0.25% (v/v) Triton-X 100 in DPBS for 15 min, followed by incubating with 1 % (w/v) bovine serum albumin (BSA) in PBST (0.1 % v/v Triton-X 100 in DPBS) to prevent non-specific antibody binding. Next, samples were incubated with dye-labelled primary antibodies(anti-EpCAM Fluoro488) overnight at 4 ℃, then washed with twice with PBST and three times with DPBS. Afterwards, samples were stained with DAPI for 60 minutes in room temperature, followed by washing with PBST and DPBS. Immunofluorescence images were obtained using Leica SP8 confocal microscope.

Tumor Spheroid formation:

Cancer cells were prepared as suspension in RPMI-1640 medium at concentration of 2 x 10^5 cells/ml. Hydrogels with volume of 200 µL were made in 48-well plates. After all the gel components were added and well-mixed (Table S1), 50 µL of cell suspension (containing 10^4 cells) was to be encapsulated into one hydrogel by mixing again with all the gel components. After 3 hours, the hydrogel networks were thoroughly formed. Then 300 uL of RPMI-1640 medium was added to each well with hydrogels. The hydrogels were incubated at 37 ℃ with 5 % CO_2 in the 48-well plate, medium was changed every second day. During the cell growth, bright field images of cells were obtained by Zeiss Axio Observer Z1 microscope.

Different number cell seeding was done in a similar way in 96 well plate (with 10/100/500/1000 cells seeding in hydrogel with total volume of 100 µm).

Drug screening and cell viability test

Grown tumoroids and 2D cells were treated with doxorubicin hydrochloride (DOX, Sigma-Aldrich, 98% purity), paclitaxel (PTX, Thermo-Fischer Scientific) and their combination (DOX:PTX = 1:1) at concentration of 1 µg/mL, 10 µg/mL and 30 µg/mL, respectively. After 24 h and 48 h of drug treatment, the viability of cells was performed with CellTiter-Glo® luminescent

cell viability assay according to provided protocol. Luminescence signals were measured by Spark® microplate reader (TECAN, Männedorf, Switzerland).

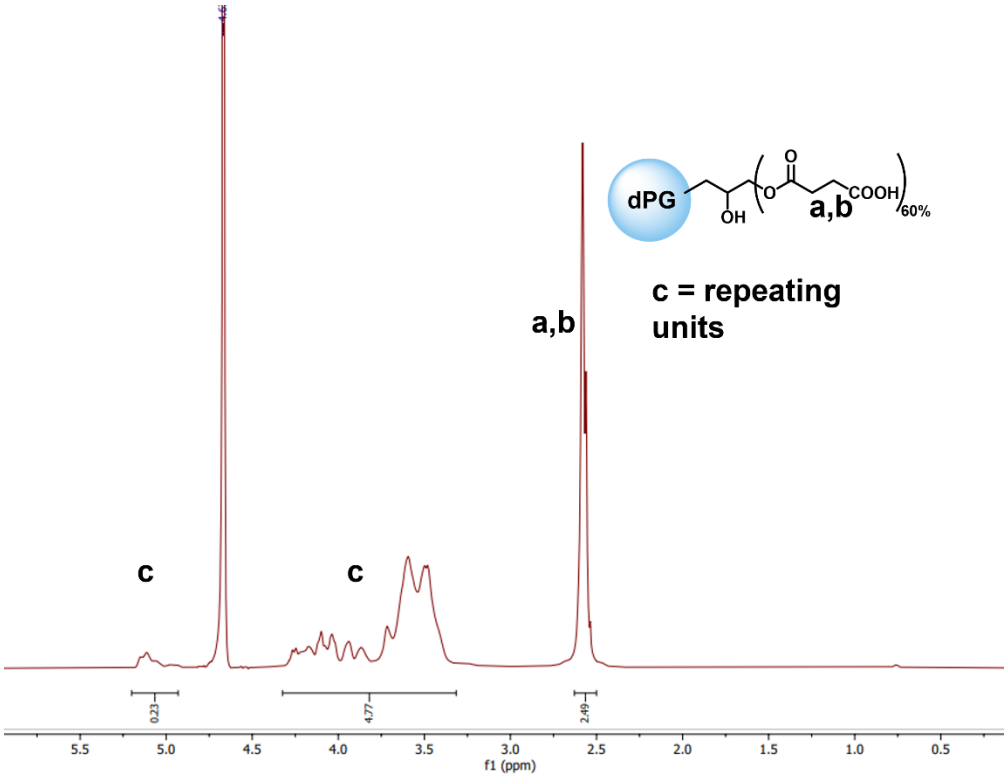

Figure S1. ^{1}H NMR (500 MHz, D_2O, δ (ppm)) of dPG-SA (dPG-succinic acid; 60% functionalized).

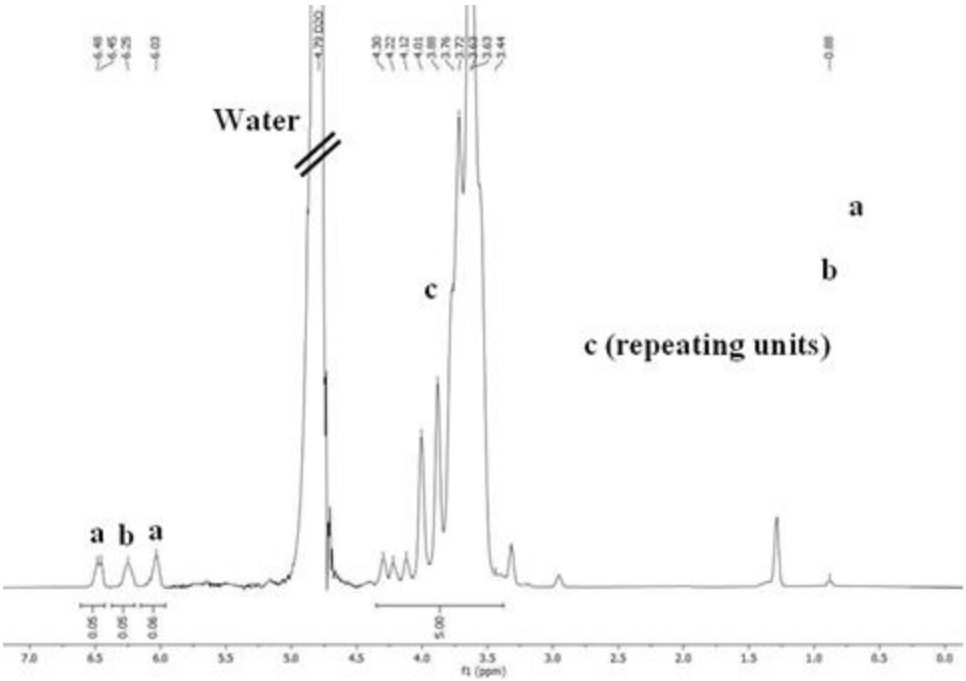

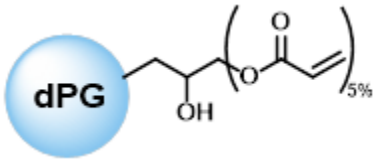

Figure S2. ^{1}H NMR (500 MHz, D_2O, δ (ppm)) of dPG-acrylate (5% functionalized).

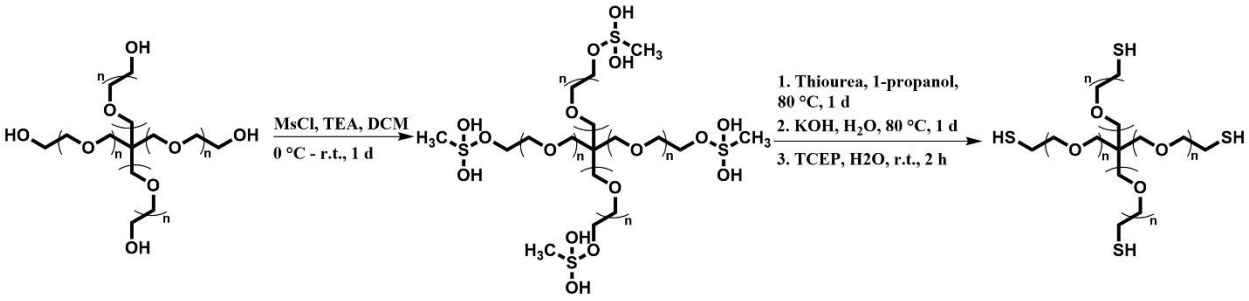

Figure S3. Synthesis of 4-arm PEG-thiol.

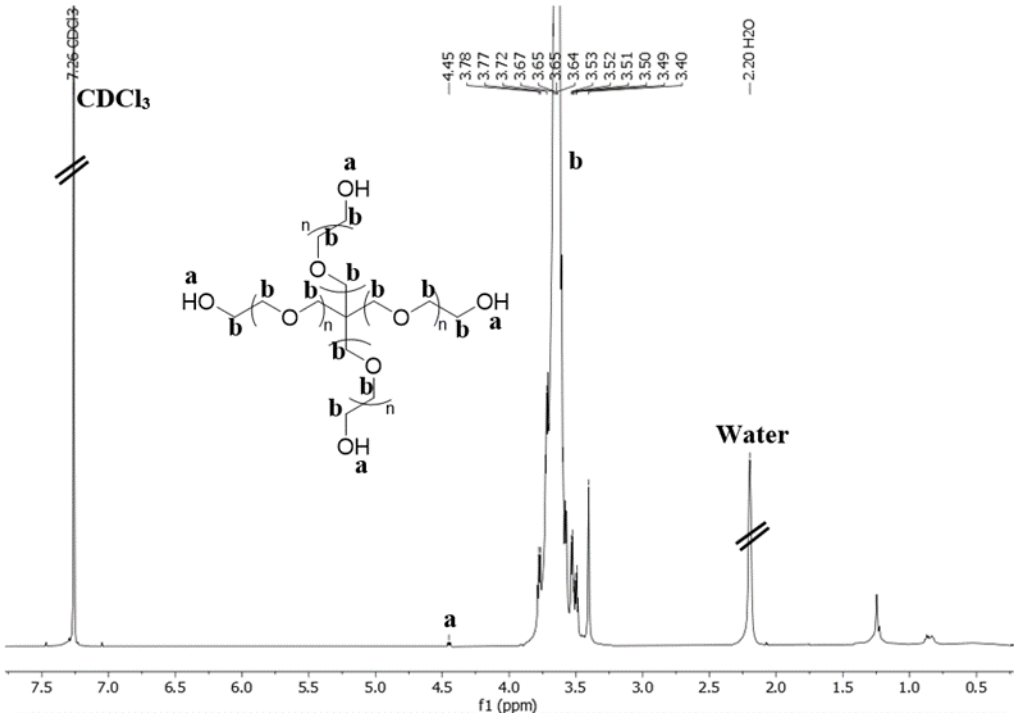

Figure S4. ^{1}H NMR (500 MHz, $CDCl_3$, δ (ppm)) of 4-arm PEG OH.

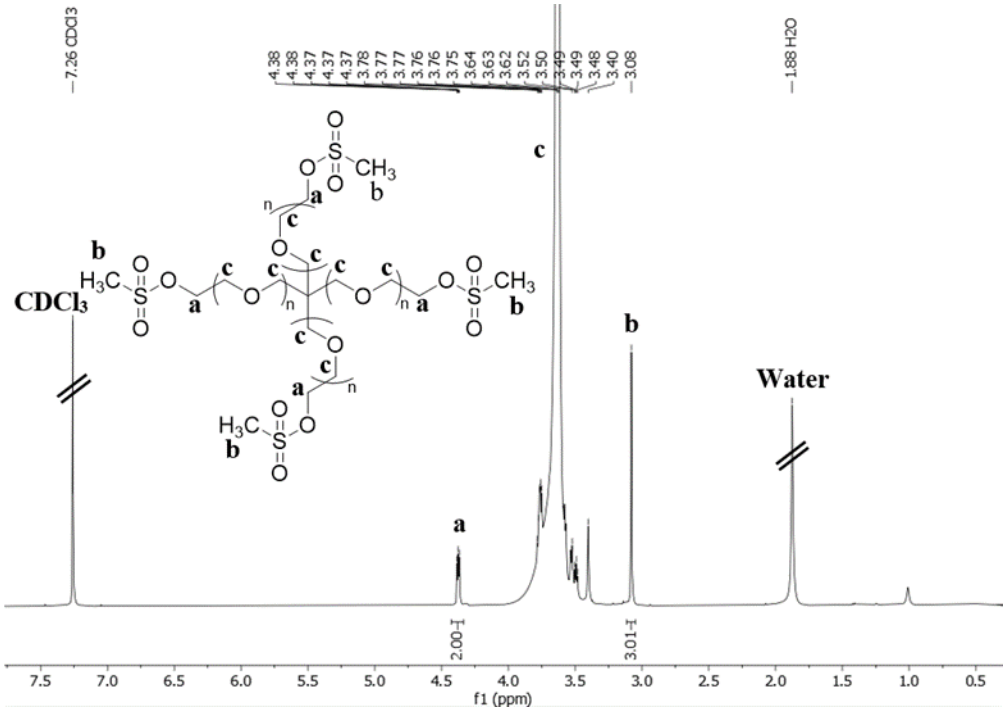

Figure S5. ^{1}H NMR (500 MHz, $CDCl_3$, δ (ppm)) of 4-arm PEG mesylate.

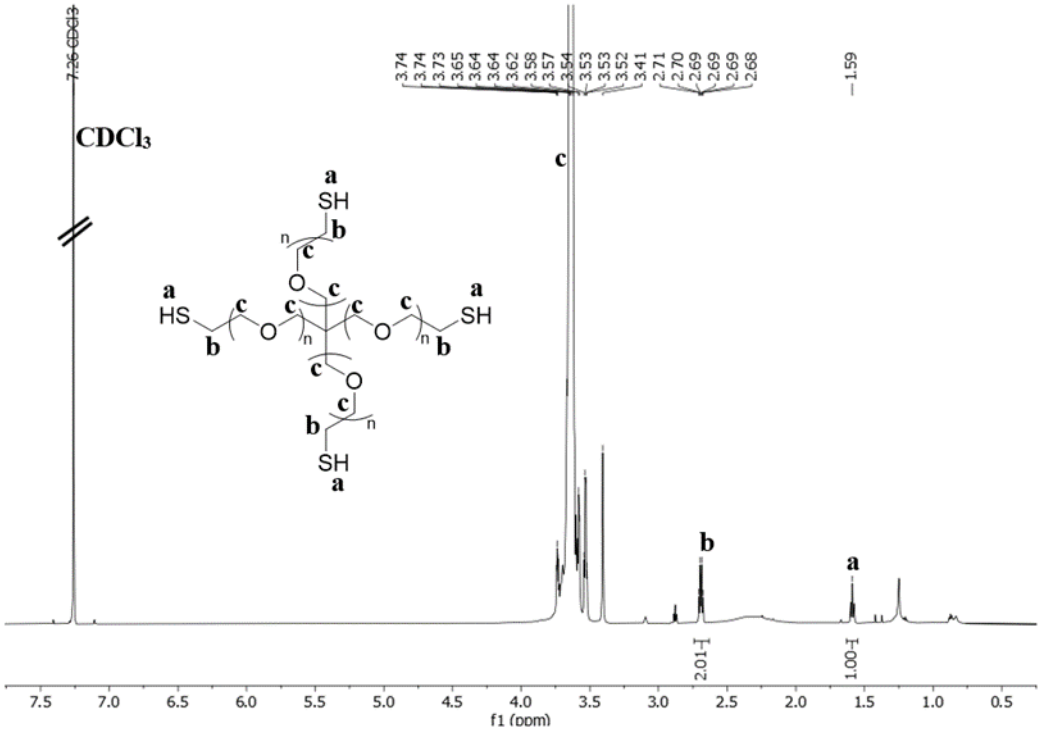

Figure S6. ^{1}H NMR (700 MHz, $CDCl_3$, δ (ppm)) of 4-arm PEG thiol.

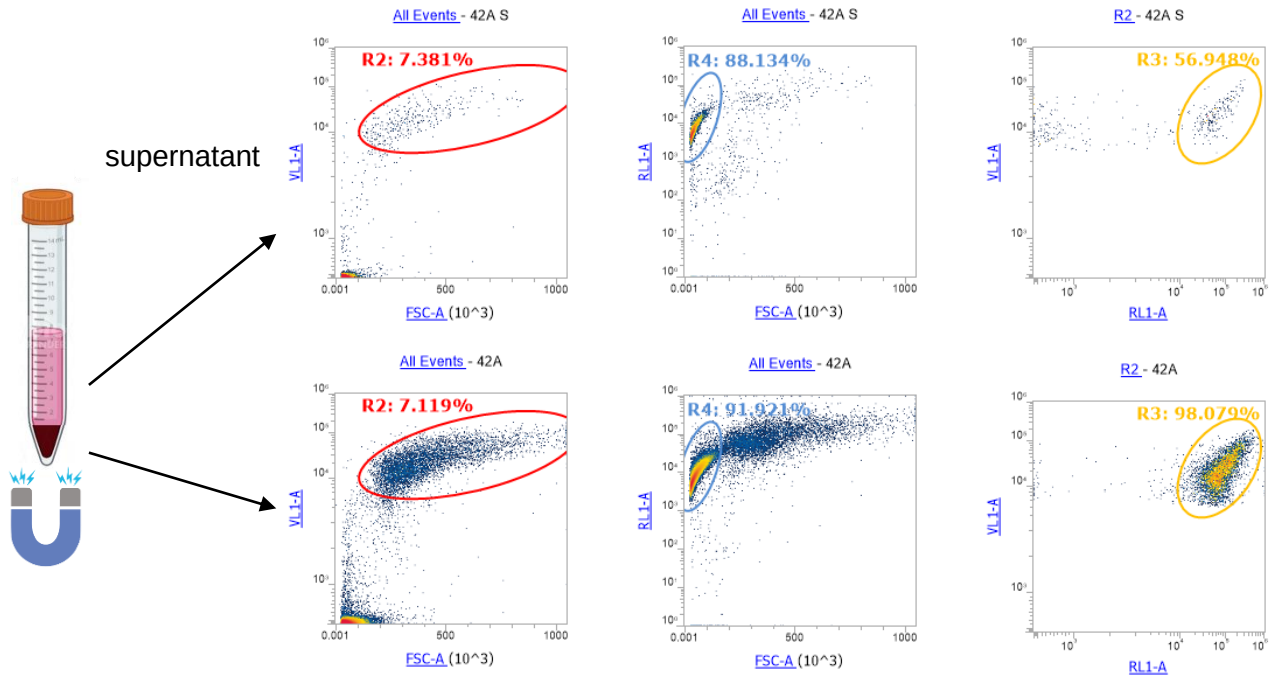

Figure S7. Representative overview of the flow cytometer analysis of immunomagnetically isolated MCF-7 cells. FeNPs were stained with red dye, MCF-7 cells were stained with violet dye, and gates were defined to progressively refine the selection. Top panel: depicts the supernatant population, Bottom panel: depicts the cells isolated after immunomagnetic isolation. R3 gate indicates the captured cells using FeNP@dPG_anti-EpCAM.

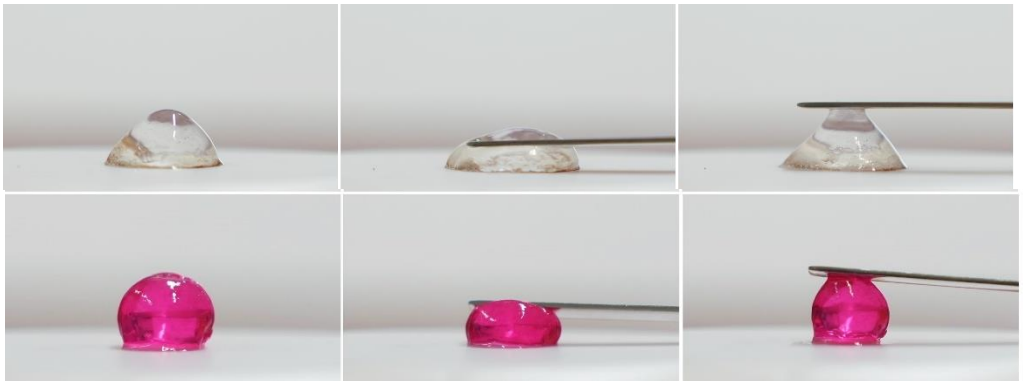

Figure S8. Motion images of = 3% gel (colorless) and 5% gel (in pink).

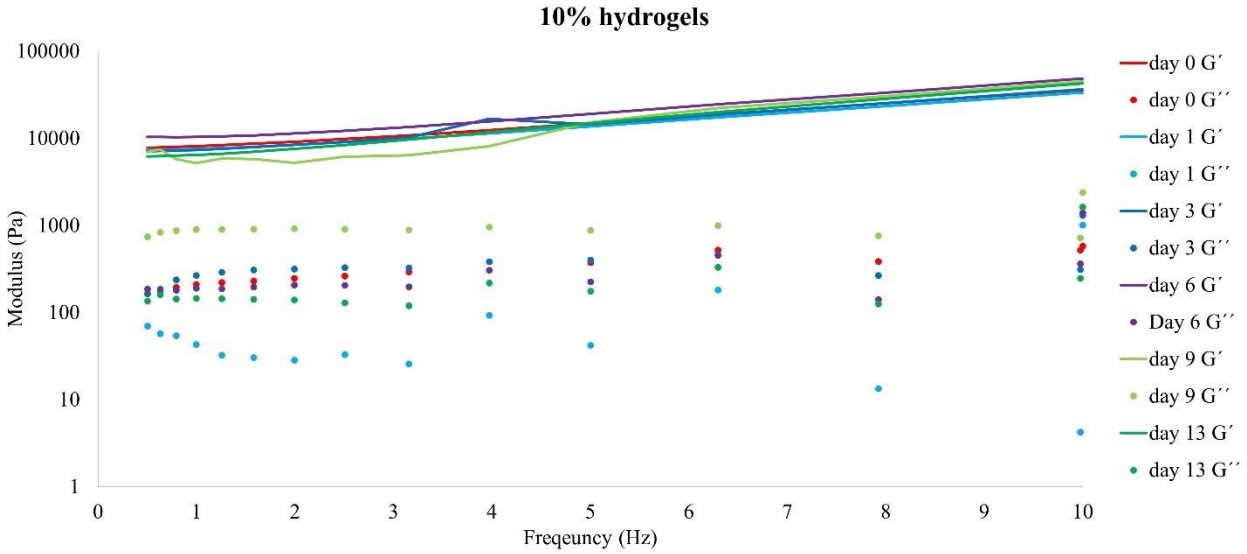

Figure S9. Storage (G´) and loss (G″) moduli as a function of frequency (Hz) for the 10% gel concentration.

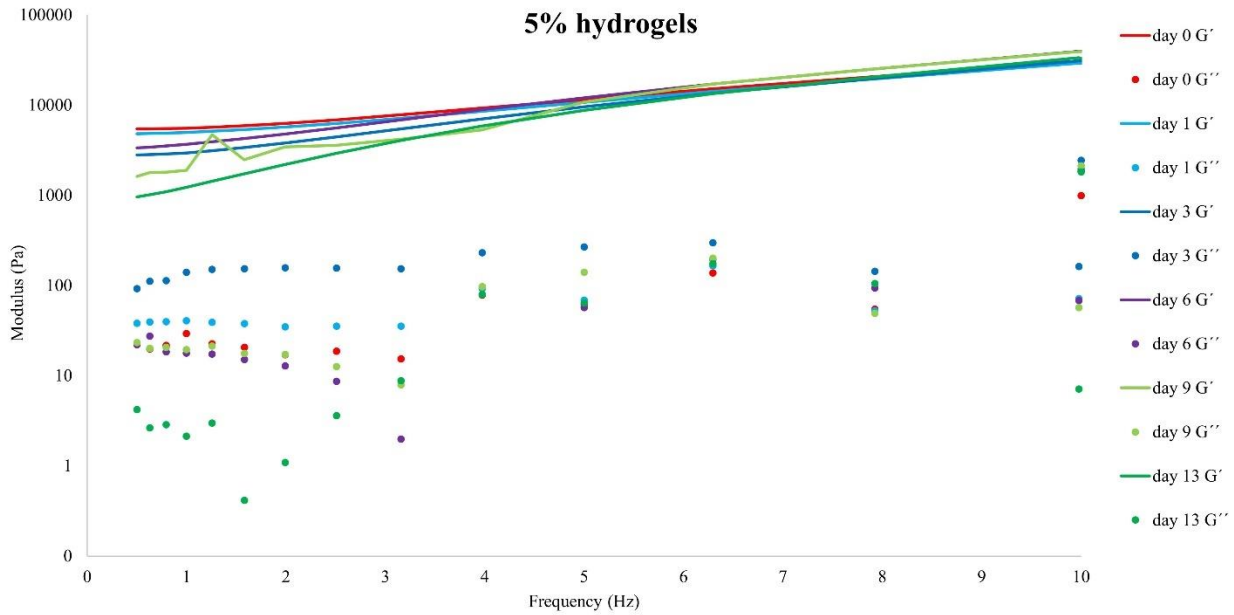

Figure S10. Storage (G´) and loss (G″) moduli as a function of frequency (Hz) for the 5% gel concentration.

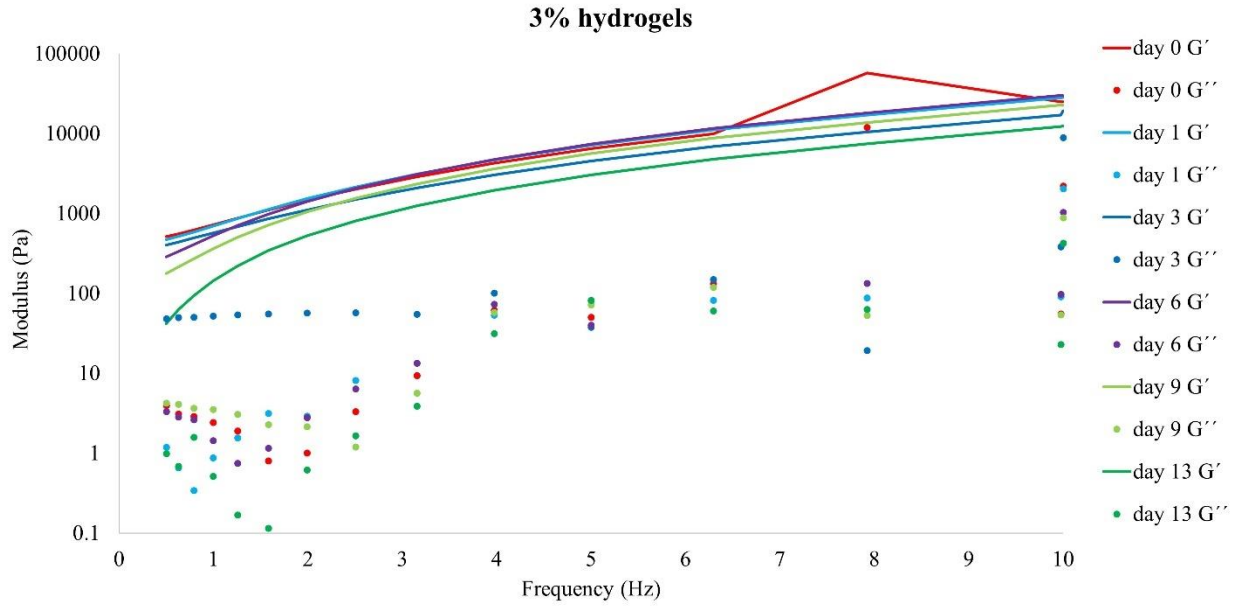

Figure S11. Storage (G´) and loss (G″) moduli as a function of frequency (Hz) for the 3% gel concentration

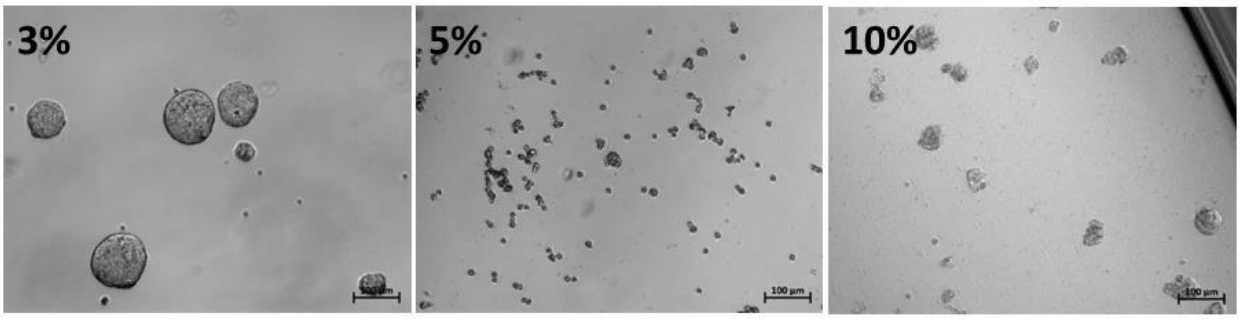

Figure S12. The tumoroid growth in different hydrogel concentrations (3, 5, 10 %).

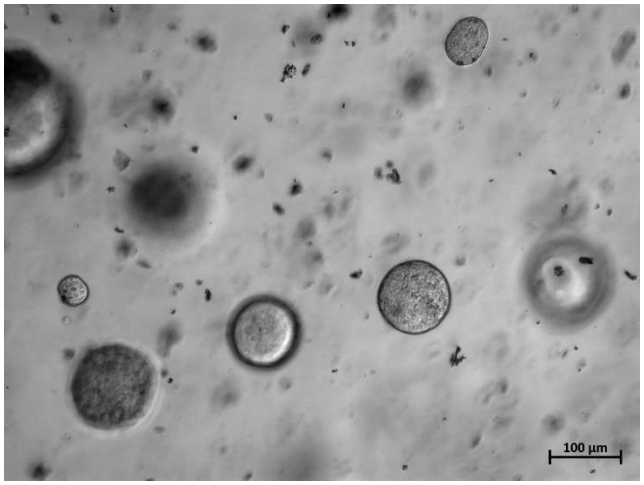

Figure S13. Brightfield image illustrating the expansion of MCF-7 cells (after immunomagnetic isolation) into 3D tumoroid when incubated in 3% hydrogel (dPG-acrylate based). The image depicts the expansion of tumor spheroids in different planes of hydrogel.

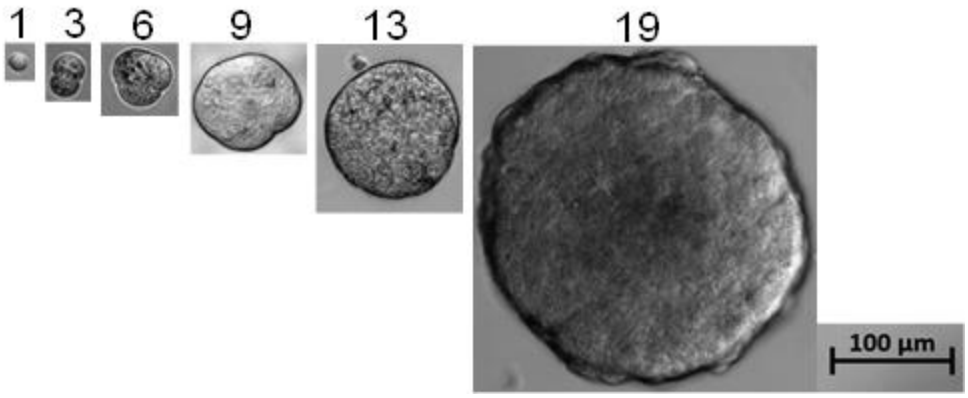

Figure S14. Brightfield images illustrating the expansion of MCF-7 cells (without immunomagnetic isolation) into 3D tumoroid when incubated in 3% hydrogel (dPG-acrylate based)

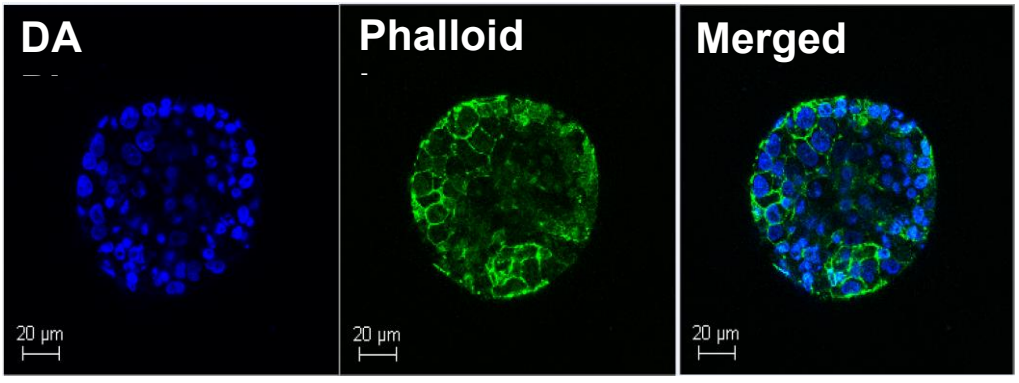

Figure S15. Confocal microscopy images of 3D tumoroid cultured for 15 days, stained with DAPI (nuclei), Phalloidin Fluoro594 (cellular cytoskeleton).

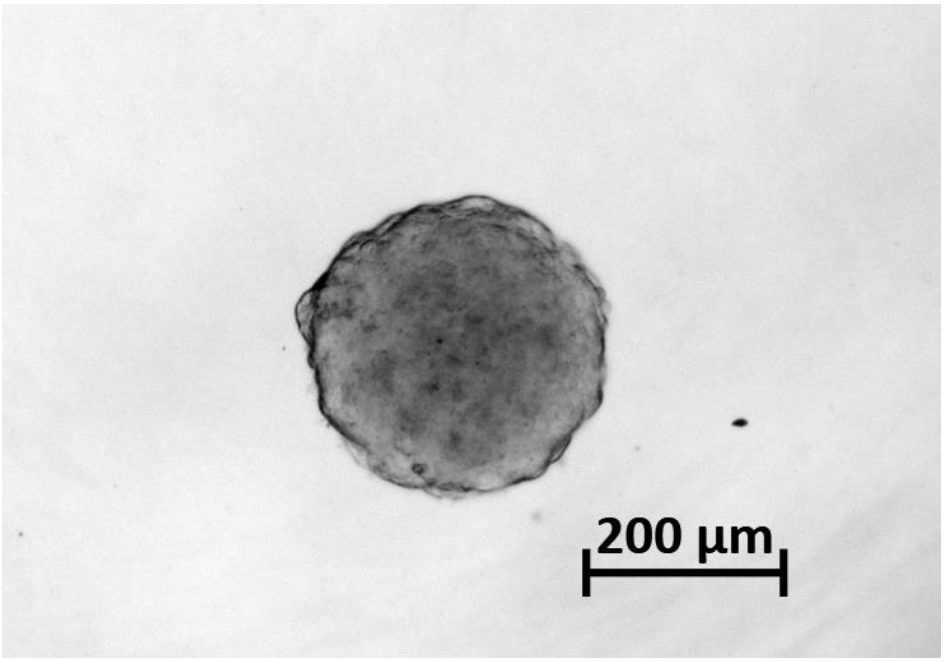

Figure S16. MCTS grown from 10 MCF-7 cells seeded within the hydrogel.

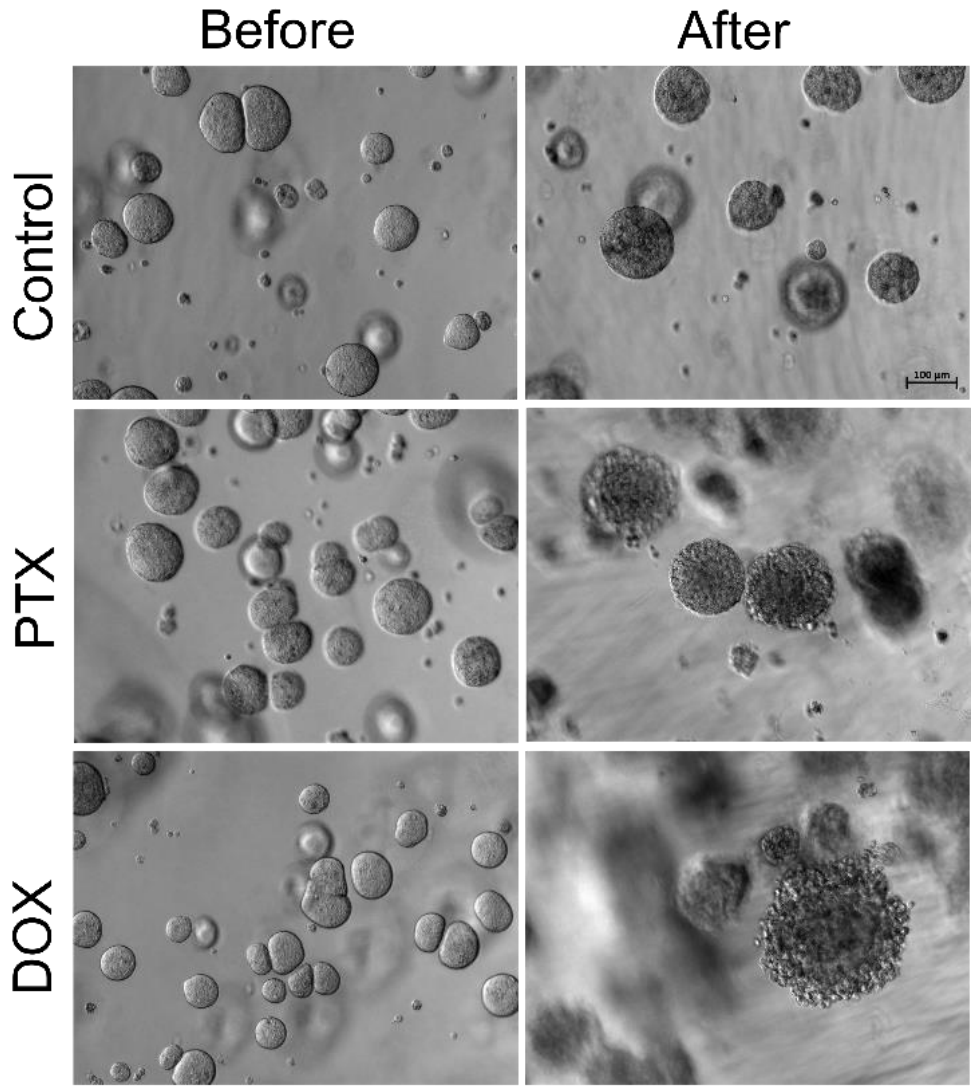

Figure S17. The morphological changes in grown tumoroids grown using the polyglycerol-based hydrogel on impact of different anticancer drugs, paclitaxel (PTX), doxorubicin (DOX).

Table S1. Preparation of the MCF-7 encapsulated *in situ* hydrogel formation at different gel concentration and different numbers of cells encapsulated.

No.	PEG(10% w/v)		dPG(24.5% w/v)		MCF-7*	PBS	Total	Conc.
	Volume (µL)	Mol (µmol)	Volume (µL)	Mol (µmol)	Amount (cells)	volume (µL)	volume (µL)	(%w/v)
1	55	0.55	18.5	0.45	3000	16.5	100	10
2	27.7	0.28	9.3	0.23	3000	53	100	5
3	16.7	0.17	5.7	0.14	3000	67.6	100	3
4	16.7	0.17	5.7	0.14	1000	67.6	100	3
5	16.7	0.17	5.7	0.14	500	67.6	100	3
6	16.7	0.17	5.7	0.14	100	67.6	100	3
7	16.7	0.17	5.7	0.14	10	67.6	100	3

*The volume of MCF-7 solution added is always 10 µL.

Table S2. Dose dependent effect of different drugs on grown 3D tumoroids in comparison to control hydrogels (with no drug treatment) in dPG based hydrogel over an incubation time of 24 h and 48 h.

Drugs	Dosage (µg/mL)	% Live cells	
		24 h post-drug treatment	48 h post-drug treatment
Doxorubicin	1	96.71 ± 0.16	88.25 ± 0.05
	10	71.94 ± 0.16	54.01 ± 0.08
	30	70.50 ± 0.10	45.46 ± 0.01
Paclitaxel	1	109.17 ± 0.14	70.28 ± 0.09
	10	93.51 ± 0.14	70.23 ± 0.11
	30	69.88 ± 0.12	85.58 ± 0.14

References

[1] aA. Sunder, R. Hanselmann, H. Frey, R. Mülhaupt, *Macromolecules* **1999**, *32*, 4240-4246; bR. Haag, A. Sunder, J.-F. Stumbé, *Journal of the American Chemical Society* **2000**, *122*, 2954-2955.

[2] M. Wallert, J. Plaschke, M. Dimde, V. Ahmadi, S. Block, R. Haag, *Macromolecular Materials and Engineering* **2021**, *306*, 2000688.

[3] J. Park, K. An, Y. Hwang, J.-G. Park, H.-J. Noh, J.-Y. Kim, J.-H. Park, N.-M. Hwang, T. Hyeon, *Nature Materials* **2004**, *3*, 891-895.

[4] J. Sherwood, Y. Xu, K. Lovas, Y. Qin, Y. Bao, *Journal of Magnetism and Magnetic Materials* **2017**, *427*, 220-224.

[5] B. Thongrom, M. Dimde, U. Schedler, R. Haag, *Macromolecular Chemistry and Physics* **2023**, *224*, 2200271.

4.3 Polyglycerol-Based Hydrogel as Versatile Support Matrix for 3D Multicellular Tumor Spheroid Formation

Boonya Thongrom[1], Peng Tang[1], Smriti Arora*, Rainer Haag*

Gels **2023**, *9*, 938

https://doi.org/10.3390/gels9120938

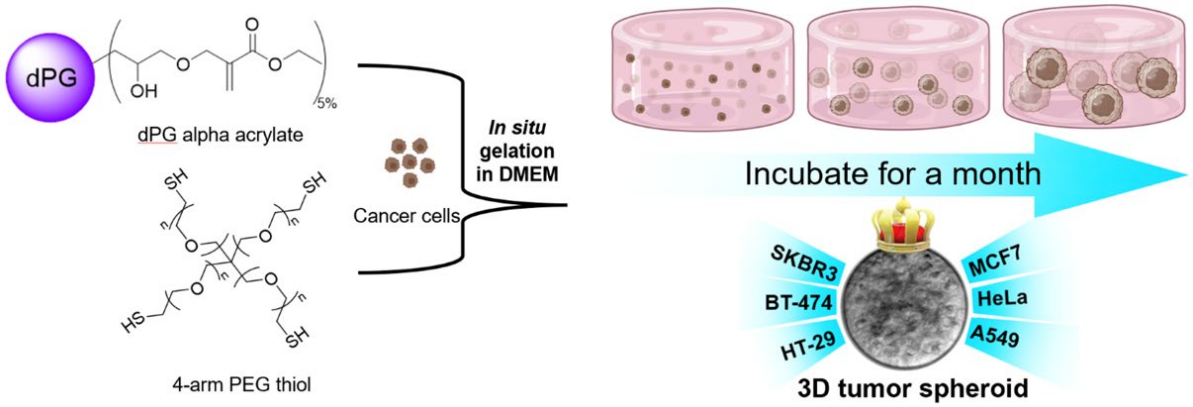

Figure 17: Graphical abstract of project 3. Reprinted with permission from ref.[167] Copyright 2023 MDPI

Contributions of authors: In this publication, Boonya Thongrom and Peng Tang are shared first authors. Boonya Thongrom synthesized all the hydrogel components and characterized them, wrote the hydrogel-related part of the manuscript. Peng Tang researched all the biological related part of the project including the cell seeding, culture and characterizations, wrote the biological part of the manuscript. Both Boonya Thongrom and Peng Tang took care of the revision procedures. Smriti Arora wrote the introduction part of the manuscript and along with Rainer Haag, they both supervised the project and offered suggestions and guidance, proofread the manuscript.

gels

MDPI

Article

Polyglycerol-Based Hydrogel as Versatile Support Matrix for 3D Multicellular Tumor Spheroid Formation

Boonya Thongrom †, Peng Tang †, Smriti Arora * and Rainer Haag *

Institute for Chemistry and Biochemistry, Freie Universität Berlin, Takustr. 3, 14195 Berlin, Germany; peng.tang@fu-berlin.de (P.T.)
* Correspondence: smriti@zedat.fu-berlin.de (S.A.); haag@zedat.fu-berlin.de (R.H.)
† These authors contributed equally to this work.

Abstract: Hydrogel-based artificial scaffolds are essential for advancing cell culture models from 2D to 3D, enabling a more realistic representation of physiological conditions. These hydrogels can be customized through crosslinking to mimic the extracellular matrix. While the impact of extracellular matrix scaffolds on cell behavior is widely acknowledged, mechanosensing has become a crucial factor in regulating various cellular functions. cancer cells' malignant properties depend on mechanical cues from their microenvironment, including factors like stiffness, shear stress, and pressure. Developing hydrogels capable of modulating stiffness holds great promise for better understanding cell behavior under distinct mechanical stress stimuli. In this study, we aim to 3D culture various cancer cell lines, including MCF-7, HT-29, HeLa, A549, BT-474, and SK-BR-3. We utilize a non-degradable hydrogel formed from alpha acrylate-functionalized dendritic polyglycerol (dPG) and thiol-functionalized 4-arm polyethylene glycol (PEG) via the thiol-Michael click reaction. Due to its high multivalent hydroxy groups and bioinert ether backbone, dPG polymer was an excellent alternative as a crosslinking hub and is highly compatible with living microorganisms. The rheological viscoelasticity of the hydrogels is tailored to achieve a mechanical stiffness of approximately 1 kPa, suitable for cell growth. Cancer cells are in situ encapsulated within these 3D network hydrogels and cultured with cell media. The grown tumor spheroids were characterized by fluorescence and confocal microscopies. The average grown size of all tumoroid types was ca. 150 µm after 25 days of incubation. Besides, the stability of a swollen gel remains constant after 2 months at physiological conditions, highlighting the nondegradable potential. The successful formation of multicellular tumor spheroids (MCTSs) for all cancer cell types demonstrates the versatility of our hydrogel platform in 3D cell growth.

Keywords: polyglycerol-based hydrogel; thiol-Michael click reaction; stiffness; ECM-mimicking platform; 3D tumor spheroids

Citation: Thongrom, B.; Tang, P.; Arora, S.; Haag, R. Polyglycerol-Based Hydrogel as Versatile Support Matrix for 3D Multicellular Tumor Spheroid Formation. *Gels* **2023**, *9*, 938. https://doi.org/10.3390/gels9120938

Academic Editor: Yuqi Jin

Received: 1 November 2023
Revised: 21 November 2023
Accepted: 25 November 2023
Published: 29 November 2023

1. Introduction

There is a strong emphasis on developing promising strategies to advance therapeutic approaches, including tissue engineering, regenerative medical treatments, and personalized therapies [1–3]. These strategies involve the extraction of a patient's cells and their encapsulation within a three-dimensional scaffold. This scaffold serves as a temporary structural support for in vitro cell/tissue culture. Ideally, the scaffold's design should closely mimic the composition, rigidity, and structure of the native tissue's extracellular matrix or enable cells to remodel it, creating an environment conducive to cell function [4,5]. It is well recognized that the rigidity of the extracellular matrix plays a critical role in influencing cell behavior, such as spreading [6], migration [7], proliferation [8], and stem cell differentiation [9]. Thus, the development of a three-dimensional matrix with adjustable dynamic properties to replicate the temporal, structural, and mechanical aspects of extracellular matrix dynamics is of utmost importance in understanding its impact on

cell behavior [10–15]. An oversimplified 2D model, which lacks tumor microenvironment and tumor heterogeneity, does not meet the requirements for advanced biological analysis. However, ethical problems evoked by animal experiments are not to be neglected. In order to bridge the gap between 2D cell cultures and in vivo models, it is necessary to establish multicellular tumor spheroids (MCTSs) models [16]. The traditional methodologies for tumoroid fabrication, e.g., hanging droplets and [17]. non-adherent plate cultures [18], can form large tumoroids relatively fast. However, these techniques are still limited in their applications, lacking further support for long time preservation. Employing hydrogels as a platform for 3D culture not only can offer cell suspension and nonadherent conditions for aggregation into multicellular tumor spheroids (MCTSs) but also allows cancer stem cells (CSCs) expansion in a controllable manner [19].

Hydrogels, particularly synthetic ones, have emerged as primary candidates for in vitro cell/tissue culture due to their ability to closely mimic native cellular environments, including matrix rigidity [20], and sequester proteins [21]. Native tissues exhibit a wide range of stiffness, from soft brain tissue (260–490 Pa) to stiffer bone tissue (2–4 GPa) [22]. The mechanical rigidity of the matrix is a critical factor in modulating cell interactions with the surrounding extracellular matrix (ECM) and thereby influences fundamental cellular processes. The choice of a hydrogel is contingent upon the specific experimental requirements, such as the needed stiffness, optical characteristics, and conductive properties. One example of a synthetic hydrogel is using crosslinked polymers where the crosslinking between individual polymer molecules maintains the overall 3D structure of the hydrogel after it swells in an aqueous medium. When used for 3D cell culture, it is essential that not only the polymer material but also the crosslinking reaction is compatible with cell viability. Furthermore, the hydrogel's stiffness and the pore architecture can be tuned by using two main approaches: varying the concentration of crosslinkers in the pre-polymer solution and adjusting the degree of polymerization.

Generally, a synthetic polymeric gel precursor comprising several hydroxy groups, and a polyether backbone like polysaccharides, can be an excellent option for the fabrication of a hydrogel since it provides hydrophilicity toward water which is vital to all living beings and is inert to microorganisms [23,24]. Dendritic polyglycerol (dPG), a bioinert multivalent polyether polymer, can be a potential alternative gel precursor for the formationof a hydrogel network. With the benefit of a large number of multivalent hydroxy groups on the surface of dPG, any postpolymerization modifications of potential moieties including crosslinking functional groups can be made with ease. Furthermore, dPG serves as a biocompatible material and has been studied exclusively in the field of biomedical applications [25–27]. The polyether-polyol scaffold is therefore an ideal hub for fabricating a biocompatible hydrogel network.

The primary objective of this study is to uncover the distinct roles of matrix stiffness in regulating the 3D culture patterns of different cancer cell lines originating from different cancerous tissues. This investigation is conducted using a non-degradable hydrogel system based on cytocompatible bioinert dendritic polyglycerol (dPG) and 4-arm polyethylene glycol (4-arm PEG). These 2 combinations are excellent not only for building biocompatible hydrogels but also for cost-effective upscale synthesis based on thiol-click chemistry. Notably, key matrix properties such as swelling capacity and hydrolytic stability remain constant.

2. Results and Discussion

2.1. Synthesis of Gel Precursors and Hydrogel Formation

The hydrogel was specifically designed to facilitate the growth of cancer cells, which are embedded in situ during the gelation process. The primary objective for this hydrogel is to maintain a stable and durable crosslinked structure that can securely hold the encapsulated cells within a 3D network for an extended period until a noticeable increase in their size is observed. The gel stiffness and consistency were influenced by the previous study from our group [28]. In the former study, we showed that cancer cell MCF7 could

grow well in a 3D softer texture gel matrix whose shear storage modulus or stiffness is approximately in the range of 0.1–0.7 kPa and they successfully formed multicellular tumor spheroids (MCTSs) after the incubation for roughly 2 weeks. With this result, we have been inspired to further investigate the growth of other cancer cell lines by using the same hydrogel components which are dendritic polyglycerol (dPG) as a multivalency hub and 4-arm polyethylene glycol (4-arm PEG) as a crosslinker. The average size of the synthesized dPG polymer used in this study is approximately 10 kDa, based on a chromatogram result from Gel Permeation chromatography (GPC), and its hyperbranched architecture is demonstrated in Figure 1. However, the degradability has been modified in this study in order to prolong the stability of a hydrogel for intensive monitoring of MCTSs growth in a long incubation period.

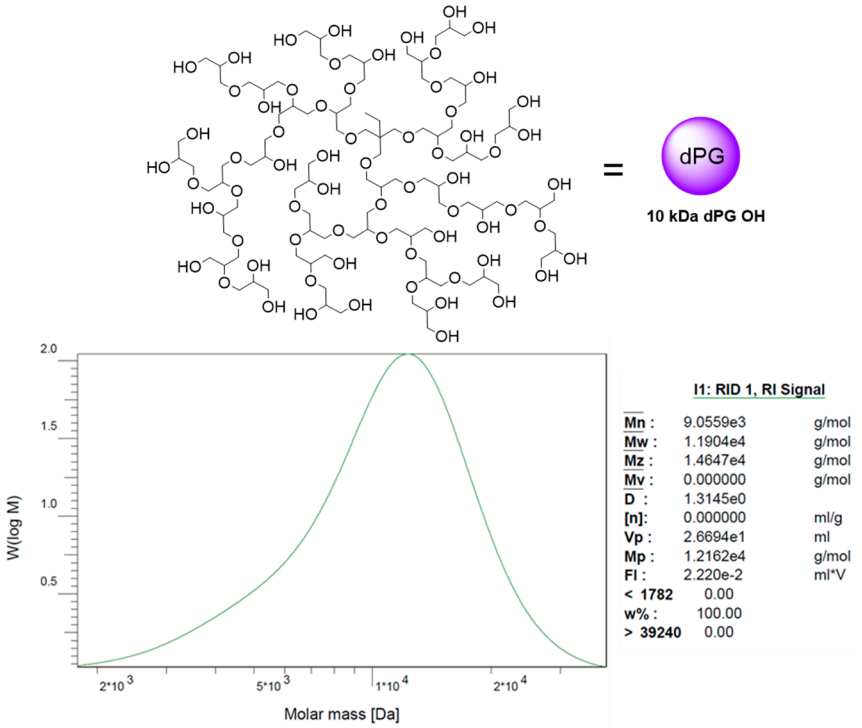

Figure 1. GPC chromatogram of 10 kDa dendritic polyglycerol (dPG) and illustrating picture of dPG structure.

dPG was designed to be functionalized with a nondegradable functional group which has similar reactivity as the acrylate group in the previous study. By using ethyl 2-(bromomethyl) acrylate as a reagent, the dPG alpha-acrylate was synthesized (Figure 2). This alpha-acrylate moiety serves as a nondegradable part of a hydrogel, with only ether and thioether bonds forming after the synthesis and gelation respectively [29]. The number of alpha-acrylate moieties decorated on the dPG was approximately 7 groups (the calculation can be seen in Supplementary Information). On the other hand, the crosslinker 4-arm PEG thiol was synthesized following the previous reports [30,31] with slight modification, thereby obtaining 4-arm PEG thiol with approximately 3.5 thiol groups, determined from Ellman's assay (Figure 2).

The hydrogel is formed through a Michael addition reaction between the alpha-acrylate part and the thiol part by combining both gel components, including dPG alpha-acrylate and 4-arm PEG thiol, in either an aqueous solution or cell culture medium, as depicted in Figure 2. In the case of the encapsulation of cancer cells, both gel components and a culture medium solution containing the cancer cells were prepared and simultaneously loaded into a well within a 48-well plate (refer to Supplementary Information for specific details). After forming the hydrogel, it was allowed to set for approximately 4 h before the addition of culture medium for the subsequent cell growth experiment.

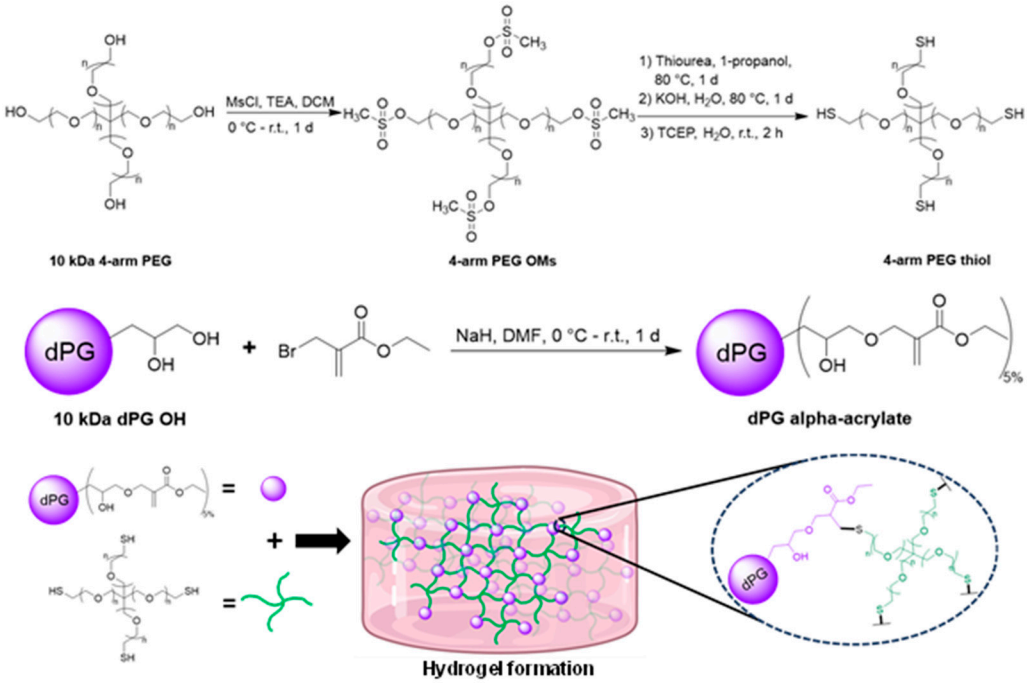

Figure 2. Synthetic routes of dPG alpha acrylate and 4-arm PEG thiol, and the schematics showing hydrogel formation.

2.2. Characterizations of Hydrogel

As mentioned in the earlier study, the optimal storage modulus or stiffness for the ideal 3D matrix consistency for cancer cell growth falls within the range of 0.1–0.7 kPa. Therefore, we fine-tuned the hydrogel stiffness and determined that at a gel concentration of 3% *w*/*v* and a mole ratio of 3:1 between dPG alpha-acrylate and 4-arm PEG dithiol, the gel exhibited an approximate stiffness of 1 kPa, showing soft texture (Figure 3c,d).

The hydrogel created with dPG alpha-acrylate and 4-arm PEG thiol is typically non-degradable, primarily because of its ether and thioether linkages. This is in contrast to our earlier studies, where we employed degradable hydrogels linked by acrylate groups containing degradable ester bonds [28,30]. To prove the degradation concept, we, therefore, performed the degradation study for 2 weeks by using the hydrogel candidate without encapsulating cells. The gel sample was incubated at 37 °C with an excess of culture medium and the gel was picked at each time point for the rheological characterization of a shear storage modulus performed by rheometer. The resulting graph of shear storage (G′) and loss (G″) moduli of the sample at different time points (1 d, 3 d, 6 d, 9 d, 12 d, and 14 d) is shown in Figure 3a. By analyzing the storage modulus (G′) which represents the solid behavior or energy storage inside the chemically crosslinked networks, it is obvious that there is no difference between the G′ of 1 d, 6 d, and 14 d gel incubation. In addition, we can simply investigate the stiffness which represents a G′ value picked at 1 Hz, and the mesh size which was calculated from the stiffness value. The stiffness bar chart shows that sample at different incubation times has quite comparable stiffness value at approximately 0.9–1 kPa (Figure 3b). Similarly, the hydrogel mesh size of each time point also shows the same value close to 20 nm (Figure 4a). These results, hence, support that the hydrogel is unable to degrade in a cell culture medium at physiological pH and temperature for at least 2 weeks of incubation.

Besides the rheological data, the hydrogel sample was characterized by a mass swelling ratio. This mass swelling ratio can be calculated by dividing the mass of a swollen gel by the mass of a dried gel [32]. The hydrogel samples at day 1, day 6, and day 14 of incubation were chosen and the resulting mass swelling ratio can be seen in Figure 4b. From the bar chart, the gel samples at all 3 different time points show a high-water swelling capacity up to approximately 25 times from the dried state. The viscosity data obtained from a

viscosity test with shear rate ramping from 0.1 to 10 s^{-1} in 2 min of the sample at different incubation times was also present (Figure S6). The data show the shear thinning behavior of the hydrogel, meaning that it has a lower viscosity at a higher shear rate. Based on the findings related to mass swelling ratio, shear stiffness, and viscosity, we anticipate that the sample should possess a soft texture with excellent network flexibility. We aimed to have this hydrogel effectively serve as a supportive ECM-mimicking platform for the formation of 3D multicellular tumor structures.

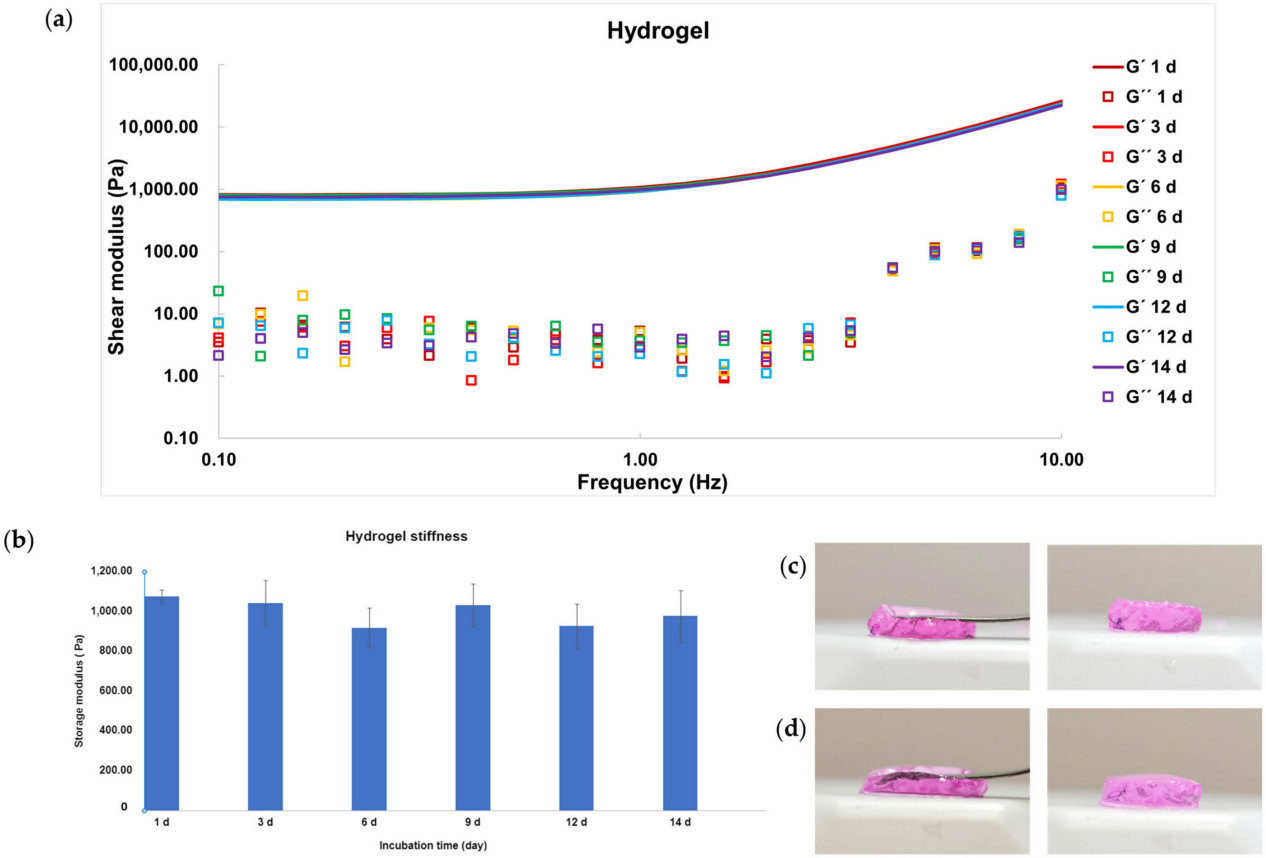

Figure 3. Hydrogel characterization: (**a**) Shear modulus graph performed by frequency sweep test at 37 °C of hydrogel sample at different incubation times; (**b**) Stiffness bar chart obtained from G′ value at 1 Hz from frequency sweep test of hydrogel sample at each incubation time; (**c**,**d**) Photographs of hydrogel prepared by using culture medium at 1 day and 14 days of incubation, respectively.

2.3. Formation of 3D Multicellular Tumor Spheroids (MCTSs)

To closely mimic the mechanical properties of extracellular matrix (ECM) for studying cell-environment interactions in ex vivo models, hydrogels emerge as an excellent choice due to their straightforward tunability [26]. Acrylate-based hydrogels are notable for their impressive biocompatibility and intriguing mechanical attributes [28,30,33]. Therefore, a meticulously engineered acrylate-based hydrogel platform greatly enhances the feasibility of various cellular investigations.

In order to demonstrate the potential of our alpha-acrylate hydrogel in ECM-mimicking applications, we utilize the hydrogel as a 3D scaffold for tumor spheroid formation. Employing hydrogels as a platform for 3D culture not only can offer cell suspension and nonadherent conditions for aggregation into MCTSs but also allows cancer stem cells (CSC) expansion in a controllable manner [19]. To explore how hydrogels accommodate and facilitate cell growth, we adjusted the mechanical properties of the hydrogels based on our prior research findings [28]. We discovered that softer gels, with a stiffness of around 1 kPa, promote cell expansion into tumor spheroids. Therefore, 3% of hydrogel was

chosen. At this concentration, the gelation took place slowly, allowing the homogenous distribution of the cell suspension in the mixture to avoid aggregation and precipitation. After around 5 min, a relatively strong network formed, where the cells positions were fixed. Complete gelation was achieved in 30 min, then the cell medium was added. We chose 6 different cell lines, A549 (human lung cancer), BT-474 (ER/HER2-positive human breast cancer), MCF-7 (human breast cancer), HeLa (human cervical cancer), HT-29 (human colorectal cancer), and SK-BR-3 (HER2-positive human breast cancer), for encapsulation in the well-tuned hydrogel. The growth was monitored by using brightfield microscopy. The encapsulated cells were homogeneously distributed in the hydrogel and were nourished by cell medium (Figure S7). At first, single cells expanded into small spheroids with the support of the hydrogel's structure. As the hydrogel swelled, the mesh size of the network increased, providing a highly flexible network environment for the spheroids to grow into larger tumor spheroids. Besides, due to the dynamic nature of the hydrogel, higher cell concentration in the later stages of the culture allowed cells to aggregate into substantially bigger tumor spheroids (Figure 5a,b). All cell lines successfully formed tumor spheroids after 3 weeks of culture. Notably, the growth patterns were similar across all the cell lines despite their distinct cell types and characteristics. In Figure 5c, a 3D scan of a stained tumor spheroid was imaged under a confocal microscope. Due to the limitation of the microscope, only the upper part of the tumor spheroid was presented. The sphere clearly demonstrated that the cells not only aggregated into clusters but formed spherical morphology, thereby developing into MCTSs.

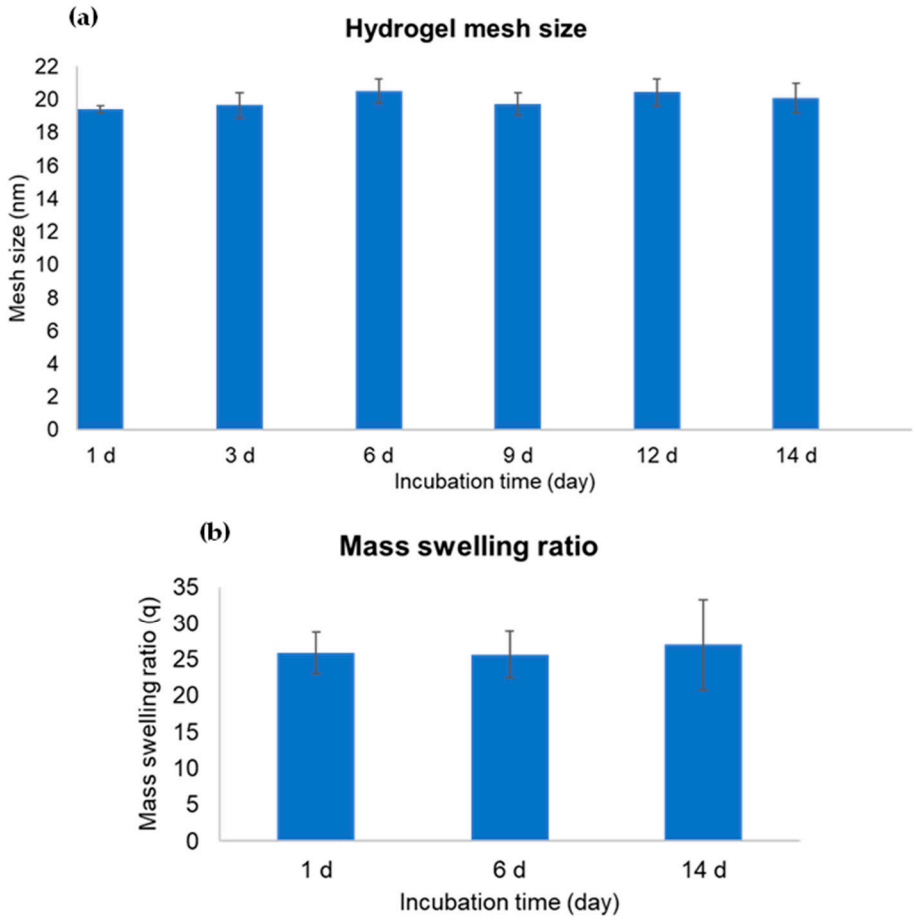

Figure 4. Hydrogel characterization: (**a**) Mesh size bar chart calculated from the stiffness value of the gel sample at each incubation time; (**b**) Mass swelling ratio of hydrogel sample at different incubation times.

The A549 cell line grew into tumor spheroids with an average size of 149.87 µm, with an average size of 134.19 µm for HeLa, 126.59 µm for HT-29, 112.07 µm for BT-474, 137.56 µm for MCF-7 and 157.86 µm for SK-BR-3 was observed after 25 days of incubation, respectively (Figure 6a). The microscopic images show the progression of the tumor spheroids from Day 1 to Day 25. All grown tumor spheroids are of similar shape with different sizes (Figure 5a,b). The difference could be attributed to the preferences of different cell lines in the tumor microenvironment (TME). The spheroid growth is influenced not only by the hydrogel's stiffness but also by the compatibility of the mesh size with the rate of growth, which can impose constraints on expansion. Observations revealed that tumor spheroids tend to be larger with the size of 150–200 µm when positioned on the upper surface of the hydrogel, comparing to those at the bottom of the gel (~50 µm). This is because they benefit from improved access to oxygen and fresh cell medium. Furthermore, a relatively greater swollen hydrogel layer and increased network flexibility anticipated at the interface could facilitate tumoroids to grow bigger. MCTSs with relatively homogeneous size distributions can be observed in Figure S7. Nevertheless, the evidence demonstrates that alpha-acrylate hydrogel can serve as a universal platform for tumor spheroid's growth while remaining structurally stable even after being immersed in a cell medium for a duration of two months (Figure 6b). This nondegradable nature ensures consistent stiffness over the desired timeframe, preserving the microenvironment necessary for specific cell lines. Unlike degradable hydrogels, which alter in stiffness through degradation, this characteristic raises the potential for a 3D culture of organoids, particularly considering the extended culture period required in contrast to tumoroids. It also holds promise for applications in tissue engineering and stem cell research.

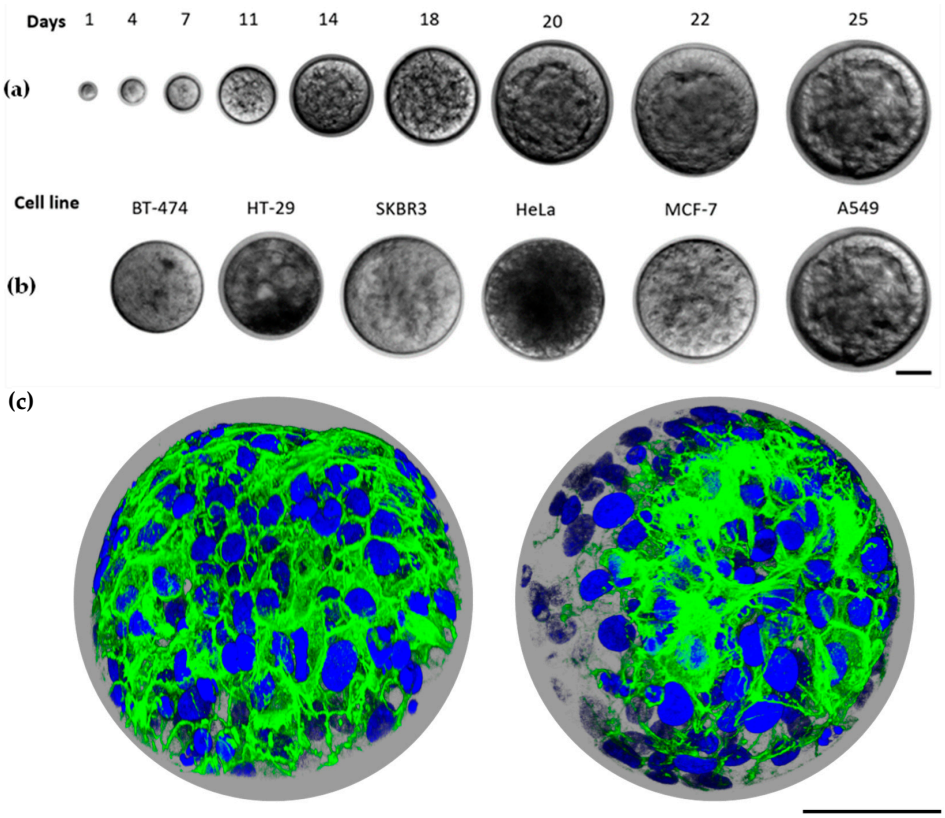

Figure 5. Tumor spheroids growth in the hydrogel: (**a**) Brightfield images of A549 cell line cells growing from single cells on Day 1 to tumor spheroids with an average size of around 150 µm on Day 25; (**b**) Grown tumor spheroids of BT-474, HT-29, SK-BR-3, HeLa, MCF-7 and A549 cell lines on Day 25, scale bar indicates 50 µm; (**c**) Confocal image of MCTSs, cells were stained with DAPI and Phalloidin, scale bar indicates 50 µm.

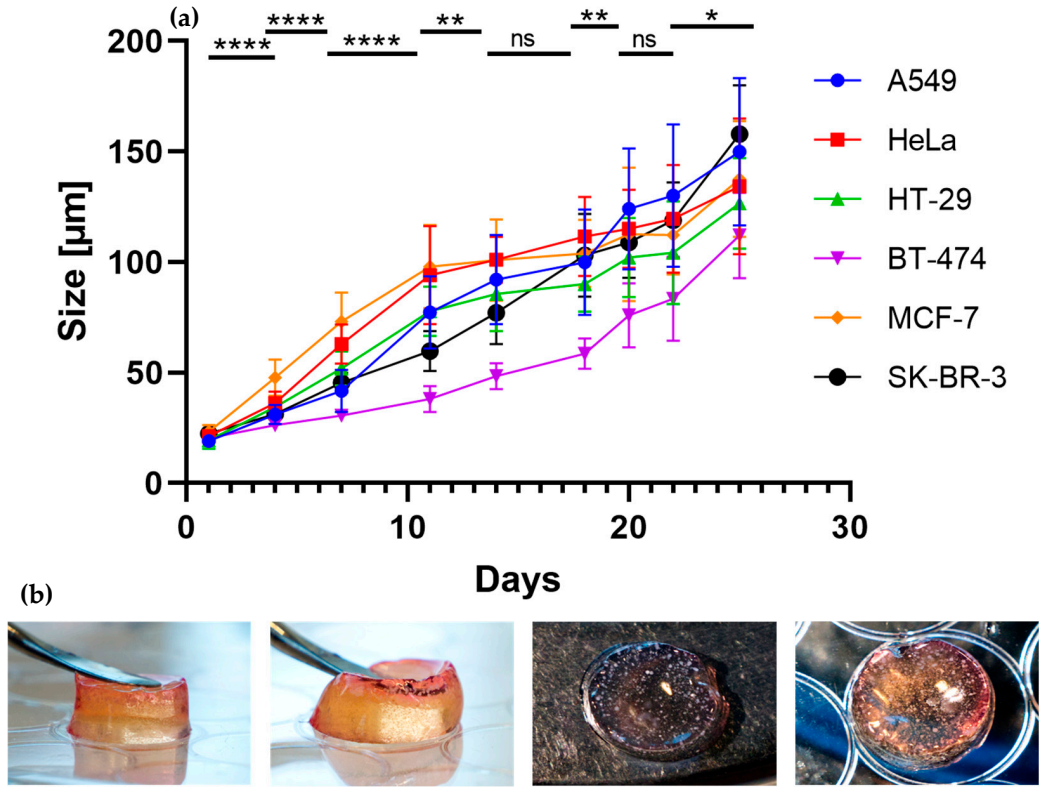

Figure 6. Size determination of tumor spheroids in hydrogel matrix; (**a**) Comparative size changes with all six different cell lines from within a culture period of 25 days. Data are presented as mean ± standard deviation, n = 25, *t*-test, shown for A549 cell line (see Table S1), * $p < 0.05$, ** $p < 0.01$, **** $p < 0.0001$, ns denotes no significance $p > 0.05$; (**b**) Photographs of tumoroids-encapsulated hydrogel after incubation in cell medium for 2 months. The numerous white dots inside the gel are grown MCTSs whose size is visible to the eyes.

3. Conclusions

In summary, the nondegradable hydrogel made from alpha-acrylate functionalized dPG and 4-arm PEG thiol at 3% *w*/*v* with 1 kPa stiff serves as an excellent supporting scaffold for various types of cancer cell lines such as A549, HeLa, HT-29, BT-474, MCF-7, and SK-BR-3. These cell lines are in situ encapsulated into a gel matrix and later form 3D tumor spheroids with standard culturing protocol and yet achieve an average tumoroid size at approximately 150 µm after 25 days of incubation with no observable toxicity. We believe that this gel platform can be a potential alternative not only for 3D tumoroid growth but also for organoid formation since the hydrogel has been proven to be stable for long time preservation.

4. Materials and Methods

4.1. Materials

All chemicals were purchased from Merck KGaA, Darmstadt, Germany and/or its affiliates and used without any further purification unless otherwise declared. Diethyl ether (100%) and DCM (100%) were purchased from VWR chemicals. N,N-Dimethylformamide (DMF) (99.8%), KOH (pellets), NaN_3 (99%), MeOH (99.9%), THF (99.8%) and Chloroform were purchased from Thermo Fisher Scientific, Waltham, MA, USA. Ethyl 2-(bromomethyl)acrylate was purchased from TCI Deutschland GmbH (Eschborn, Germany). The average weight molecular weight of 10 kDa of dPG (Figure 1) was prepared as a previously reported procedure [34] in our group.

4.2. Synthesis of dPG alpha acrylate

The functionalization degree of alpha acrylate group onto dendritic polyglycerol (dPG) was calculated based on the number of theoretical free OH groups of the glycidol monomer. Ideally, a glycidol has 1 free OH group. So a 10 kDa dPG should contains approximately 135 groups of free OH (calculated by 10,000/74). If all 135 groups of free OH convert to a new functional group, it means this 10 kDa dPG polymer has 100% functionalization degree. Therefore, all the estimated equivalents of each reagent in the synthetic reaction are based on this calculation of the degree functionalization. 10 kDa dPG (1 eq., 0.1 mmol, 1 g, Figure S1) was dried in vacuum prior to being dissolved by DMF (10 mL). NaH (8 eq., 0.8 mmol, 0.019 g) was added to the solution which was then stirred at room temperature for 1 h. The reaction flask was later cooled down by an ice bath and ethyl 2-(bromomethyl)acrylate (9 eq., 0.9 mmol, 0.124 mL) was added dropwise to the reaction mixture and it was run for 1 day. Afterward, the crude mixture was purified by dialysis with a 2 kDa cutoff dialysis tube in water for 2 days. After the purification, the pure product was stored as an aqueous solution and its concentration was calculated. Based on the concentration and total volume, the final yield was calculated and resulted in 83%. The functionalization degree of alpha acrylate was calculated by the area under a peak in the ^{1}H NMR spectrum based on the NMR end-group analysis. It shows that there is 5% alpha acrylate decorated onto the dPG polymer (calculated by 0.05 × 100/1), which is roughly estimated to be 7 groups (calculated by 135 × 5%). ^{1}H NMR (700 MHz, D_2O, δ (ppm)): 0.92 (3H, broad s, initiator backbone), 1.36 (3H, broad s), 3.58–4.43 (m, backbone repeating units), 6.02–6.06 (1H, d), and 6.41 (1H, s) (Figure S2).

4.3. Synthesis of 4-arm PEG OMs

To a DCM (30 mL) solution of dried 10 kDa 4-arm polyethylene glycol (4-arm PEG, 1 eq., 0.3 mmol, 3 g, Figure S3)) was added an excess of Triethylamine (15 eq., 4.5 mmol, 0.63 mL). The reaction flask was then cooled down by an ice bath, followed by adding an excess of methanesulfonyl chloride (12 eq., 3.6 mmol, 0.28 mL). The reaction mixture was stirred for 1 day. The next day, the crude mixture was washed quickly with brine, later dried with Na_2SO_4 for 30 min and concentrated. The product in con-centrated DCM solution was then precipitated in cooled Ether and finally dried for 1 day in vacuum at room temperature. The final precipitated product is white with a 92% yield. 1H NMR (500 MHz, $CDCl_3$, δ (ppm)): 3.08 (3H, s), 3.40–3.78 (m, polymer backbone), 4.36–4.38 (2H, t, J = 5 Hz) (Figure S4).

4.4. Synthesis of 4-arm PEG Thiol

4-arm PEG OMs (1 eq., 0.276 mmol, 2.76 g) was suspended in 1-propanol (30 mL), followed by the addition of an excess of thiourea (20 eq., 5.52 mmol, 0.42 g). The reaction mixture was then heated up at 80 °C which made all suspension become solution and it was stirred for 1 day. Next, the solvent was removed from the reaction flask and water (30 mL) was then added to dissolve the crude mixture, followed by the excessive addition of KOH (20 eq., 5.52 mmol, 0.31 g). The solution was then heated up and 80 °C and stirred for 1 day. Afterward, tris(2-carboxyethyl)phosphine hydrochloride (4 eq., 1.1 mmol, 0.32 g) was added to the reaction flask which was then run for 2 h at room temperature. Next, The purification took place. The crude product was first extracted quickly by DCM, then dried with Na_2SO_4 and concentrated with a rotary evaporator. The product in DCM solution was precipitated in cooled Ether and dried in vacuum for 1 day at room temperature. The resulting product was pale yellowish precipitated with 81% yield. 1H NMR (500 MHz, $CDCl_3$, δ (ppm)): 1.57–1.60 (1H, t, J = 5 and 10 Hz), 2.67–2.70 (2H, quat, J = 5 Hz), 3.40–3.75 (m, polymer backbone) (Figure S5). The amount of thiol groups at the end chain of each arm was quantified by Ellman's assay protocol from Thermo Fischer Scientific by using the standard calibration curve of cys-teine in different concentrations. The resulting number of thiol groups is approximate-ly 3.5 groups per 4-arm PEG molecule.

4.5. Rheological Experiment

The Rheological performance was conducted by Malvern Kinexus Prime Lab+. The hydrogel samples were mechanically characterized in triplication by using an 8-mm parallel plate at 37 °C with 0.05 N force and analyzed by oscillatory amplitude sweep and frequency sweep (0.1% strain) as well as viscosity (2 min ramp time) tests. The stiffness values of hydrogel samples were directly related to the shear storage modulus at 1 Hz. The mesh size was calculated from the stiffness or shear storage modulus at 1 Hz, by using the classical theory of rubber elasticity [35–37] as shown below:

$$r = \left(\frac{6RT}{\pi N_{Av} G}\right)^{\frac{1}{3}}$$

where r is mesh size (nm), R is the gas constant (8.314 $m^3 \cdot Pa \cdot K^{-1} \cdot mol^{-1}$), T is the temperature (K), π is Pi constant (3.142), N_{Av} is Avogadro's number (6.022 × 1023 mol^{-1}) and G is shear storage modulus (Pa).

4.6. Cell Culture

All cell lines were obtained from DSMZ (German Collection of Microorganisms and Cell Cultures GmbH, Braunschweig, Germany), cultured in Dulbecco's Modified Eagle Medium (DMEM, high glucose, GlutaMAX, Gibco), which was supplemented with 10% (v/v) fetal bovine serum (FBS, Gibco) and 1% (v/v) of penicillin-streptomycin solution (Gibco). Cells were cultured at 37 °C with 5% CO_2 in a culture flask.

4.7. Hydrogelation for MCTSs Formation

To prepare 300 µL hydrogel at 3% w/v concentration for the MCTSs formation experiment, 10% w/v DMEM solution of 4-arm PEG thiol (0.7 µmol, 70 µL), 21.3% w/v dPG alpha acrylate aqueous solution (0.23 µmol, 11 µL), cell solution (estimated 10,000 cells, 50 µL) and 219 µL DMEM were simply mixed in a well of a 48-well plate. All cells were in situ encapsulated during gelation. The hydrogel sample was left in a cell incu-bator for 4 h prior to the addition of 400 µL DMEM on top of the gel for cell growth, fresh medium was changed every other day. The growth of MCTS was monitored under BrightField with Zeiss Axio Observer Z1 microscope (Jena, Germany).

4.8. MCTSs Staining and Imaging

The grown MCTSs were firstly fixed with 4% paraformaldehyde at room temper-ature for 30 min, then washed with DPBS 3 times. Then, DAPI and Phal-loidin-iFluoro594 reagent (Abcam, Cambridge, UK) were used to stain the cell nuclei and cytoskeletons for 30 min, followed by washing with DPBS 3 times. The stained MCTSs were carefully transferred from a 48-well plate to an 8-well Miccroscope µ-Slide (ibidi, Gräfelfing, Germany) and imaged by Leica SP8 confocal microscope (Wetzlar, Germany).

4.9. Statistical Analysis

All tests were conducted in at least three independent sessions. The quantified data are expressed as mean ± SD. GraphPad Prism was employed for statistical analysis. Differences between the tumoroid growth with time were analyzed using two sample unpaired *t*-test.

Supplementary Materials: The following supporting information can be downloaded at: https://www.mdpi.com/article/10.3390/gels9120938/s1, Figure S1: 1H NMR (500 MHz, D_2O, δ (ppm)) spectrum of 10 kDa dPG; Figure S2: 1H NMR (700 MHz, D_2O, δ (ppm)) spectrum of 10 kDa dPG alpha acrylate; Figure S3: 1H NMR (500 MHz, $CDCl_3$, δ (ppm)) spectrum of 10 kDa 4-arm polyethylene glycol (PEG); Figure S4: 1H NMR (500 MHz, $CDCl_3$, δ (ppm)) spectrum of 10 kDa 4-arm PEG OMs; Figure S5: 1H NMR (500 MHz, $CDCl_3$, δ (ppm)) spectrum of 10 kDa 4-arm PEG thiol; Figure S6: Shear viscosity graph of hydrogel sample at 37 °C at different incubation times; Table S1: *p*-value for the MCTS growth of each cell line; Figure S7: Brightfield images of cancer cell line A549, BT-474, HT-29,

SK-BR-3, HeLa, and MCF-7 growing from single cells on Day 1 to tumor spheroids with an average size of around 150 µm on Day 25, scale bar indicates 100 µm.

Author Contributions: Conceptualization, S.A. and R.H.; Investigation, B.T. and P.T.; Resources, R.H.; Writing–original draft, B.T. and P.T.; Writing–review & editing, B.T., P.T., S.A. and R.H.; Supervision, S.A.; Project administration, R.H.; Funding acquisition, R.H. All authors have read and agreed to the published version of the manuscript.

Funding: This research was funded by The Federal Ministry of Education and Research (BMBF) and Collaborative Research Center "Dynamic Hydrogels at Biological Interfaces" (CRC 1449), Deutsche Forschungsgemeinschaft (DFG, German Research Foundation)—Project ID 431232613—SFB 1449.

Institutional Review Board Statement: Not applicable.

Informed Consent Statement: Not applicable.

Data Availability Statement: The data presented in this study are openly available in article.

Acknowledgments: The authors would like to greatly thank the Core Facility BioSupraMol for the NMR measurements and our technician, Cathleen Hudziak, for measuring GPC and providing a starting material, 10 kDa dendritic polyglycerol (dPG).

Conflicts of Interest: The authors declare no conflict of interest.

References

1. Dzobo, K.; Thomford, N.E.; Senthebane, D.A.; Shipanga, H.; Rowe, A.; Dandara, C.; Pillay, M.; Shirley, K.; Motaung, C.M. Innovation and Transformation of Medicine. *Stem Cells Int.* **2018**, *2018*, 2495848. [CrossRef] [PubMed]
2. Vicente, A.M.; Ballensiefen, W.; Jönsson, J.I. How Personalised Medicine Will Transform Healthcare by 2030: The ICPerMed Vision. *J. Transl. Med.* **2020**, *18*, 180. [CrossRef]
3. Goetz, L.H.; Schork, N.J. Personalized Medicine: Motivation, Challenges and Progress. *Fertil. Steril.* **2018**, *109*, 952–963. [CrossRef]
4. Ahearne, M. Introduction to Cell-Hydrogel Mechanosensing. *Interface Focus* **2014**, *4*, 20130038. [CrossRef] [PubMed]
5. Yang, C.; Tibbitt, M.W.; Basta, L.; Anseth, K.S. Mechanical Memory and Dosing Influence Stem Cell. *Nat. Mater.* **2014**, *13*, 645–652. [CrossRef] [PubMed]
6. Yeung, T.; Georges, P.C.; Flanagan, L.A.; Marg, B.; Ortiz, M.; Funaki, M.; Zahir, N.; Ming, W.; Weaver, V.; Janmey, P.A. Effects of Substrate Stiffness on Cell Morphology, Cytoskeletal Structure, and Adhesion. *Cell Motil. Cytoskeleton* **2005**, *60*, 24–34. [CrossRef]
7. Barriga, E.H.; Franze, K.; Charras, G.; Mayor, R. Tissue Stiffening Coordinates Morphogenesis by Triggering Collective Cell Migration in Vivo. *Nature* **2018**, *554*, 523–527. [CrossRef]
8. Gjorevski, N.; Sachs, N.; Manfrin, A.; Giger, S.; Bragina, E.; Ordóñez-Morán, P.; Clevers, H.; Lutolf, M.P. Designer Matrices for Intestinal Stem Cell and Organoid Culture. *Nature* **2016**, *539*, 560–564. [CrossRef]
9. Trappmann, B.; Gautrot, J.E.; Connelly, J.T.; Strange, D.G.T.; Li, Y.; Oyen, M.L.; Stuart, M.A.C.; Boehm, H.; Li, B.; Vogel, V.; et al. Extracellular-Matrix Tethering Regulates Stem-Cell Fate. *Nat. Mater.* **2012**, *11*, 642–649. [CrossRef]
10. Li, L.; Eyckmans, J.; Chen, C.S. Designer Biomaterials for Mechanobiology. *Nat. Mater.* **2017**, *16*, 1164–1168. [CrossRef] [PubMed]
11. Madl, C.M.; Heilshorn, S.C.; Blau, H.M. Bioengineering Strategies to Accelerate Stem Cell Therapeutics. *Nature* **2018**, *557*, 335–342. [CrossRef]
12. Gaharwar, A.K.; Singh, I.; Khademhosseini, A. Engineered Biomaterials for in Situ Tissue Regeneration. *Nat. Rev. Mater.* **2020**, *5*, 686–705. [CrossRef]
13. Trappmann, B.; Chen, C.S. How Cells Sense Extracellular Matrix Stiffness: A Material's Perspective. *Curr. Opin. Biotechnol.* **2013**, *24*, 948–953. [CrossRef] [PubMed]
14. Chaudhuri, O.; Cooper-White, J.; Janmey, P.A.; Mooney, D.J.; Shenoy, V.B. Effects of Extracellular Matrix Viscoelasticity on Cellular Behaviour. *Nature* **2020**, *584*, 546. [CrossRef] [PubMed]
15. Zhao, H.; Xu, K.; Zhu, P.; Wang, C.; Chi, Q. Smart Hydrogels with High Tunability of Stiffness as a Biomimetic Cell Carrier. *Cell Biol. Int.* **2019**, *43*, 84–97. [CrossRef] [PubMed]
16. Gunti, S.; Hoke, A.T.K.; Vu, K.P.; London, N.R. Organoid and Spheroid Tumor Models: Techniques and Applications. *Cancers* **2021**, *13*, 874. [CrossRef] [PubMed]
17. Timmins, N.E.; Nielsen, L.K. Generation of Multicellular Tumor Spheroids by the Hanging-Drop Method. In *Meth-ods in Molecular Medicine*; Hauser, H., Fussenegger, M., Eds.; Humana Press Inc.: Totowa, NJ, USA, 2007; pp. 141–151.
18. Dangles-Marie, V.; Pocard, M.; Richon, S.; Weiswald, L.B.; Assayag, F.; Saulnier, P.; Judde, J.G.; Janneau, J.L.; Auger, N.; Validire, P.; et al. Establishment of Human Colon Cancer Cell Lines from Fresh Tumors versus Xenografts: Comparison of Success Rate and Cell Line Features. *Cancer Res.* **2007**, *67*, 398–407. [CrossRef] [PubMed]
19. Weiswald, L.B.; Bellet, D.; Dangles-Marie, V. Spherical Cancer Models in Tumor Biology. *Neoplasia* **2015**, *17*, 1–15. [CrossRef]
20. Sawicki, L.A.; Choe, L.H.; Wiley, K.L.; Lee, K.H.; Kloxin, A.M. Isolation and Identification of Proteins Secreted by Cells Cultured within Synthetic Hydrogel-Based Matrices. *ACS Biomater. Sci. Eng.* **2018**, *4*, 836–845. [CrossRef]

21. Tibbitt, M.W.; Anseth, K.S. Hydrogels as Extracellular Matrix Mimics for 3D Cell Culture. *Biotechnol. Bioeng.* **2009**, *103*, 655–663. [CrossRef]
22. Levental, I.; Georges, P.C.; Janmey, P.A. Soft Biological Materials and Their Impact on Cell Function. *Soft Matter* **2007**, *3*, 299–306. [CrossRef]
23. Kanimozhi, K.; Khaleel Basha, S.; Sugantha Kumari, V.; Kaviyarasu, K.; Maaza, M. In Vitro Cytocompatibility of Chitosan/PVA/Methylcellulose—Nanocellulose Nanocomposites Scaffolds Using L929 Fibroblast Cells. *Appl. Surf. Sci.* **2018**, *449*, 574–583. [CrossRef]
24. Lang, K.; Sánchez-Leija, R.J.; Gross, R.A.; Linhardt, R.J. Review on the Impact of Polyols on the Properties of Bio-Based Polyesters. *Polymers* **2020**, *12*, 2969. [CrossRef] [PubMed]
25. Iocozzia, J.; Lin, Z. A Clean and Simple Route to Soft, Biocompatible Nanocapsules via UV-Cross-Linkable Az-ido-Hyperbranched Polyglycerol. *Macromolecules* **2017**, *50*, 4906–4912. [CrossRef]
26. Son, S.; Shin, E.; Kim, B.-S. Redox-Degradable Biocompatible Hyperbranched Polyglycerols: Synthesis, Copolymeri-zation Kinetics, Degradation, and Biocompatibility. *Macromolecules* **2015**, *48*, 600–609. [CrossRef]
27. Gerecke, C.; Edlich, A.; Giulbudagian, M.; Schumacher, F.; Zhang, N.; Said, A.; Yealland, G.; Lohan, S.B.; Neumann, F.; Meinke, M.C.; et al. Biocompatibility and Characterization of Polyglycerol-Based Thermoresponsive Nanogels Designed as Novel Drug-Delivery Systems and Their Intracellular Localization in Keratinocytes. *Nanotoxicology* **2017**, *11*, 267–277. [CrossRef]
28. Tang, P.; Thongrom, B.; Arora, S.; Haag, R. Polyglycerol-Based Biomedical Matrix for Immunomagnetic Circulating Tumor Cell Isolation and Their Expansion into Tumor Spheroids for Drug Screening. *Adv. Healthc. Mater.* **2023**, *12*, 2300842. [CrossRef]
29. Tong, X.; Lai, J.; Guo, B.-H.; Huang, Y. A New End Group Structure of Poly(Ethylene Glycol) for Hydroly-sis-Resistant Biomaterials. *J. Polym. Sci. A Polym. Chem.* **2011**, *49*, 1513–1516. [CrossRef]
30. Thongrom, B.; Dimde, M.; Schedler, U.; Haag, R. Thiol-Click Based Polyglycerol Hydrogels as Biosensing Platform with In Situ Encapsulated Streptavidin Probes. *Macromol. Chem. Phys.* **2022**, *224*, 2200271. [CrossRef]
31. Mahadevegowda, S.H.; Stuparu, M.C. Amphiphilic Corannulene Derivatives: Synthetic Access and Development of a Struc-ture/Property Relationship in Thermoresponsive Buckybowl Amphiphiles. *Eur. J. Org. Chem.* **2017**, *2017*, 570–576. [CrossRef]
32. Salinas, C.N.; Anseth, K.S. Mixed Mode Thiol-Acrylate Photopolymerizations for the Synthesis of PEG-Peptide Hy-drogels. *Macromolecules* **2008**, *41*, 6019–6026. [CrossRef]
33. Khan, A.H.; Cook, J.K.; Wortmann, W.J., III; Kersker, N.D.; Rao, A.; Pojman, J.A.; Melvin, A.T. Synthesis and Charac-terization of Thiol-Acrylate Hydrogels Using a Base-Catalyzed Michael Addition for 3D Cell Culture Applications. *J. Biomed. Mater. Res. Part B Appl. Biomater.* **2020**, *108*, 2294–2307. [CrossRef] [PubMed]
34. Wallert, M.; Plaschke, J.; Dimde, M.; Ahmadi, V.; Block, S.; Haag, R. Automated Solvent-Free Polymerization of Hyperbranched Polyglycerol with Tailored Molecular Weight by Online Torque Detection. *Macromol. Mater. Eng.* **2021**, *306*, 2000688. [CrossRef]
35. Anseth, K.S.; Bowman, C.N.; Brannon-Peppas, L. Mechanical Properties of Hydrogels and Their Experimental Determination. *Biomaterials* **1996**, *17*, 1647–1657. [CrossRef] [PubMed]
36. Kuijpers, A.J.; Engbers, G.H.M.; Feijen, J.; De Smedt, S.C.; Meyvis, T.K.L.; Demeester, J.; Krijgsveld, J.; Zaat, S.A.J.; Dankert, J. Characterization of the Network Structure of Carbodiimide Cross-Linked Gelatin Gels. *Macromolecules* **1999**, *32*, 3325–3333. [CrossRef]
37. Li, J.; Mooney, D.J.; Paulson, J.A. Designing Hydrogels for Controlled Drug Delivery HHS Public Access. *Nat. Rev. Mater.* **2016**, *1*, 16071. [CrossRef] [PubMed]

Supplementary materials

Polyglycerol-Based Hydrogel as Versatile Support Matrix for 3D Multicellular Tumor Spheroid Formation

Boonya Thongrom [1#], Peng Tang [2#], Smriti Arora* and Rainer Haag*

[1] b.thongrom@fu-berlin.de
[2] mauricetangp@zedat.fu-berlin.de
* Correspondence: smriti@zedat.fu-berlin.de and haag@zedat.fu-berlin.de
[#] These authors contributed equally to this work.

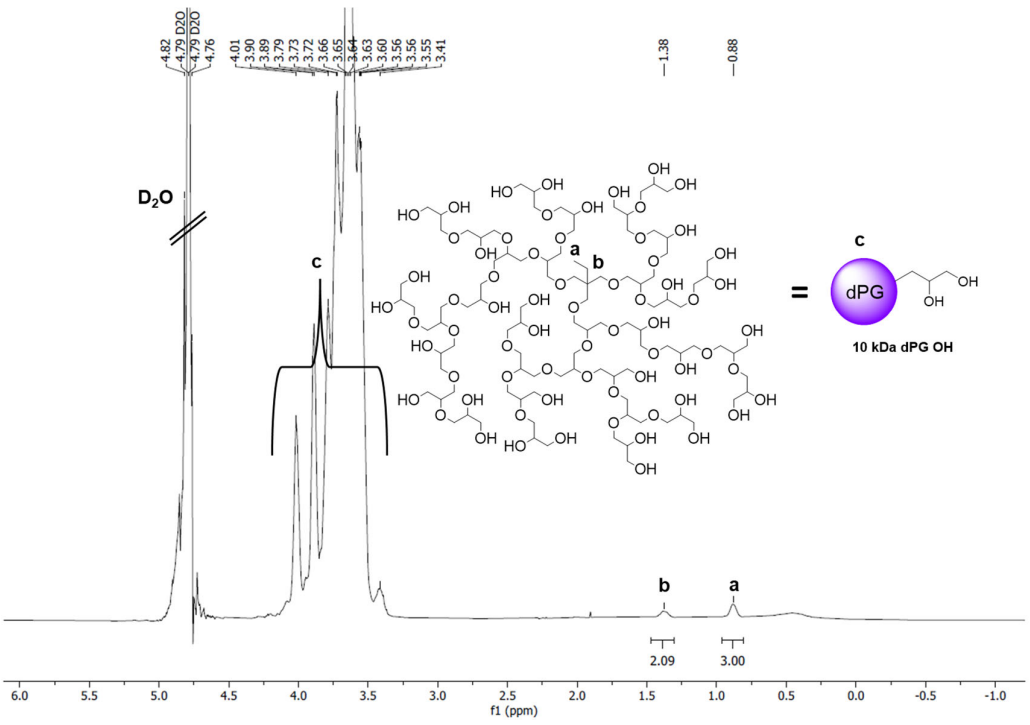

Figure S1. ^{1}H NMR (500 MHz, D_2O, δ (ppm)) spectrum of 10 kDa dPG.

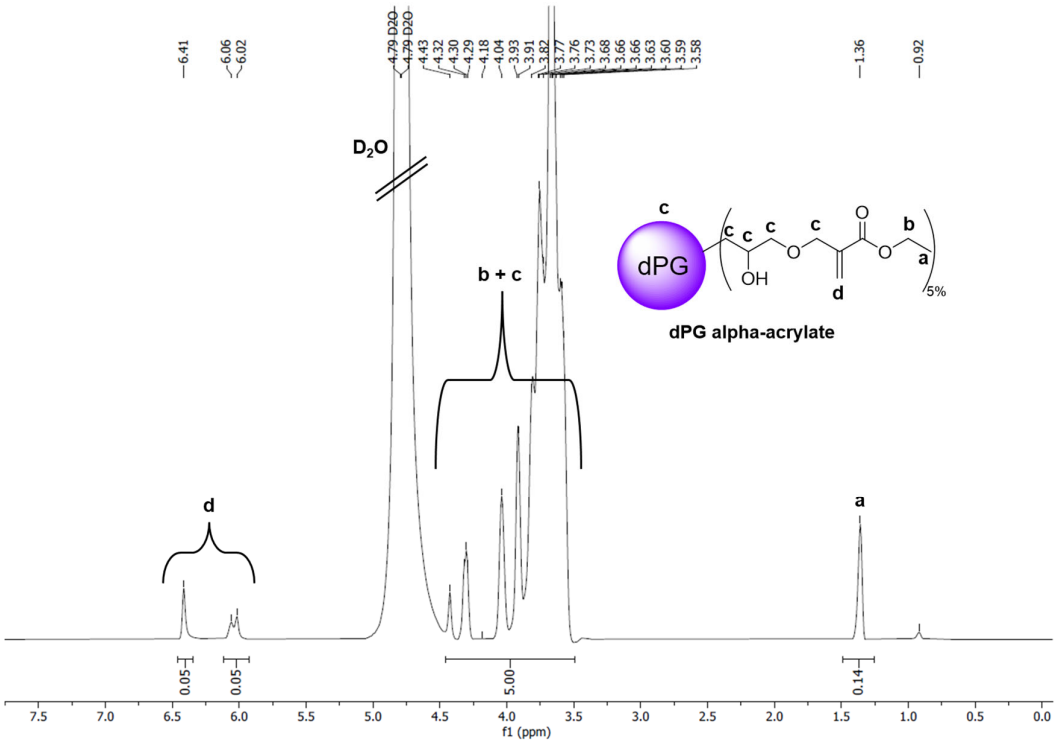

Figure S2. ^{1}H NMR (700 MHz, D_2O, δ (ppm)) spectrum of 10 kDa dPG alpha acrylate.

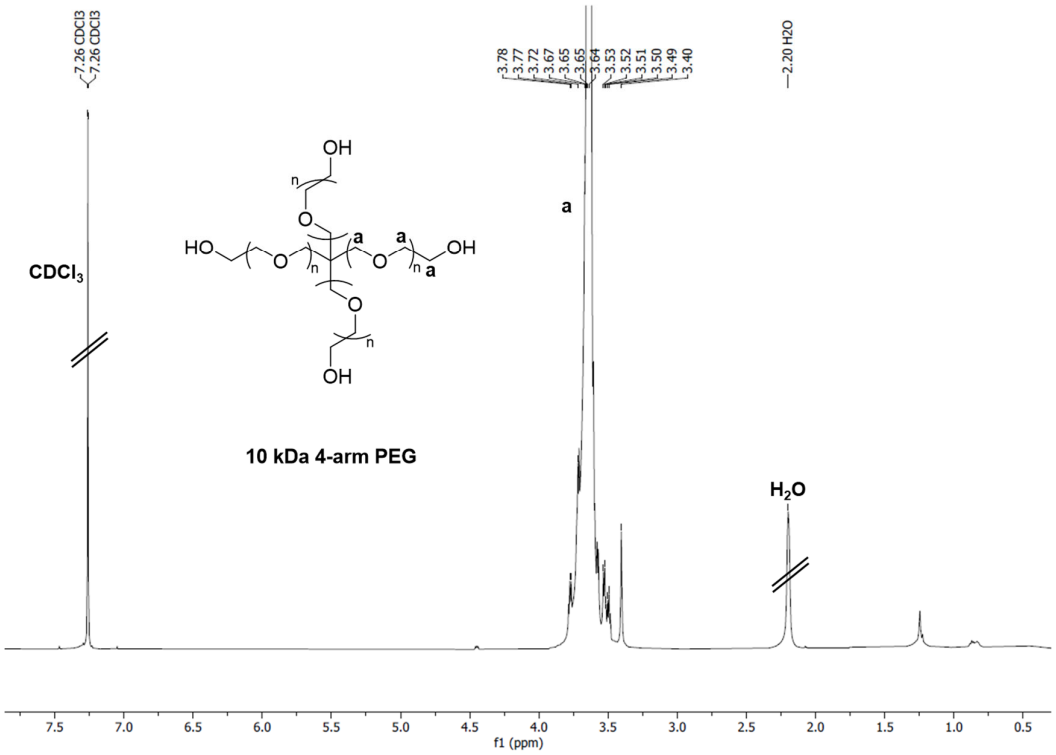

Figure S3. ^{1}H NMR (500 MHz, $CDCl_3$, δ (ppm)) spectrum of 10 kDa 4-arm polyethylene glycol (PEG).

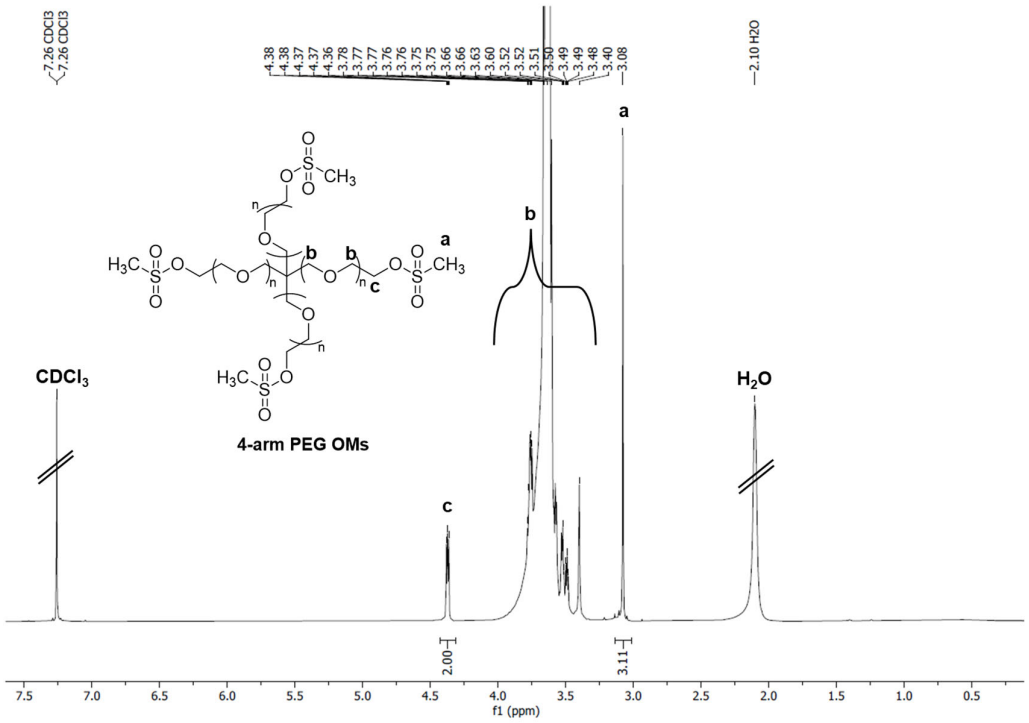

Figure S4. ^{1}H NMR (500 MHz, $CDCl_3$, δ (ppm)) spectrum of 10 kDa 4-arm PEG OMs.

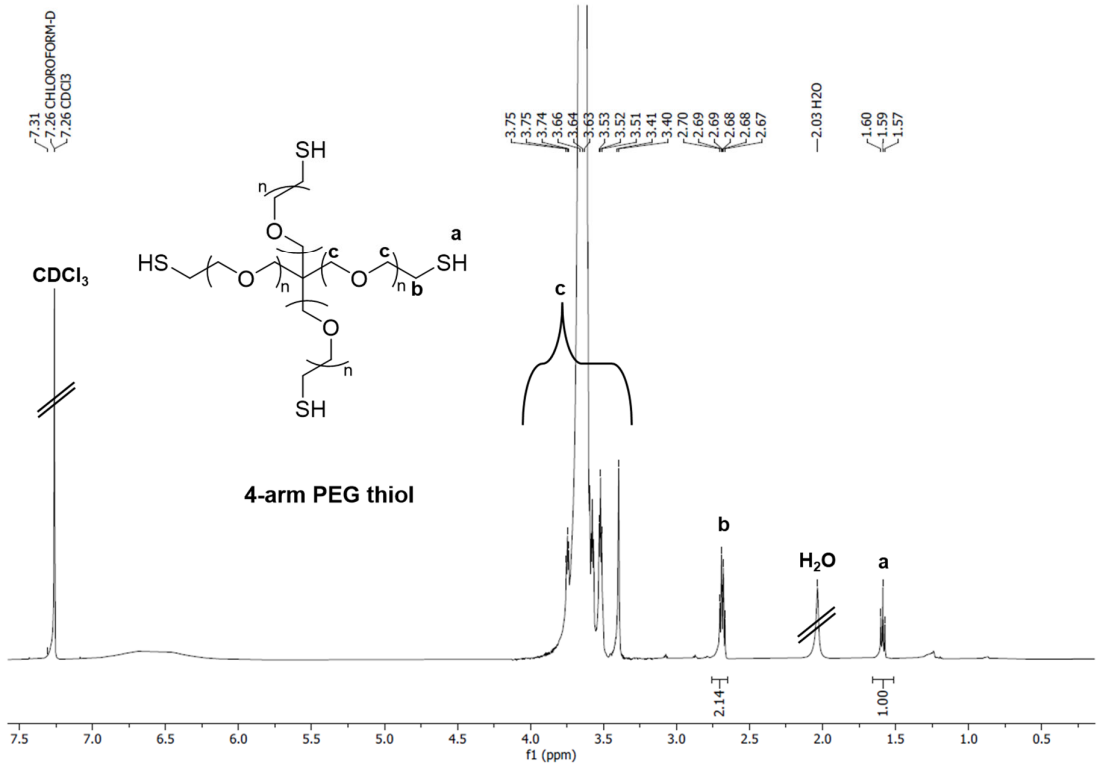

Figure S5. ^{1}H NMR (500 MHz, $CDCl_3$, δ (ppm)) spectrum of 10 kDa 4-arm PEG thiol.

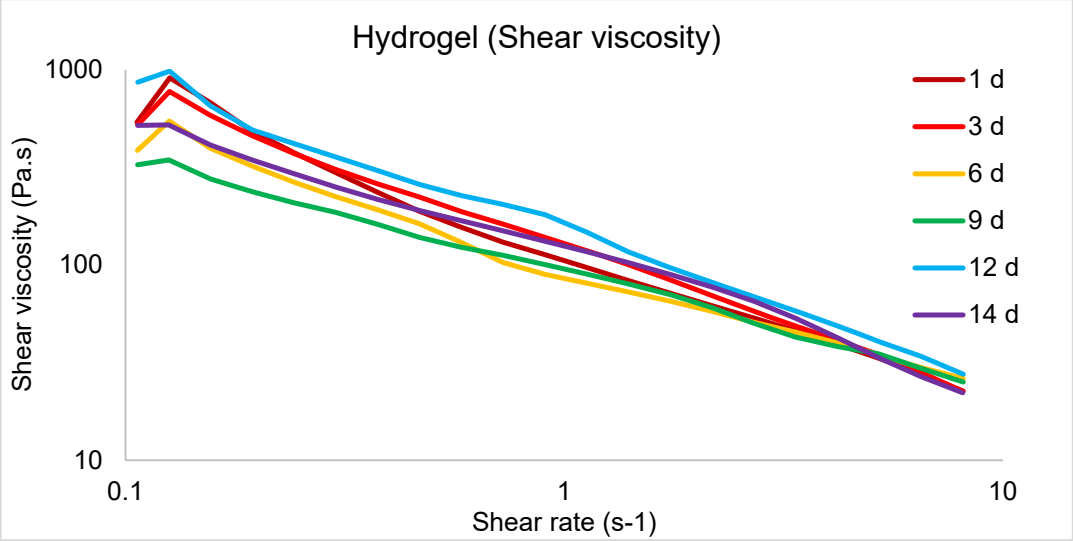

Figure S6. Shear viscosity graph of hydrogel sample at 37 °C at different incubation times.

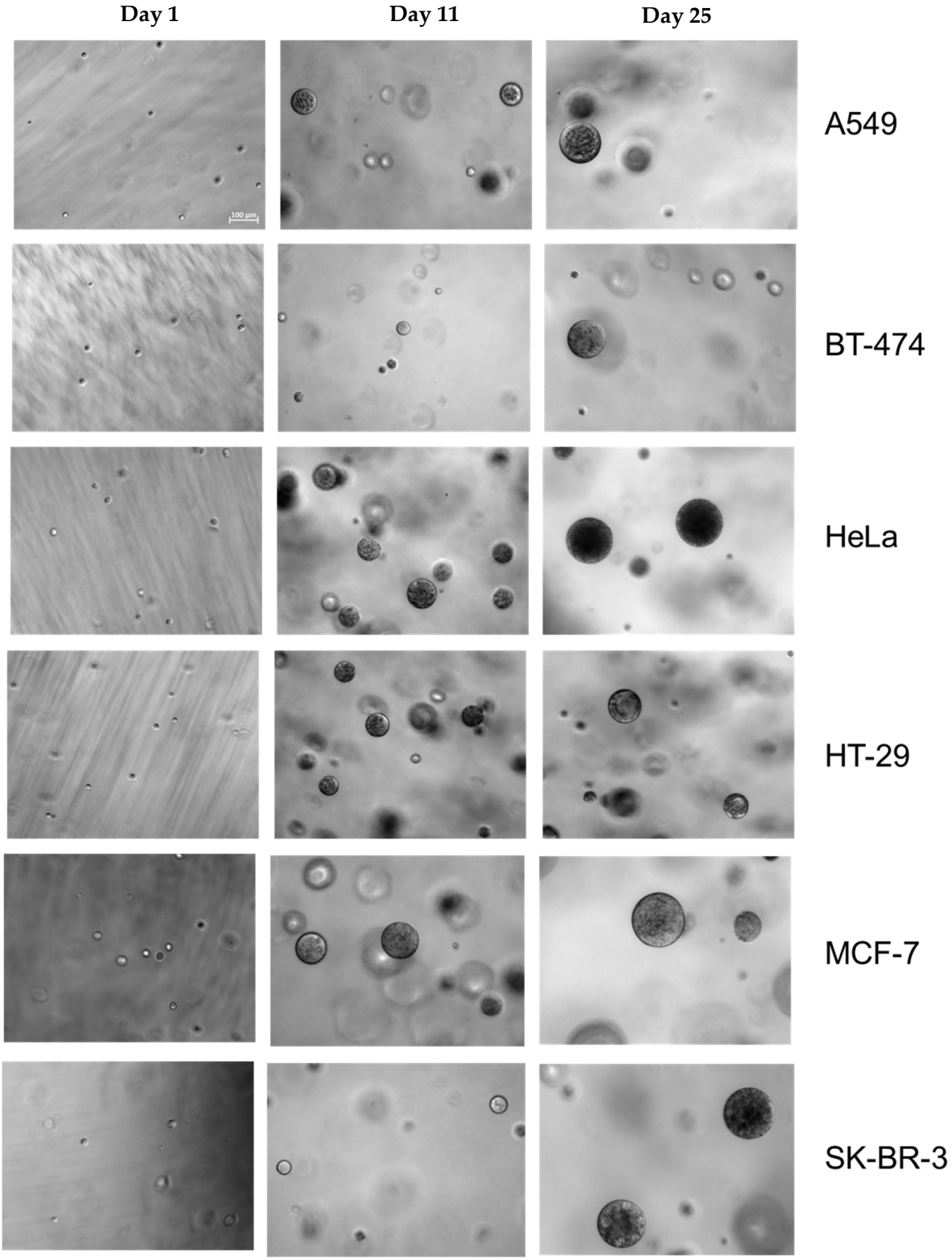

Figure S7. Brightfield images of cancer cell line A549, BT-474, HT-29, SK-BR-3, HeLa, and MCF-7 growing from single cells on day 1 to tumor spheroids with an average size of around 150 μm on day 25, scale bar indicates 100 μm.

Table S1. p-value for the MCTS growth of each cell line.

	D1 vs. D4	D4 vs. D7	D7 vs.D11	D11 vs. D14	D14. vs. D18	D18 vs. D20	D20 vs. D22	D22 vs. D25
A549	****	****	****	**	ns	**	ns	*
HeLa	****	****	****	ns	*	ns	ns	ns
HT29	****	****	****	ns	ns	**	ns	***
BT474	****	****	****	****	****	****	ns	****
MCF7	****	****	****	ns	ns	ns	ns	***
SKBR3	****	****	****	****	****	ns	*	****

5. Summary and Conclusion

The projects presented in this dissertation focus mainly on the interplay between cells and synthetic polymer materials. Owing to the outstanding chemical and biological properties of polyglycerol and its derivatives, a variety of functional materials were designed. From two-dimensional surfaces with certain topographical structures to three-dimensional immunomagnetic particles and hydrogels, cell adhesion, recognition and proliferation were studied, and corresponding applications were suggested.

In the first project, three mussel-inspired polyglycerol macromolecules were synthesized with differences in molecular structures and chemical compositions. Serving as versatile coating materials, by comparing either two of them, the influences of the variates, i.e. the linear/dendritic structure and catechol/amine composition, on the coating results were investigated. In the coating process, the catechol content plays the most important part in the oxidation, while the amines help with the crosslinking of the oxidants. Hence, a higher catechol concentration indicates a faster coating rate. On the other hand, attributed to the high reaction efficiency of dendritic structures, the coating process of dendritic polyglycerol exceeds the linear ones, despite a higher catechol functionalization. Therefore, among the three types of MiPG, dPG40 can achieve thick, rough coating within one hour, lPG80 requires several hours while the lPG40 can only make monolayer coating. Depending on the results, applications on each of them can be suggested. For instance, as cells have preference for surface with certain roughness, dPG40 and lPG80 with good tunability on roughness are able to fabricate suitable substrates for cells to adhere to.

In the second project, we first introduced polyglycerol to iron nanoparticles for specific cell capture, then employed polyglycerol as hydrogel platform for captured cell culture. The fascinating properties of polyglycerol. e.g. bio-antifouling, easy post-functionalization and outstanding biocompatibility were demonstrated. In the first part, the immunomagnetic nanoparticles were shielded with polyglycerol from unwanted cells or molecules, cell recognition and capture were done by the antibody-antigen interaction. High efficiency, selectivity and specificity were achieved. Later, the captured cells were directly encapsulated in acrylate-based polyglycerol hydrogels for 3D culture. We successfully grew multicellular tumor spheroids out from the captured cells, then the anti-tumor drug screening was done, showing that our model excel in liquid biopsy for CTC-related research and could be potentially used for personalized treatment for cancer patients.

Encouraged by the successful 3D culture from the second project, we continued to explore the possibilities of polyglycerol-based hydrogels as ECM mimetics. By changing the crosslinking chemistry, we designed a non-degradable hydrogel as a comparison to the degradable acrylate hydrogel we reported in project 2, and employed it as platform for 3D culture. Different cell lines were used, and we were able to grow them into MCTS from single cell suspensions. The sizes and morphology of the MCTSs were characterized and we proved our platform serves as a versatile scaffold for MCTSs generation. As oppose to the advantages of degradable hydrogel, in which it is applicable in release-required case, the non-degradable nature can in situations like organoid formation, where a long culture period is needed.

6. Kurzzusammenfassung

Die in dieser Dissertation vorgestellten Projekte befassen sich hauptsächlich mit dem Zusammenspiel zwischen Zellen und synthetischen Polymermaterialien. Aufgrund der hervorragenden chemischen und biologischen Eigenschaften von Polyglycerin und seinen Derivaten wurde eine Vielzahl funktioneller Materialien entwickelt. Von zweidimensionalen Oberflächen mit bestimmten topographischen Strukturen bis hin zu dreidimensionalen immunmagnetischen Partikeln und Hydrogelen wurden Zelladhäsion, -erkennung und -proliferation untersucht und entsprechende Anwendungen vorgeschlagen.

Im ersten Projekt wurden drei von Muscheln inspirierte Polyglycerin-Makromoleküle mit unterschiedlichen Molekularstrukturen und chemischen Zusammensetzungen synthetisiert. Als vielseitige Beschichtungsmaterialien wurden sie durch den Vergleich von jeweils zwei von ihnen die Einflüsse der Variante, d.h. der linearen/dendritischen Struktur und der Catechin/Amin-Zusammensetzung, auf die Beschichtungsergebnisse untersucht. Im Beschichtungsprozess spielt der Catechin-Gehalt bei der Oxidation die wichtigste Rolle, während die Amine bei der Vernetzung der Oxidationsmittel helfen. Eine höhere Catechol-Konzentration bedeutet daher eine schnellere Beschichtungsrate. Andererseits übertrifft der Beschichtungsprozess von dendritischem Polyglycerin trotz höherer Catechinfunktionalisierung den von linearem Polyglycerin, was auf die hohe Reaktionseffizienz von dendritischen Strukturen zurückzuführen ist. Daher kann dPG40 unter den drei MiPG-Typen innerhalb einer Stunde eine dicke, raue Beschichtung erreichen, lPG80 benötigt mehrere Stunden, während lPG40 nur eine einschichtige Beschichtung erzeugen kann. Je nach den Ergebnissen können für jedes dieser Produkte Anwendungen vorgeschlagen werden. Da Zellen beispielsweise eine Oberfläche mit einer bestimmten Rauheit bevorzugen, können dPG40 und lPG80 mit ihrer guten Abstimmbarkeit der Rauheit geeignete Substrate herstellen, an denen Zellen haften.

Im zweiten Projekt brachten wir zunächst Polyglycerin in Eisennanopartikel ein, um gezielt Zellen einzufangen, und setzten dann Polyglycerin als Hydrogel-Plattform für die Zellkultur ein. Die faszinierenden Eigenschaften von Polyglycerin, wie z. B. Bio-Antifouling, einfache Nachfunktionalisierung und hervorragende Biokompatibilität, wurden nachgewiesen. Im ersten Teil wurden die immunmagnetischen Nanopartikel mit Polyglycerin von unerwünschten Zellen oder Molekülen abgeschirmt, die Zellerkennung und der Einfang erfolgten durch die Antikörper-Antigen-Interaktion. Es wurde eine hohe Effizienz, Selektivität und Spezifität erreicht. Später wurden die eingefangenen Zellen direkt in

Polyglycerin-Hydrogelen auf Acrylatbasis für die 3D-Kultur verkapselt. Wir haben aus den vercapselten Zellen erfolgreich multizelluläre Tumor-Sphäroide gezüchtet und anschließend das Screening von Antitumor-Medikamenten durchgeführt. Dies zeigt, dass unser Modell in der Flüssigbiopsie für die CTC-Forschung hervorragend geeignet ist und potenziell für die personalisierte Behandlung von Krebspatienten eingesetzt werden könnte.

Ermutigt durch die erfolgreiche 3D-Kultur aus dem zweiten Projekt setzten wir die Erforschung der Möglichkeiten von Hydrogelen auf Polyglycerinbasis als ECM-Mimetika fort. Durch Änderung der Vernetzungschemie entwickelten wir ein nicht abbaubares Hydrogel als Vergleich zu dem abbaubaren Acrylat-Hydrogel, über das wir in Projekt 2 berichteten, und verwendeten es als Plattform für die 3D-Kultur. Es wurden verschiedene Zelllinien verwendet, die wir aus einzelnen Zellsuspensionen zu MCTS züchten konnten. Die Größe und Morphologie der MCTS wurden charakterisiert und wir konnten beweisen, dass unsere Plattform als vielseitiges Gerüst für die Erzeugung von MCTS dient. Im Gegensatz zu den Vorteilen des abbaubaren Hydrogels, das sich für die Freisetzung eignet, kann die nicht abbaubare Beschaffenheit in Situationen wie der Organoidbildung eingesetzt werden, in denen eine lange Kulturdauer erforderlich ist.

7. References

[1] *Biointerfaces: Where Material Meets Biology*, The Royal Society Of Chemistry, **2014**.

[2] J. V. L. Nguyen, E. Ghafar-Zadeh, *Actuators* **2020**, *9*, 137.

[3] K. Hori, S. Yoshimoto, T. Yoshino, T. Zako, G. Hirao, S. Fujita, C. Nakamura, A. Yamagishi, N. Kamiya, *Journal of Bioscience and Bioengineering* **2022**, *133*, 195.

[4] C. Jensen, Y. Teng, *Frontiers in Molecular Biosciences* **2020**, *7*.

[5] S. Cai, C. Wu, W. Yang, W. Liang, H. Yu, L. Liu, *Nanotechnology Reviews* **2020**, *9*, 971.

[6] J. W. Haycock, in *3D Cell Culture: Methods and Protocols* (Ed.: J. W. Haycock), Humana Press, Totowa, NJ, **2011**, pp. 1–15.

[7] O. Habanjar, M. Diab-Assaf, F. Caldefie-Chezet, L. Delort, *International Journal of Molecular Sciences* **2021**, *22*, 12200.

[8] M. W. Tibbitt, K. S. Anseth, *Biotechnology and Bioengineering* **2009**, *103*, 655.

[9] M. Mozetič, *Materials (Basel)* **2019**, *12*, 441.

[10] S. K. Nemani, R. K. Annavarapu, B. Mohammadian, A. Raiyan, J. Heil, Md. A. Haque, A. Abdelaal, H. Sojoudi, *Advanced Materials Interfaces* **2018**, *5*, 1801247.

[11] A. Saberi, H. R. Bakhsheshi-Rad, S. Abazari, A. F. Ismail, S. Sharif, S. Ramakrishna, M. Daroonparvar, F. Berto, *Coatings* **2021**, *11*, 747.

[12] Y. Ikada, *Biomaterials* **1994**, *15*, 725.

[13] B. D. Ratner, *Biosensors and Bioelectronics* **1995**, *10*, 797.

[14] P. Alves, J. F. J. Coelho, J. Haack, A. Rota, A. Bruinink, M. H. Gil, *European Polymer Journal* **2009**, *45*, 1412.

[15] M. M. Demir, K. Koynov, Ü. Akbey, C. Bubeck, I. Park, I. Lieberwirth, G. Wegner, *Macromolecules* **2007**, *40*, 1089.

[16] D. Briggs, D. G. Rance, C. R. Kendall, A. R. Blythe, *Polymer* **1980**, *21*, 895.

[17] M. Ozdemir, C. U. Yurteri, H. Sadikoglu, *Critical Reviews in Food Science and Nutrition* **1999**, *39*, 457.

[18] Z. Zhang, L. Yu, W. Liu, Z. Song, *Applied Surface Science* **2010**, *256*, 3856.

[19] W. M. da Silva, M. P. Suarez, A. R. Machado, H. L. Costa, *Wear* **2013**, *302*, 1230.

[20] M. W. Laschke, V. A. Augustin, F. Sahin, D. Anschütz, W. Metzger, C. Scheuer, M. Bischoff, C. Aktas, M. D. Menger, *Journal of Biomedical Materials Research Part B: Applied Biomaterials* **2016**, *104*, 1738.

[21] A. Jordá-Vilaplana, V. Fombuena, D. García-García, M. D. Samper, L. Sánchez-Nácher, *European Polymer Journal* **2014**, *58*, 23.

[22] O. Lyutakov, J. Tůma, I. Huttel, V. Prajzler, J. Siegel, V. Švorčík, *Appl. Phys. B* **2013**, *110*, 539.

[23] N. Chen, D. H. Kim, P. Kovacik, H. Sojoudi, M. Wang, K. K. Gleason, *Annual Review of Chemical and Biomolecular Engineering* **2016**, *7*, 373.

[24] F. Khelifa, S. Ershov, Y. Habibi, R. Snyders, P. Dubois, *Chem. Rev.* **2016**, *116*, 3975.

[25] E. Biazar, M. Kamalvand, F. Avani, *International Journal of Polymeric Materials and Polymeric Biomaterials* **2022**, *71*, 493.

[26] O. Neděla, P. Slepička, V. Švorčík, *Materials* **2017**, *10*, 1115.

[27] A. Z. Unal, J. L. West, *Bioconjugate Chem.* **2020**, *31*, 2253.

[28] E. Ruoslahti, M. D. Pierschbacher, *Science* **1987**, *238*, 491.

[29] E. Ruoslahti, *Annual Review of Cell and Developmental Biology* **1996**, *12*, 697.

[30] L. S. Barbarash, E. N. Bolbasov, L. V. Antonova, V. G. Matveeva, E. A. Velikanova, E. V. Shesterikov, Y. G. Anissimov, S. I. Tverdokhlebov, *Materials Letters* **2016**, *171*, 87.

[31] P. Das, N. Ojah, R. Kandimalla, K. Mohan, D. Gogoi, S. K. Dolui, A. J. Choudhury, *International Journal of Biological Macromolecules* **2018**, *114*, 1026.

[32] S. Eve, J. Mohr, *Procedia Engineering* **2009**, *1*, 237.

[33] Z. Kolská, R. Polanský, P. Prosr, M. Zemanová, P. Ryšánek, P. Slepička, V. Švorčík, *Materials Letters* **2018**, *214*, 264.

[34] A. Satish, P. S. Korrapati, *Journal of Tissue Engineering and Regenerative Medicine* **2019**, *13*, 753.

[35] B. Kong, W. Sun, G. Chen, S. Tang, M. Li, Z. Shao, S. Mi, *Sci Rep* **2017**, *7*, 970.

[36] I. Jun, Y.-W. Chung, Y.-H. Heo, H.-S. Han, J. Park, H. Jeong, H. Lee, Y. B. Lee, Y.-C. Kim, H.-K. Seok, H. Shin, H. Jeon, *ACS Appl. Mater. Interfaces* **2016**, *8*, 3407.

[37] S. Mädler, C. Bich, D. Touboul, R. Zenobi, *Journal of Mass Spectrometry* **2009**, *44*, 694.

[38] S.-N. Park, H. J. Lee, K. H. Lee, H. Suh, *Biomaterials* **2003**, *24*, 1631.

[39] Q. He, R. Kusumi, S. Kimura, U.-J. Kim, K. Deguchi, S. Ohki, A. Goto, T. Shimizu, M. Wada, *Carbohydrate Polymers* **2020**, *237*, 116189.

[40] E. Mirzaei B., A. Ramazani S. A., M. Shafiee, M. Danaei, *International Journal of Polymeric Materials and Polymeric Biomaterials* **2013**, *62*, 605.

[41] H. Awada, A. Al Samad, D. Laurencin, R. Gilbert, X. Dumail, A. El Jundi, A. Bethry, R. Pomrenke, C. Johnson, L. Lemaire, F. Franconi, G. Félix, J. Larionova, Y. Guari, B. Nottelet, *ACS Appl. Mater. Interfaces* **2019**, *11*, 9519.

[42] A. A. Nada, F. H. H. Abdellatif, E. A. Ali, R. A. Abdelazeem, A. A. S. Soliman, N. Y. Abou-Zeid, *Carbohydrate Polymers* **2018**, *199*, 610.

[43] S. I. Goreninskii, R. O. Guliaev, K. S. Stankevich, N. V. Danilenko, E. N. Bolbasov, A. S. Golovkin, A. I. Mishanin, V. D. Filimonov, S. I. Tverdokhlebov, *Colloids and Surfaces B: Biointerfaces* **2019**, *177*, 137.

[44] Q. Yang, J. Zhao, A. Muhammad, L. Tian, Y. Liu, L. Chen, P. Yang, *Materials Today Bio* **2022**, *16*, 100407.

[45] L. Chen, C. Yan, Z. Zheng, *Materials Today* **2018**, *21*, 38.

[46] Q. Wei, R. Haag, *Materials Horizons* **2015**, *2*, 567.

[47] N. Roberto Barros, Y. Chen, V. Hosseini, W. Wang, R. Nasiri, M. Mahmoodi, E. Pinar Yalcintas, R. Haghniaz, M. Magan Mecwan, S. Karamikamkar, W. Dai, S. A. Sarabi, N. Falcone, P. Young, Y. Zhu, W. Sun, S. Zhang, J. Lee, K. Lee, S. Ahadian, M. Remzi Dokmeci, A. Khademhosseini, H.-J. Kim, *Biomaterials Science* **2021**, *9*, 6653.

[48] E. C. Bell, J. M. Gosline, *Journal of Experimental Biology* **1996**, *199*, 1005.

[49] B. P. Lee, P. B. Messersmith, J. N. Israelachvili, J. H. Waite, *Annual Review of Materials Research* **2011**, *41*, 99.

[50] J. Yang, M. A. C. Stuart, M. Kamperman, *Chemical Society Reviews* **2014**, *43*, 8271.

[51] B. K. Ahn, *J. Am. Chem. Soc.* **2017**, *139*, 10166.

[52] Q. Wei, F. Zhang, J. Li, B. Li, C. Zhao, *Polymer Chemistry* **2010**, *1*, 1430.

[53] H. Lee, S. M. Dellatore, W. M. Miller, P. B. Messersmith, *Science* **2007**, *318*, 426.

[54] H.-C. Yang, J. Luo, Y. Lv, P. Shen, Z.-K. Xu, *Journal of Membrane Science* **2015**, *483*, 42.

[55] Q. Ye, F. Zhou, W. Liu, *Chemical Society Reviews* **2011**, *40*, 4244.

[56] Z. Xu, *Sci Rep* **2013**, *3*, 2914.

[57] M. J. Sever, J. T. Weisser, J. Monahan, S. Srinivasan, J. J. Wilker, *Angewandte Chemie International Edition* **2004**, *43*, 448.

[58] Q. Lu, D. X. Oh, Y. Lee, Y. Jho, D. S. Hwang, H. Zeng, *Angewandte Chemie* **2013**, *125*, 4036.

[59] S. Kim, A. Faghihnejad, Y. Lee, Y. Jho, H. Zeng, D. Soo Hwang, *Journal of Materials Chemistry B* **2015**, *3*, 738.

[60] S. C. T. Nicklisch, J. H. Waite, *Biofouling* **2012**, *28*, 865.

[61] J. Yu, in *Adhesive Interactions of Mussel Foot Proteins* (Ed.: J. Yu), Springer International Publishing, Cham, **2014**, pp. 21–30.

[62] J. J. Wilker, *Angewandte Chemie International Edition* **2010**, *49*, 8076.

[63] D. Soo Hwang, H. Zeng, Q. Lu, J. Israelachvili, J. Herbert Waite, *Soft Matter* **2012**, *8*, 5640.

[64] M. Li, C. Schlaich, M. W. Kulka, I. S. Donskyi, T. Schwerdtle, W. E. S. Unger, R. Haag, *J. Mater. Chem. B* **2019**, *7*, 3438.

[65] J. Yu, Y. Kan, M. Rapp, E. Danner, W. Wei, S. Das, D. R. Miller, Y. Chen, J. H. Waite, J. N. Israelachvili, *Proceedings of the National Academy of Sciences* **2013**, *110*, 15680.

[66] M. W. Kulka, I. S. Donskyi, N. Wurzler, D. Salz, Ö. Özcan, W. E. S. Unger, R. Haag, *ACS Appl. Bio Mater.* **2019**, *2*, 5749.

[67] J. H. Waiter, *Annals of the New York Academy of Sciences* **1999**, *875*, 301.

[68] Q. Guo, J. Chen, J. Wang, H. Zeng, J. Yu, *Nanoscale* **2020**, *12*, 1307.

[69] H. Ma, J. Luo, Z. Sun, L. Xia, M. Shi, M. Liu, J. Chang, C. Wu, *Biomaterials* **2016**, *111*, 138.

[70] M. Xu, A. Khan, T. Wang, Q. Song, C. Han, Q. Wang, L. Gao, X. Huang, P. Li, W. Huang, *ACS Appl. Bio Mater.* **2019**, *2*, 3329.

[71] Md. S. Islam, N. Akter, Md. M. Rahman, C. Shi, M. T. Islam, H. Zeng, Md. S. Azam, *ACS Sustainable Chem. Eng.* **2018**, *6*, 9178.

[72] X. Wang, Z. Gu, B. Jiang, L. Li, X. Yu, *Biomaterials Science* **2016**, *4*, 678.

[73] F. Xiong, S. Wei, H. Sheng, X. Han, W. Jiang, Z. Zhang, B. Li, H. Xuan, Y. Xue, H. Yuan, *International Journal of Biological Macromolecules* **2022**, *201*, 338.

[74] A. S. Hoffman, *Advanced Drug Delivery Reviews* **2012**, *64*, 18.

[75] O. Wichterle, D. Lím, *Nature* **1960**, *185*, 117.

[76] F. Lim, A. M. Sun, *Science* **1980**, *210*, 908.

[77] J. George, C.-C. Hsu, L. T. B. Nguyen, H. Ye, Z. Cui, *Biotechnology Advances* **2020**, *42*, 107370.

[78] F. Puza, Y. Zheng, L. Han, L. Xue, J. Cui, *Polymer Chemistry* **2020**, *11*, 2339.

[79] C. Norioka, Y. Inamoto, C. Hajime, A. Kawamura, T. Miyata, *NPG Asia Mater* **2021**, *13*, 1.

[80] Y. Huang, P. G. Lawrence, Y. Lapitsky, *Langmuir* **2014**, *30*, 7771.

[81] S. Ma, S. Wang, Q. Li, Y. Leng, L. Wang, G.-H. Hu, *Ind. Eng. Chem. Res.* **2017**, *56*, 7971.

[82] G. Li, Q. Yan, H. Xia, Y. Zhao, *ACS Appl. Mater. Interfaces* **2015**, *7*, 12067.

[83] M. Mihajlovic, M. Staropoli, M.-S. Appavou, H. M. Wyss, W. Pyckhout-Hintzen, R. P. Sijbesma, *Macromolecules* **2017**, *50*, 3333.

[84] Z. Rao, M. Inoue, M. Matsuda, T. Taguchi, *Colloids and Surfaces B: Biointerfaces* **2011**, *82*, 196.

[85] W. E. Hennink, C. F. van Nostrum, *Advanced Drug Delivery Reviews* **2012**, *64*, 223.

[86] D. L. Taylor, M. in het Panhuis, *Advanced Materials* **2016**, *28*, 9060.

[87] S.-J. Jeon, A. W. Hauser, R. C. Hayward, *Acc. Chem. Res.* **2017**, *50*, 161.

[88] I. Tokarev, S. Minko, *Soft Matter* **2009**, *5*, 511.

[89] K. Nakamae, T. Miyata, A. Jikihara, A. S. Hoffman, *Journal of Biomaterials Science, Polymer Edition* **1995**, *6*, 79.

[90] J. E. Morris, A. S. Hoffman, R. R. Fisher, *Biotechnology and Bioengineering* **1993**, *41*, 991.

[91] S. Mondal, S. Das, A. K. Nandi, *Soft Matter* **2020**, *16*, 1404.

[92] E. M. Ahmed, *Journal of Advanced Research* **2015**, *6*, 105.

[93] A. S. Hoffman, *Advanced Drug Delivery Reviews* **2012**, *64*, 18.

[94] H. C. Kolb, M. G. Finn, K. B. Sharpless, *Angewandte Chemie International Edition* **2001**, *40*, 2004.

[95] C. D. Hein, X.-M. Liu, D. Wang, *Pharm Res* **2008**, *25*, 2216.

[96] R. Randriantsilefisoa, Y. Hou, Y. Pan, J. L. C. Camacho, M. W. Kulka, J. Zhang, R. Haag, *Advanced Functional Materials* **2020**, *30*, 1905200.

[97] C. E. Hoyle, C. N. Bowman, *Angewandte Chemie International Edition* **2010**, *49*, 1540.

[98] P. M. Kharkar, M. S. Rehmann, K. M. Skeens, E. Maverakis, A. M. Kloxin, *ACS Biomater. Sci. Eng.* **2016**, *2*, 165.

[99] W. Hu, Z. Wang, Y. Xiao, S. Zhang, J. Wang, *Biomaterials Science* **2019**, *7*, 843.

[100] V. X. Truong, I. Donderwinkel, J. E. Frith, *Journal of Polymer Science Part A: Polymer Chemistry* **2019**, *57*, 1872.

[101] B. Fu, X. Wang, Z. Chen, N. Jiang, Z. Guo, Y. Zhang, S. Zhang, X. Liu, L. Liu, *Journal of Materials Chemistry B* **2022**, *10*, 656.

[102] A. R. Fajardo, S. L. Fávaro, A. F. Rubira, E. C. Muniz, *Reactive and Functional Polymers* **2013**, *73*, 1662.

[103] J. Chen, S. K. Spear, J. G. Huddleston, R. D. Rogers, *Green Chemistry* **2005**, *7*, 64.

[104] A. A. D'souza, R. Shegokar, *Expert Opinion on Drug Delivery* **2016**, *13*, 1257.

[105] Q. Yang, S. K. Lai, *WIREs Nanomedicine and Nanobiotechnology* **2015**, *7*, 655.

[106] H. Frey, R. Haag, *Reviews in Molecular Biotechnology* **2002**, *90*, 257.

[107] A. Thomas, S. S. Müller, H. Frey, *Biomacromolecules* **2014**, *15*, 1935.

[108] H. E. H. Meijer, L. E. Govaert, *Progress in Polymer Science* **2005**, *30*, 915.

[109] D. Hölter, A. Burgath, H. Frey, *Acta Polymerica* **1997**, *48*, 30.

[110] V. T. Wyatt, G. D. Strahan, *Polymers* **2012**, *4*, 396.

[111] D. Wilms, S.-E. Stiriba, H. Frey, *Acc. Chem. Res.* **2010**, *43*, 129.

[112] A. Sunder, R. Hanselmann, H. Frey, R. Mülhaupt, *Macromolecules* **1999**, *32*, 4240.

[113] S. McMahon, R. Kennedy, P. Duffy, J. M. Vasquez, J. G. Wall, H. Tai, W. Wang, *ACS Appl. Mater. Interfaces* **2016**, *8*, 26648.

[114] M. H. M. Oudshoorn, R. Rissmann, J. A. Bouwstra, W. E. Hennink, *Biomaterials* **2006**, *27*, 5471.

[115] B. Thongrom, A. Sharma, C. Nie, E. Quaas, M. Raue, S. Bhatia, R. Haag, *Macromolecular Bioscience* **2022**, *22*, 2100507.

[116] A. Herrmann, L. Kaufmann, P. Dey, R. Haag, U. Schedler, *ACS Appl. Mater. Interfaces* **2018**, *10*, 11382.

[117] L. T. Saldin, M. C. Cramer, S. S. Velankar, L. J. White, S. F. Badylak, *Acta Biomaterialia* **2017**, *49*, 1.

[118] F. T. Bosman, I. Stamenkovic, *The Journal of Pathology* **2003**, *200*, 423.

[119] C. Frantz, K. M. Stewart, V. M. Weaver, *Journal of Cell Science* **2010**, *123*, 4195.

[120] A. D. Theocharis, S. S. Skandalis, C. Gialeli, N. K. Karamanos, *Advanced Drug Delivery Reviews* **2016**, *97*, 4.

[121] H. Geckil, F. Xu, X. Zhang, S. Moon, U. Demirci, *Nanomedicine* **2010**, *5*, 469.

[122] Y. Ma, T. Han, Q. Yang, J. Wang, B. Feng, Y. Jia, Z. Wei, F. Xu, *Advanced Functional Materials* **2021**, *31*, 2100848.

[123] J. Fukuda, A. Khademhosseini, J. Yeh, G. Eng, J. Cheng, O. C. Farokhzad, R. Langer, *Biomaterials* **2006**, *27*, 1479.

[124] A. K. Azab, B. Orkin, V. Doviner, A. Nissan, M. Klein, M. Srebnik, A. Rubinstein, *Journal of Controlled Release* **2006**, *111*, 281.

[125] M. p. Lutolf, G. p. Raeber, A. h. Zisch, N. Tirelli, J. a. Hubbell, *Advanced Materials* **2003**, *15*, 888.

[126] E. C. González-Díaz, S. Varghese, *Gels* **2016**, *2*, 20.

[127] K. A. Kyburz, K. S. Anseth, *Acta Biomaterialia* **2013**, *9*, 6381.

[128] J. J. Moon, M. S. Hahn, I. Kim, B. A. Nsiah, J. L. West, *Tissue Engineering Part A* **2009**, *15*, 579.

[129] Z. Wang, Z. Wang, W. W. Lu, W. Zhen, D. Yang, S. Peng, *NPG Asia Mater* **2017**, *9*, e435.

[130] P. R. Kuhl, L. G. Griffith-Cima, *Nat Med* **1996**, *2*, 1022.

[131] Z. Lin, G. Luo, W. Du, T. Kong, C. Liu, Z. Liu, *Small* **2020**, *16*, 1903899.

[132] S. Vanharanta, J. Massagué, *Cancer Cell* **2013**, *24*, 410.

[133] S. J. Cohen, C. J. A. Punt, N. Iannotti, B. H. Saidman, K. D. Sabbath, N. Y. Gabrail, J. Picus, M. A. Morse, E. Mitchell, M. C. Miller, G. V. Doyle, H. Tissing, L. W. M. M. Terstappen, N. J. Meropol, *Annals of Oncology* **2009**, *20*, 1223.

[134] C. Alix-Panabières, H. Schwarzenbach, K. Pantel, *Annual Review of Medicine* **2012**, *63*, 199.

[135] K. Pantel, M. R. Speicher, *Oncogene* **2016**, *35*, 1216.

[136] E. Schuster, R. Taftaf, C. Reduzzi, M. K. Albert, I. Romero-Calvo, H. Liu, *Trends in Cancer* **2021**, *7*, 1020.

[137] M. Yu, S. Stott, M. Toner, S. Maheswaran, D. A. Haber, *Journal of Cell Biology* **2011**, *192*, 373.

[138] P. Paterlini-Brechot, N. L. Benali, *Cancer Letters* **2007**, *253*, 180.

[139] Z. Habli, W. AlChamaa, R. Saab, H. Kadara, M. L. Khraiche, *Cancers* **2020**, *12*, 1930.

[140] R. A. Harouaka, M.-D. Zhou, Y.-T. Yeh, W. J. Khan, A. Das, X. Liu, C. C. Christ, D. T. Dicker, T. S. Baney, J. T. Kaifi, C. P. Belani, C. I. Truica, W. S. El-Deiry, J. P. Allerton, S.-Y. Zheng, *Clinical Chemistry* **2014**, *60*, 323.

[141] R. Rosenberg, R. Gertler, J. Friederichs, K. Fuehrer, M. Dahm, R. Phelps, S. Thorban, H. Nekarda, J. R. Siewert, *Cytometry* **2002**, *49*, 150.

[142] V. Gupta, I. Jafferji, M. Garza, V. O. Melnikova, D. K. Hasegawa, R. Pethig, D. W. Davis, *Biomicrofluidics* **2012**, *6*, 024133.

[143] W. J. Allard, J. Matera, M. C. Miller, M. Repollet, M. C. Connelly, C. Rao, A. G. J. Tibbe, J. W. Uhr, L. W. M. M. Terstappen, *Clinical Cancer Research* **2004**, *10*, 6897.

[144] J. C. Ahn, P.-C. Teng, P.-J. Chen, E. Posadas, H.-R. Tseng, S. C. Lu, J. D. Yang, *Hepatology* **2021**, *73*, 422.

[145] L. Yu, P. Tang, C. Nie, Y. Hou, R. Haag, *Advanced Healthcare Materials* **2021**, *10*, 2002202.

[146] L. Descamps, D. Le Roy, A.-L. Deman, *International Journal of Molecular Sciences* **2022**, *23*, 1981.

[147] M.-H. Park, E. Reátegui, W. Li, S. N. Tessier, K. H. K. Wong, A. E. Jensen, V. Thapar, D. Ting, M. Toner, S. L. Stott, P. T. Hammond, *J. Am. Chem. Soc.* **2017**, *139*, 2741.

[148] J. Lee, B. Kwak, *Biosensors and Bioelectronics* **2020**, *168*, 112564.

[149] L. P. Ferreira, V. M. Gaspar, J. F. Mano, *Acta Biomaterialia* **2018**, *75*, 11.

[150] N. Kramer, A. Walzl, C. Unger, M. Rosner, G. Krupitza, M. Hengstschläger, H. Dolznig, *Mutation Research/Reviews in Mutation Research* **2013**, *752*, 10.

[151] F. Hirschhaeuser, H. Menne, C. Dittfeld, J. West, W. Mueller-Klieser, L. A. Kunz-Schughart, *Journal of Biotechnology* **2010**, *148*, 3.

[152] G. Lazzari, P. Couvreur, S. Mura, *Polymer Chemistry* **2017**, *8*, 4947.

[153] K. Froehlich, J.-D. Haeger, J. Heger, J. Pastuschek, S. M. Photini, Y. Yan, A. Lupp, C. Pfarrer, R. Mrowka, E. Schleußner, U. R. Markert, A. Schmidt, *J Mammary Gland Biol Neoplasia* **2016**, *21*, 89.

[154] S. Nath, G. R. Devi, *Pharmacology & Therapeutics* **2016**, *163*, 94.

[155] B. Rodday, F. Hirschhaeuser, S. Walenta, W. Mueller-Klieser, *J Biomol Screen* **2011**, *16*, 1119.

[156] M. B. Oliveira, C. L. Salgado, W. Song, J. F. Mano, *Small* **2013**, *9*, 768.

[157] A. Barzegari, A. A. Saei, *Bioimpacts* **2012**, *2*, 23.

[158] F. Hirschhaeuser, T. Leidig, B. Rodday, C. Lindemann, W. Mueller-Klieser, *SLAS Discovery* **2009**, *14*, 980.

[159] L. Chen, Z. Xiao, Y. Meng, Y. Zhao, J. Han, G. Su, B. Chen, J. Dai, *Biomaterials* **2012**, *33*, 1437.

[160] N. Arya, V. Sardana, M. Saxena, A. Rangarajan, D. S. Katti, *Journal of The Royal Society Interface* **2012**, *9*, 3288.

[161] T. Hoshiba, M. Tanaka, *Biochimica et Biophysica Acta (BBA) - Molecular Cell Research* **2016**, *1863*, 2749.

[162] C.-T. Tsao, F. M. Kievit, K. Wang, A. E. Erickson, R. G. Ellenbogen, M. Zhang, *Mol. Pharmaceutics* **2014**, *11*, 2134.

[163] G. Benton, H. K. Kleinman, J. George, I. Arnaoutova, *International Journal of Cancer* **2011**, *128*, 1751.

[164] S. Pradhan, J. M. Clary, D. Seliktar, E. A. Lipke, *Biomaterials* **2017**, *115*, 141.

[165] P. Tang, G. Ma, P. Nickl, C. Nie, L. Yu, R. Haag, *Advanced Materials Interfaces* **2023**, *10*, 2300165.

[166] P. Tang, B. Thongrom, S. Arora, R. Haag, *Advanced Healthcare Materials* **2023**, *12*, 2300842.

[167] B. Thongrom, P. Tang, S. Arora, R. Haag, *Gels* **2023**, *9*, 938.

8. List of abbreviations

RGD	Arginylglycylaspartic acid
PCL	Poly-ε-caprolactone
UV	Ultra-violet
PVCi	Polyvinyl cinnamate
PLLA	Poly (L-lactic acid)
NHS	N-hydroxysuccinimide
EDC	1-ethyl-3-(3-dimethylaminopropyl) carbodiimide
EGDE	Ethylene glycol diglycidyl ether
Mfp	Mussel foot protein
Dopa	3,4-dihydroxyphenyl-L-alanine
PDA	Polydopamine
SFA	Surface force apparatus
AFM	Atom force microscope
SCPP	Strontium-doped calcium polyphosphate
ECM	Extracellular matrix
HEMA	Hydroxyethyl methacrylate
SPAAC	Strain-promoted alkyne-azide cycloaddition
hPG/dPG	Hyperbranched/dendritic polyglycerol
IEDDA	Diels-Adler reaction
PEG	Polyethylene glycol
RAFT	Reversible addition fragmentation chain transfer
PEGDA	Polyethylene glycol diacrylate
PEGMEMA	Polyethylene glycol methyl ether methacrylate
dPGS	Dendritic polyglycerol sulfates
HSV	Herpes simplex virus
GAGs	Glycosaminoglycans
EGF	Epidermal growth factor
CTC	Circulating tumor cell
EMT	Epithelia-to-mesenchymal transition
EpCAM	Epithelia cell adhesion molecule
TME	Tumor microenvironment
MCTS	Multicellular tumor spheroid

9. List of Publications, Patents

[1] P. Tang, G. Ma, P. Nickl, C. Nie, L. Yu, R. Haag, Mussel-inspired Polyglycerol Coatings for Surface Modification with Tunable Architecture. *Adv. Mater. Interfaces*, **2023**, 2300165.

[2] P. Tang, B. Thongrom, S. Arora, R. Haag, Polyglycerol-based biomedical matrix for immunomagnetic circulating tumor cell isolation and their expansion into tumor spheroids for drug screening. *Adv. Healthc. Mater*, **2023**, *12*, 2300842.

[3] B. Thongrom[1], P. Tang[1], S. Arora, R. Haag, Polyglycerol-Based Hydrogel as Versatile Support Matrix for 3D Multicellular Tumor Spheroid Formation. *Gels* **2023**, *9*, 938.

[4] L. Yu, P. Tang, C. Nie, Y. Hou, R. Haag, Well-defined Nanostructured Biointerfaces: Strengthened Cellular Interaction for Circulating Tumor Cells isolation. *Adv. Healthc. Mater.* **2021**, *10*, 2002202.

[5] Z. Tavasolyzadeh, P. Tang, M. B. Hahn, G. Hweidi, N. Nordholt, R. Haag, H. Sturm,I. Topolniak, 2D and 3D Micropatterning of Mussel-Inspired Functional Materials by Direct Laser Writing. *Small*, **2023**, 2309394.

[6] European Patent Nr. PCT/EP2022/052538
Peng Tang, Leixiao Yu, Rainer Haag
"Layered structure for specific cell capturing"